

Renormalization group theory for fermions and order parameter fluctuations in interacting Fermi systems

Von der Fakultät Mathematik und Physik der Universität Stuttgart
zur Erlangung der Würde eines Doktors der Naturwissenschaften
(Dr. rer. nat.) genehmigte Abhandlung

vorgelegt von
Philipp Strack
aus Frankfurt am Main

Hauptberichter: Prof. Dr. Walter Metzner
Mitberichter: Prof. Dr. Alejandro Muramatsu

Max-Planck-Institut für Festkörperforschung, Stuttgart, 2009

Acknowledgments

Walter Metzner's supervision privileged my scientific efforts: timely availability for questions, significant calculational help, and extremely flexible work arrangements left hardly any external factors to blame. Though not always easy to digest, his sober and matter-of-factly Wittgensteinian approach to penetrate problems has sharpened my wit during the last three years for what I am deeply thankful. Alejandro Muramatsu is thanked for co-refereeing this thesis.

Pawel Jakubczyk, So Takei, Sebastian Diehl, and Johannes Bauer are thanked wholeheartedly for contributing important stimuli and corrections during the course of this work. During initial stages of my PhD time, Sabine Andergassen, Tilman Enss, and Carsten Honerkamp were always available for questions. Roland Gersch and Julius Reiss have additionally provided me with code examples and many useful hints on programming. Further interactions with Inga Fischer, Andrey Katanin, Manfred Salmhofer, and Roland Zeyher are gratefully acknowledged.

Christof Wetterich is thanked for providing the opportunity to interact frequently with his group at the Institute for Theoretical Physics in Heidelberg. Intense discussions with Jan Pawłowski, Holger Gies, and Hans Christian Krahle have shaped some ideas of this thesis. Jens Braun, Stefan Flörchinger, Jens Müller, Georg Robbers, and Michael Scherer are also acknowledged for useful conversations.

Gil Lonzarich is gratefully acknowledged for being an inspirational host during the summer 2007 in Cambridge, UK. The Quantum Matter group at Cavendish Laboratory and especially Stephen Rowley, Leszek Spalek, Montu Saxena are thanked for insightful exchanges.

Anne Gerrit Knepel makes my life better in any respect; Rolf Dieter Strack's engineering skills made our apartment more livable and freed up valuable time; Irmgard and Georg Walter Strack's liquidity injections eased costs associated with frequent travel and coexisting apartments; Elisabeth Strack's and Uwe Gsänger's policies insured me safely; Eva Maria and Helmut Knepel enabled a most luxurious lifestyle for our two cats Mia and Momo during much of this PhD time. Thank you.

Abstract

The physics of interacting Fermi systems is extremely sensitive to the energy scale. Of particular interest is the low energy regime where correlation induced collective behavior emerges. The theory of interacting Fermi systems is confronted with the occurrence of very different phenomena along a continuum of scales calling for methods capable of computing physical observables as a function of energy scale.

In this thesis, we perform a comprehensive renormalization group analysis of two- and three-dimensional Fermi systems at low and zero temperature. We examine systems with spontaneous symmetry-breaking and quantum critical behavior by deriving and solving flow equations within the functional renormalization group framework.

We extend the Hertz-Millis theory of quantum phase transitions in itinerant fermion systems to phases with discrete and continuous symmetry-breaking, and to quantum critical points where the zero temperature theory is associated with a non-Gaussian fixed point. The order parameter is implemented by a bosonic Hubbard-Stratonovich field, which –for continuous symmetry-breaking– splits into two components corresponding to longitudinal and transversal Goldstone fluctuations. We compute the finite temperature phase boundary near the quantum critical point explicitly including non-Gaussian fluctuations.

We then set up a coupled fermion-boson renormalization group theory that captures the mutual interplay of gapless fermions with massless order parameter fluctuations when approaching a quantum critical point. As a first application, we compute the complete set of quantum critical exponents at the semimetal-to-superfluid quantum phase transition of attractively interacting Dirac fermions in two dimensions. Both, the order parameter propagator and the fermion propagator become non-analytic functions of momenta destroying the Fermi liquid behavior.

We finally compute the effects of quantum fluctuations in the superfluid ground state of an attractively interacting Fermi system, employing the attractive Hubbard model as a prototype. The flow equations capture the influence of longitudinal and Goldstone order parameter fluctuations on non-universal quantities such as the fermionic gap and the fermion-boson vertex, as well as the exact universal infrared asymptotics present in every fermionic superfluid.

Contents

1	Introduction	1
1.1	Experiments	1
1.1.1	Phase boundary close to a quantum critical point	1
1.1.2	Phase diagram of an attractive two-component Fermi gas	3
1.2	Thesis outline	4

Part I Theoretical Framework

2	Underlying concepts	9
2.1	Fermi liquid instabilities	9
2.2	Spontaneous symmetry-breaking	12
2.3	Quantum criticality	13
2.4	The renormalization group	15
3	Functional renormalization group	17
3.1	Functional integral for quantum many-particle systems	17
3.1.1	Superfield formulation for fermionic and bosonic models	18
3.1.2	One-particle irreducible generating functional	19
3.2	Flow equations	19
3.2.1	Exact flow equation	19
3.2.2	Spontaneous symmetry-breaking	22
4	Summary Part I	25

Part II Applications

5	Hertz-Millis theory with discrete symmetry-breaking	29
5.1	Introduction	29

5.2	Bosonic action	30
5.3	Method	32
5.3.1	Truncation	33
5.3.2	Flow equations	34
5.4	Zero-temperature solution at the quantum critical point	35
5.4.1	$z \geq 2$	36
5.4.2	$z = 1$	37
5.5	Finite temperatures	38
5.5.1	$z = 3$	39
5.5.2	$z = 2$	44
5.5.3	$z = 1$	45
5.6	Conclusion	48
6	Quantum critical points with Goldstone modes	49
6.1	Introduction	49
6.2	σ - Π Model for continuous symmetry-breaking	50
6.3	Method	53
6.4	Finite temperature phase boundary in three dimensions	54
6.4.1	Flow equations	54
6.4.2	Classical fixed point	56
6.4.3	Shift exponent ψ	56
6.5	Infrared asymptotics in the symmetry-broken phase	57
6.5.1	Flow equations	57
6.5.2	Analytical results	58
6.6	Conclusion	60
7	Fermi-Bose renormalization group for quantum critical fermion systems	61
7.1	Introduction	61
7.2	Dirac cone model	62
7.2.1	Mean-field theory	63
7.3	Method	64
7.3.1	Truncation	65
7.3.2	Flow equations	68
7.4	Solution at the quantum critical point	71
7.4.1	Quantum critical flows in two dimensions	72
7.4.2	Quantum critical exponents	75
7.5	Conclusion	76
8	Fermionic superfluids at zero temperature	77
8.1	Introduction	77
8.2	Bare action	78
8.3	Mean-field theory	80

8.4	Truncation	83
8.4.1	Symmetric regime	83
8.4.2	Symmetry-broken regime	85
8.4.3	Flow equations	86
8.4.4	Relation to mean-field theory	92
8.5	Results	94
8.5.1	Flow for $\Lambda \lesssim \Lambda_c$	94
8.5.2	Infrared asymptotics	95
8.5.3	Numerical results in two dimensions	97
8.6	Conclusion	99

Part III Summary

9	Conclusions	103
9.1	Key results	103
9.1.1	Non-Gaussian fixed points	103
9.1.2	Goldstone modes	104
9.1.3	Non-universal and universal quantities	104
9.2	Criticism	104
9.3	Outlook	105
9.3.1	QED ₃ (extending chapter 7)	106
9.3.2	Superfluid Kosterlitz-Thouless phase (ext. chapter 8)	107
9.3.3	BCS-Bose crossover (ext. chapter 8)	108
10	Deutsche Zusammenfassung	109

Part IV Appendices

Numerical procedure	115
Academic curriculum vitae	117
References	119

Introduction

This thesis is concerned with low- and zero-temperature properties of correlated fermion systems in two and three dimensions. Interaction effects accompanied by quantum and thermal fluctuations play an important role and produce fascinating phenomena such as, for example, new scaling laws in the vicinity of quantum critical points and exotic forms of superfluidity in cold atomic gases.

1.1 Experiments

Before presenting the outline of this thesis, we refer to two recent hallmark experiments which are related to computations performed in the present work.

1.1.1 Phase boundary close to a quantum critical point

First, we discuss the recent measurement of the finite temperature phase boundary of the antiferromagnetically ordered phase in $\text{BaCuSi}_2\text{O}_6$ performed in Stanford (Sebastian 2006). In this compound, the line of finite temperature phase transitions remains continuous down to the lowest temperatures and ends at a quantum critical point (QCP). In the vicinity of the QCP, the shape of the phase boundary becomes universal and follows the power-law: $T_c \sim (\delta - \delta_c)^\psi$, where δ is the non-thermal control parameter –in this case the external magnetic field. The so-called shift exponent ψ is independent of microscopic details and depends only on dimensionality (d) and the additional dimensionality incurred from quantum fluctuations (z):

$$\psi = \frac{z}{d + z - 2}, \quad (1.1)$$

as first derived by Millis (1993). The relevant excitations of the material measured by the Stanford group (Sebastian 2006) are spin-dimers which can be described by an interacting Bose gas undergoing Bose-Einstein condensation at the critical temperature. The original spin degrees of freedom exhibit antiferromagnetic order when the (collective) spin-dimer gas condenses. In such cases, the dynamical exponent is $z = 2$.

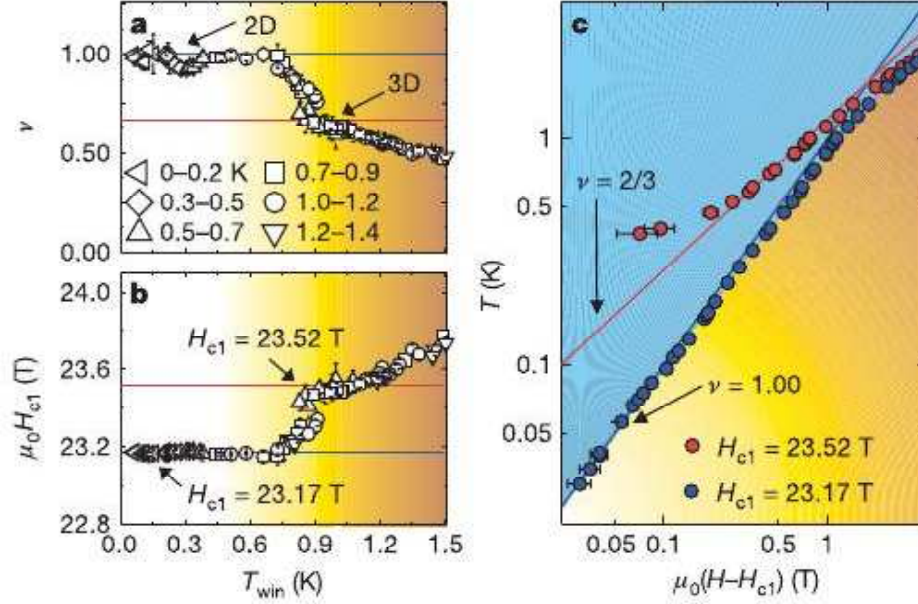


Fig. 1.1. Phase boundary of the antiferromagnetic phase in $\text{BaCuSi}_2\text{O}_6$ close to the QCP (Sebastian 2006). (a) Values of the shift exponent (here ν) obtained from fitting experimental points on the phase boundary. The data approach $\nu = 2/3$ in the intermediate regime, and there is a distinct crossover toward $\nu = 1$ before the QCP is reached. (b): Estimates of the location of the QCP, H_{c1} , obtained along with ν during the fit. (c): Best fits to the phase boundary in the intermediate and low temperature regime on a logarithmic scale.

In Fig. 1.1 (c), data from torque magnetometry for the phase boundary is exhibited, clearly in agreement with Eq. (1.1). The area coloured in blue is the paramagnetic region and the yellow area corresponds to the antiferromagnetically ordered phase. Upon lowering the temperature when approaching the QCP, there is a crossover from three-dimensional scaling to two-dimensional scaling. This has been argued to be a consequence of effective decoupling of the $2d$ -layers of the material at very low temperatures and is specific to the geometrically frustrated lattice structure of $\text{BaCuSi}_2\text{O}_6$.

In chapters 5 and 6, we compute zero- and finite-temperature properties of correlated systems close to a QCP. The interplay of thermal and quantum fluctuations makes this an interesting subject for theoretical studies. Among other things, we introduce a new way to compute the shift exponent coming from the symmetry-broken phase with and without Goldstone modes by the use of modern renormalization group equations which continuously connect the quantum fluctuation dominated regime directly at the QCP to the regime dominated by non-Gaussian classical fluctuations further up the T_c -line.

1.1.2 Phase diagram of an attractive two-component Fermi gas

As the second experiment, we make reference to the seminal measurement of the phase diagram for a spin-polarized Fermi gas performed by the Ketterle group at MIT (Shin 2008). In this experiment, a different amount of spin-up and spin-down components of ^6Li are loaded in an optical trap. By applying an external magnetic field close to a Feshbach resonance the population imbalanced gas is tuned to the resonantly (attractively) interacting regime, forms bosonic spin-singlets, and condenses to the superfluid state upon lowering the temperature. The non-thermal control parameter here is the population imbalance or polarization $\sigma = (n_\uparrow - n_\downarrow) / (n_\uparrow + n_\downarrow)$, where \uparrow and \downarrow refer to the two spin components with densities $n_{\uparrow,\downarrow}$. Increasing σ deprives the attractively interacting fermions of their respective opposite-spin pairing partner thus inhibiting the superfluid pairing beyond a critical polarization $\sigma_c(T)$.

As shown in the left plot of Fig. 1.2, an increasing polarization indeed suppresses the critical temperature and destabilizes the superfluid phase at low temperatures. In the inner region of the trap, a superfluid core forms and the spin polarization shows a

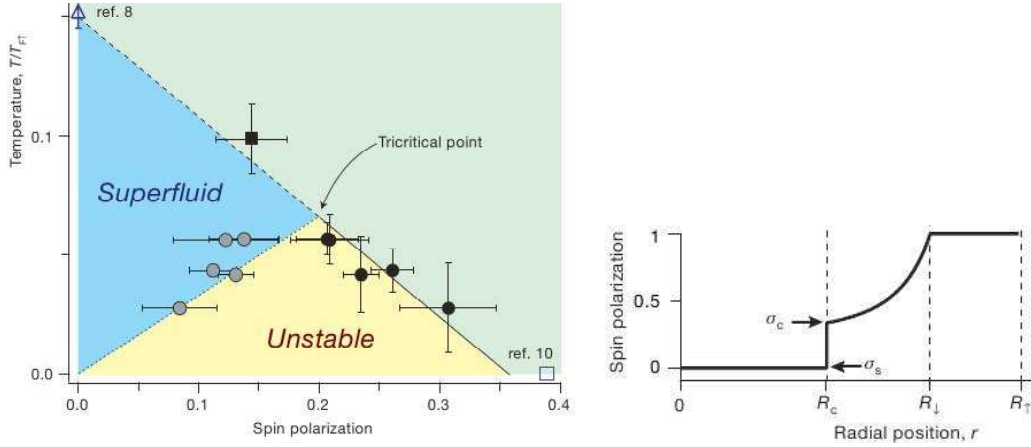


Fig. 1.2. Left: The $\sigma - T$ -phase diagram for a homogeneous spin-polarized Fermi gas with resonant interactions (Shin 2008). The critical polarizations σ_c (black solid circles and square) and σ_s (grey solid circles) are displayed along the local $T/T_{F\uparrow}$, with $T_{F\uparrow}$ the Fermi temperature of the majority component in the spin-up state, at the phase boundary. The yellow area ($\sigma_s < \sigma < \sigma_c$) represents a region with phase separation until $\sigma_s = \sigma_c$ at the tricritical point. The triangle with ref. 8 marks T_c for the unpolarized Fermi gas at unitarity from Burovski et. al (2006) and the square with ref. 10 marks the position of the first order quantum phase transition from Lobo et. al. (2006). Right: At low T , the sample has a three-layer structure (Shin 2008): the core region ($0 \leq r < R_c$) of a fully paired superfluid with $n_\uparrow = n_\downarrow$; the intermediate region ($R_c \leq r < R_\downarrow$) of a partially polarized normal gas; and the outer region ($R_\downarrow < r < R_\uparrow$) of a fully polarized normal gas.

discontinuity at the boundary of the superfluid core $r = R_c$, a signature of the phase separation of a superfluid and a normal gas (Bedaque 2003). The critical polarization $\sigma_c = \lim_{r \rightarrow R_c^+} \sigma(r)$ represents the minimum spin polarization for a stable normal gas; $\sigma_s = \lim_{r \rightarrow R_c^-} \sigma(r)$ represents the maximum spin polarization for a stable superfluid gas as illustrated in on the right plot in Fig. 1.2. At $\sigma_{c0} \approx 0.36$, in the bottom right corner of the left plot in Fig. 1.2, the Clogston limit of superfluidity which is a first order quantum phase transition was experimentally verified.

One way to achieve a *continuous* quantum phase transition in attractive fermion systems involves cold atomic gases loaded in a honeycomb optical lattice (see Zhao 2006 and references therein) and possibly graphene (Uchoa 2007, Castro Neto 2008). The attractive Hubbard model on the honeycomb lattice exhibits, at half-filling, a quantum critical point between a semimetal with massless Dirac fermions and an s-wave superconductor.

Fermionic systems displaying superfluidity form a cornerstone of this thesis. In chapter 7, we investigate attractively interacting Dirac fermions in the vicinity of a continuous semimetal-to-superfluid quantum phase transition and in chapter 8, we consider the superfluid ground state of the attractive Hubbard model at quarter-filling.

1.2 Thesis outline

This thesis is structured in two parts. In the first part, the methodological framework is presented. The second part contains various applications of these methods and concepts. In detail, the chapters in Part I have the following contents:

- In chapter 2, we introduce the fundamental concepts necessary for an understanding of the applications in the second part. First, the standard model of interacting Fermi systems, Landau's Fermi liquid theory, and instabilities thereof are phrased in the language of the renormalization group (RG). The notion of spontaneous symmetry-breaking with a focus on Goldstone bosons is introduced. These massless bosonic excitations arise when a continuous symmetry is broken, as is the case for example in magnetic or superfluid systems. Then, we –after having presented basic features of phase transitions in general– expose the conventional RG approach to quantum critical systems referred to as the Hertz-Millis theory. In transiting to chapter 3 we recapitulate the underlying ideas of the Wilsonian RG approach to quantum field theory.
- In chapter 3, the functional integral approach to many-particle systems containing fermionic and bosonic fields is laid out. At the heart of the chapter is the derivation of the functional RG framework in its one-particle irreducible representation geared toward systems with spontaneously broken symmetry.

The salient points of Part I are summarized in chapter 4. The applications presented in Part II are organized as follows.

- In chapter 5, we extend the Hertz-Millis theory for quantum criticality to phases with broken discrete symmetry. Using the Hertz action, we compute the RG flow of the bosonic propagator and the effective potential with flow equations derived from the functional RG framework. Different dynamical exponents are distinguished and the shape of the phase boundary at finite temperature is computed for each. Large parts of this chapter have been published previously in *Phys. Rev. B* **77**, 195120 (2008) and the results for the Quantum Ising model are published in *Phys. Rev. B* **80**, 085108 (2009).
- In chapter 6, we analyze quantum critical systems with Goldstone modes. We employ an exclusively bosonic effective action with two propagators: one associated with the transverse (Goldstone) dispersion and the other stemming from longitudinal fluctuations. The interactions between longitudinal and Goldstone fluctuations lead to strong renormalizations of the longitudinal propagator away from and at the phase boundary where both modes become degenerate. We compute RG flows to determine the phase boundary at finite temperatures in three dimensions.
- In chapter 7, the main inconsistency of the conventional Hertz-Millis approach –that massless fermions are integrated out in one sweep– is cured by explicitly including fermions into a coupled RG flow for (Dirac) fermions and order parameter fluctuations. This way, we assess the mutual interplay of both types of fluctuations for the semimetal-to-superfluid quantum phase transition in two dimensions. At the QCP, we find that both the order parameter propagator and the single-particle propagator are non-analytic functions of frequency and momenta signalling the breakdown of the Fermi liquid. An improved version of this chapter is published in *Phys. Rev. B* **81**, 125103 (2010).
- In chapter 8, the low energy behavior of the attractive Hubbard model at quarter-filling as a prototype for systems with a superfluid ground state is analyzed. Various non-universal quantities such as the fermionic gap are computed. At the same time, the universal infrared behavior correctly emerges from the flow of the coupled fermion-boson action in agreement with the exact behavior of an interacting Bose gas. This chapter has been published in *Phys. Rev. B* **78**, 014522 (2008).

Part III contains the conclusions of this thesis, criticism, and a description of future research projects. The numerical procedure developed to solve the flow equations is explained in Appendix A.

Part I

Theoretical Framework

Underlying concepts

2.1 Fermi liquid instabilities

This section investigates conditions under which an interacting Fermi system might not be described well anymore by its original degrees of freedom, namely fermionic (quasi-) particles. To lay a basis, we first describe the standard model of interacting fermions: the Landau Fermi liquid theory (for references and review see Nozieres 1964). This theory is formulated entirely in terms of fermionic quasi-particles –bare fermions dressed by interaction effects, hence the prefix quasi. The validity of the Landau Fermi liquid theory rests upon fulfillment of the following conditions:

- the existence of a well-defined Fermi surface, that is, a $(d - 1)$ -dimensional hypersurface in momentum space, to the vicinity of which the low-energy fermionic excitations are restricted to,
- the existence of quasi-particles with a one-to-one correspondence to the non-interacting particles by adiabatically turning on the interaction.

In the functional integral terminology of the renormalization group, the Fermi liquid is said to be described by the *fixed point* or *scale-invariant* action:

$$S [\bar{\psi}, \psi] = \int_k^{<\Lambda} \bar{\psi}_k (ik_0 - v_{\mathbf{k}_F} k_r) \psi_k - \frac{1}{2} \int_{k,k',q}^{<\Lambda} f_{\mathbf{k}_F, \mathbf{k}'_F} \bar{\psi}_{k-q/2} \bar{\psi}_{k'+q/2} \psi_{k'-q/2} \psi_{k+q/2} , \quad (2.1)$$

where $\int_k = T \sum_{k_0} \int \frac{d^d k}{(2\pi)^d}$ comprises (Matsubara) frequency summation and momentum integration restricted to a shell of width 2Λ around the Fermi surface, $\bar{\psi}$, ψ are renormalized Grassmann fields rescaled by the fermionic $Z_{\mathbf{k}_F}$ -factor, k_r is the momentum deviation in radial direction from the Fermi surface, $v_{\mathbf{k}_F}$ is the Fermi velocity projected on the Fermi surface, and $f_{\mathbf{k}_F, \mathbf{k}'_F}$ the Landau function obtained as the (non-commutative) limit $\lim_{q_0 \rightarrow 0} \lim_{\mathbf{q} \rightarrow 0}$ with $\mathbf{q}/q_0 \rightarrow 0$ of the two-particle vertex (for a review see Metzner 1998). Here and in the following, we employ the four-vector notation $k = (k_0, \mathbf{k})$. Considering only processes with zero-momentum transfer by taking

the limit $q \rightarrow 0$, the Hartree mean-field theory of this action leads to the energy functional phenomenologically postulated by Landau

$$\delta E [\delta n] = \int_{\mathbf{k}} v_{\mathbf{k}_F} k_r \delta n_{\mathbf{k}} + \frac{1}{2} \int_{\mathbf{k}, \mathbf{k}'} f_{\mathbf{k}_F, \mathbf{k}'_F} \delta n_{\mathbf{k}_F} \delta n_{\mathbf{k}'_F}, \quad (2.2)$$

with $\delta n_{\mathbf{k}}$ the quasi-particle distribution function. In addition to constituting the standard model of interacting fermions, the merit of Landau's theory lies in its predictive power for systems with spherical Fermi surfaces, the epitome being liquid ^3He . Upon expanding the Landau function $f_{\mathbf{k}_F, \mathbf{k}'_F}$ in Legendre polynomials, one can –with knowledge of only the first few Legendre coefficients– compute a larger number of physical observables such as, e.g., the specific heat or compressibility (Negele 1987).

An important trademark of the Fermi liquid is the renormalized single-particle propagator determined by the quadratic part of the fixed point action as

$$G_f(k) = \frac{1}{ik_0 - v_{\mathbf{k}_F} k_r}, \quad (2.3)$$

which describes *stable* quasi-particle excitations with a velocity $v_{\mathbf{k}_F}$. Note that the interaction-induced reduction in quasi-particle weight by $Z_{\mathbf{k}_F}$ has been absorbed into renormalized field variables. Standard higher-order corrections to the fermion self-energy of Landau's theory are expected to be quadratic in frequency and temperature (Chubukov 2003). Fresh research by Millis, Chubukov and others, however, revealed –already for the generic weakly and locally interacting Fermi gas– non-analytic corrections to the Fermi liquid behavior of the susceptibilities and the specific heat (Chitov 2001, Chubukov 2003, Chubukov 2005).

Indeed, much of the more recent research in correlated fermion systems has been devoted to systems where the Fermi liquid paradigm breaks down and other theoretical descriptions must be invoked (Stewart 2001). Often, tendencies to destabilize the Fermi liquid are already visible in the bare bosonic response functions of the particle-particle (pp) channel:

$$\Pi_{\text{pp}}(q_0, \mathbf{q}) = - \int_k G_{f0}(k+q) G_{f0}(-k) \propto \text{diagram} \quad (2.4)$$

and the particle-hole (ph) channel,

$$\Pi_{\text{ph}}(q_0, \mathbf{q}) = - \int_k G_{f0}(k+q) G_{f0}(k) \propto \text{diagram}, \quad (2.5)$$

where $G_{f0}^{-1} = ik_0 - \xi_{\mathbf{k}}$ is the bare propagator with $\xi_{\mathbf{k}}$ the single-particle energy relative to the Fermi surface. The magnitudes of $\Pi_{\text{ph}}(q_0, \mathbf{q})$ and $\Pi_{\text{pp}}(q_0, \mathbf{q})$ in conjunction with the sign and momentum structure of the interaction may point at the low-energy fate

of the system. If, in a lattice structure for example, the interaction is local and repulsive and $\max\{\Pi_{\text{pp}}(q_0, \mathbf{q}), \Pi_{\text{ph}}(q_0, \mathbf{q})\}$ occurs at $\Pi_{\text{ph}}(0, \mathbf{Q} = 2\mathbf{k}_F)$, the system may form a charge- or spin-density wave eventually leading to charge or magnetic order. On the other hand, strong particle-hole fluctuations in some cases enhance pairing phenomena in the particle-particle channel via the Kohn-Luttinger effect. Therefore, the interplay of both channels has to be assessed to make a statement about the true low-energy fate of the system. Moreover, possible infrared singularities in one or sometimes even multiple scattering channels invalidate perturbative approaches. For certain geometries, such as a nested Fermi surface or when the Fermi surface intersects the van-Hove points, Π_{ph} exhibits a logarithmic divergence for small energies. Π_{pp} also diverges logarithmically as a function of energy for an inflection-symmetric Fermi surface in *any* dimension (for a review see Abrikosov 1975).

A situation of competing Fermi liquid instabilities where both, Π_{ph} and Π_{pp} are important, occurs for example in the repulsive Hubbard model and can be analyzed within a fermionic functional RG treatment which takes into account both, the particle-particle and particle-hole channel (and their mutual interplay) on equal footing (Zanchi 2000, Halboth 2000, Honerkamp 2001). In these RG flows, it is the summed up *non-universal* contributions to the flow that determine which of the several *universal* fixed points (Fermi liquid, antiferromagnetic, superconducting, etc.) the system scales towards.

A drawback of the hitherto employed fermionic functional RG is its failure to penetrate phases with broken-symmetry as the vertex functions grow large at a critical scale thus invalidating the truncation devised for weakly to intermediately coupled systems. If one attempts to go beyond this scale, the vertices eventually diverge and the flow has to be stopped. To continue the flow into phases with broken symmetry is clearly desirable because many systems have symmetry-broken ground states and many experiments are able to verify or falsify quantitative predictions from calculations in the symmetry-broken phase such as, for instance, the magnitude and symmetry properties of the superconducting gap in the cuprates.

At present, two remedial approaches have been developed. In the first approach, a small initial anomalous self-energy for one or multiple channels is added to the bare action and as such offered to the flow (Salmhofer 2004, Gersch 2005, 2006, 2008). If now the symmetry-breaking occurs in one of the offered channels, this initial anomalous self-energy regularizes the vertices around the critical scale and the flow can be continued into the symmetry-broken phase. This method requires no decoupling of the interaction.

In the second approach, the fermionic interaction is decoupled with a suitable Hubbard-Stratonovich field and one subsequently deals with a coupled fermion-boson theory (Baier 2004, Strack 2008). This approach yields easy access to the phenomena associated with spontaneous symmetry-breaking alluded to in section 2.2 and we employ it in chapter 8 of this thesis in the context of fermionic superfluids.

2.2 Spontaneous symmetry-breaking

Spontaneous symmetry-breaking occurs if the energetically lowest state of a system described by a quantum or statistical field theory exhibits different symmetry properties than the original Lagrangian. The importance of spontaneous symmetry-breaking for physics can hardly be overestimated as has been recognized by the Nobel committee in the last 50 years with a series of Nobel prizes. At the time of writing, Nambu has been awarded the Nobel prize “for the discovery of the mechanism of spontaneously broken symmetry in subatomic physics” (Nambu 2008). Quite appropriately, we will in parts employ Nambu’s formalism in chapter 8 of this thesis.

In elementary particle physics as well as condensed matter physics, a stunning range of observed phenomena finds an explanation with the help of symmetry considerations (Negele 1987, Peskin 1996). Perhaps most fundamentally, the Anderson-Higgs mechanism (Negele 1987) bridges the gap between quantum excitations of the vacuum in high-energy physics and statistical many-particle systems at low temperatures. In the former context, this mechanism is the generally accepted scenario for dynamical mass generation of fundamental particles such as gauge bosons: by (spontaneous) condensation of the Higgs field the order parameter thereof generates a mass term for particles covariantly coupled to the Higgs field. In the latter context of statistical physics, it was Anderson who first proposed this mechanism in 1958 to explain the Meissner effect in superconductors (Negele 1987): the photon (gauge boson) mediating the electromagnetic interaction becomes massive from the superconducting condensate (Higgs field).

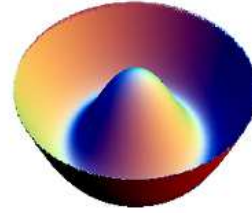


Fig. 2.1. *Potential for spontaneous breaking of continuous $O(N)$ -symmetry, drawn for the case $N = 2$. Fluctuations along the trough in the potential correspond to the Goldstone excitations (Peskin 1996).*

Goldstone bosons emerge when spontaneously breaking a continuous symmetry. In the low-energy sector of massless Quantum Chromodynamics, for example, the formation of mesonic two-quark bound states spontaneously breaks the chiral symmetry of the original Lagrangian. As a result, the emergent pions can be understood as the Goldstone bosons of massless QCD (Peskin 1996). Many striking properties of low-temperature condensed matter systems such as magnets, superfluid Helium, and superconducting materials are attributed to Goldstone bosons. In superfluid systems, Goldstone bosons are an indicator of long-range phase coherence. In this case, the order parameter contains two degrees of freedom, one associated with the amplitude and the other with the phase of the order parameter. Above the critical temperature, the Hamiltonian is invariant under the rotational symmetry group $O(2)$. Below the

critical temperature, the potential attains the form shown in Fig. 2.1 and the energetically lowest state is *degenerate* with the respect to phase transformations (i.e. location in the trough). Generalized to an N -component order parameter, the original $O(N)$ -symmetry is hidden leaving only the subgroup $O(N - 1)$, which rotates the Goldstone modes among themselves (Peskin 1996). Note that the form of the potential must respect the full $O(N)$ -symmetry even below the critical temperature, but the field evaluated at its *minimum* breaks and reduces the symmetry. Theoretically, Goldstone modes are difficult to cope with in perturbation theory as the massless propagators cause severe infrared singularities in low enough dimensions necessitating a renormalization group (RG) treatment.

In this thesis, the physics of Goldstone modes plays a central role. In chapter 6, we consider a quantum critical point adjacent to an ordered phase with Goldstone bosons. In magnetic systems, for instance, the original $O(3)$ symmetry is broken down to $O(2)$ and the Goldstone bosons are collective, gapless fluctuations in the direction of the electron spins with respect to which the ground state is degenerate. For antiferromagnetically ordered spins, these excitations form spin waves.

In chapter 8, we compute the RG flow of various observables in fermionic superfluids. Here, the Goldstone bosons correspond to fluctuations in the phase of the superfluid order parameter and the original $O(2)$ symmetry is broken spontaneously.

2.3 Quantum criticality

In certain cases, the departure from the Fermi liquid occurs in the vicinity of a quantum critical point (QCP) where spontaneous symmetry-breaking occurs at zero temperature. This quantum criticality induced breakdown of the Fermi liquid has attracted enormous attention in recent years (Stewart 2001, Loehneysen 2007). This section recollects the most popular approach to quantum critical fermion systems, the Hertz-Millis theory (Hertz 1976, Millis 1993) and its shortcomings, after having recapitulated similarities and differences between classical and quantum phase transitions.

The amount of thermal agitation in a multi-particle system can severely alter its macroscopic properties although it is described by the same particles, the same interactions, and the same Hamiltonian (Goldenfeld 1992). The point separating the two distinct –for example para- versus ferromagnetic– phases by tuning the temperature to T_c , is referred to as the critical point if the correlation length among the constituent particles diverges. At T_c , thermal fluctuations are so strong that the system becomes *self-similar* on all scales, i.e., it becomes *scale-invariant*. The free energy develops non-analyticities which can be subsumed under a set of critical exponents two of which are independent related to the existence of two relevant scaling fields, namely temperature and the external symmetry-breaking field (Goldenfeld 1992). It now turns

out that –rather remarkably– lavish reservoirs of physical systems can be described by the *same* set of critical exponents distinguished only by their most basic symmetry properties and spatial dimensionality into universality classes.

In recent times, one has come to envisage systems where continuous phase transitions occur at zero temperature. Here, a non-thermal control parameter drives the phase transition and zero-point quantum fluctuations trigger quantum critical scaling of various quantities often described by different exponents than their classical counterparts (Sachdev 1999, Loehneysen 2007). Such a quantum critical point lies between neighboring ground states –the generic situation is exhibited in Fig. 2.2. A peculiarity of quantum phase transitions is their increased effective dimensionality incurred by quantum fluctuations in the direction of imaginary time (Hertz 1976). In the functional integral formalism, the frequency term in the quadratic part of the action, $\phi (|\Omega|^{2/z} + \mathbf{q}^2) \phi$ for $z = 1, 2$, and $\phi (|\Omega|/|\mathbf{q}|^{z-2} + \mathbf{q}^2) \phi$ for $z \geq 3$, with ϕ being the bosonic order parameter field, indicates that characteristic frequencies scale as $\Omega \sim |\mathbf{q}|^z$. When approaching the transition at $T = 0$, both the order parameter correlation length ξ and correlation time ξ_τ diverge as function of control parameter:

$$\xi \sim |\delta - \delta_c|^{-\nu}, \quad \xi_\tau \sim \xi^z. \quad (2.6)$$

At finite temperature, however, the $(d + z)$ -dimensional quantum system has finite length in the time direction, $L_\tau \sim 1/T$. In Fig. 2.2, we observe that the existence of a QCP shapes large portions of the phase diagram. The black line of finite-temperature classical phase transitions separates the thermally disordered phase from the ordered phase and terminates at the QCP. Its shape is determined by the shift-exponent as alluded to in chapter 1. A completely different regime is the high-temperature regime above the QCP where $\xi_\tau \gg L_\tau$, the critical singularity is cut off by the finite temperature, and the boundaries are the crossover lines $T \sim |\delta - \delta_c|^{1/z}$. Strikingly, in this quantum critical regime one can measure power-law dependencies of physical observables up to rather high temperature with exponents *not* assuming the expected Fermi liquid values (Loehneysen 2007).

For a computation of these non-Fermi liquid power-laws in itinerant fermion systems, Millis (1993) has set up RG equations capitalizing on the fact that the zero-

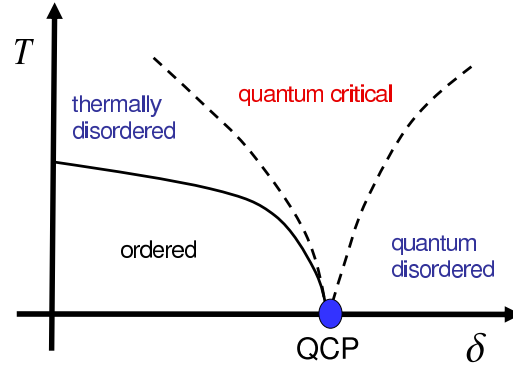


Fig. 2.2. Generic phase diagram in the vicinity of a continuous quantum phase transition.

temperature fixed point for the order parameter is Gaussian as long as $d + z > 4$. The procedure is the following. The microscopic four-fermion interaction is decoupled with a Hubbard-Stratonovich field corresponding to the incipient order. The fermions are integrated out from the functional integral in one sweep, but leaving their mark on the subsequent, usually polynomial, expansion in powers of the order parameter field. One then integrates out order parameter fluctuations on a Gaussian level (Millis 1993). Already this results in a rich phase diagram with some materials fulfilling the Hertz-Millis exponents but others not (Stewart 2001, Sebastian 2006, Loehneysen 2007). For certain cases, such as the SU(2)-symmetric antiferromagnetic channel, this procedure is ill-defined as the coefficients are singular functions of frequency and momentum (Chubukov 2003, Belitz 2005, Rech 2006, Loehneysen 2007). Experimental discrepancies and the questionable procedure to integrate out gapless fermions *before* considering order parameter fluctuations suggest that there is room for improving the Hertz-Millis theory.

In this thesis, we go beyond the Hertz-Millis approach in three ways. First, we show how to account for discrete symmetry-breaking and non-Gaussian classical fluctuations by use of truncated functional RG equations in chapter 5. Second, possible effects of Goldstone modes and their fluctuations on the quantum phase transition when breaking a continuous symmetry are analyzed in chapter 6. Third, we present a coupled fermion-boson RG that is able to assess the interplay of gapless fermions with massless order parameter fluctuations in chapter 7.

2.4 The renormalization group

The perturbative expansion of most quantum field theories is plagued by unbounded expressions. Either the integrands are singular for small momenta and the phase space volume in low dimensions does not shrink fast enough to tame the infrared divergence or the phase space volume blows up for large momenta leading to ultraviolet divergences in higher-dimensional continuum theories. These divergences are either of *physical* origin signalling for instance the proximity to a phase transition with truly infinite observables, or of *technical* origin as result of an inefficient organization of the perturbation theory with all physical observables being in fact finite.

In the 1950's and 60's, the obnoxious presence of these singularities in calculations proved a pertinacious problem to solve and severely hindered progress in statistical and quantum field theory. Then, in the beginning of the 1970's, Wilson –at the top of a scientist iceberg– reformulated the functional integral in terms of differential equations along the continuous flow parameter Λ . Typically, but not always, Λ is associated with the characteristic *kinetic* energy scale implemented by a cutoff for the propagator. This cutoff carves out the singularity from the spectrum and excludes modes with

$|\text{energy}| < \Lambda$ from the functional integral. This way, the singularity is approached peu-à-peu only at the end of the functional integration when $\Lambda \rightarrow 0$ and the renormalized theory is delivered. The solution of these so-called RG or flow equations enabled, among countless other groundbreaking discoveries, a controlled computation of critical exponents for bosonic field theories (for a review see Wilson 1974). The extension of these ideas to non-Abelian gauge theories involving fermions and bosons led to the discovery of asymptotic freedom (Politzer 1973, Gross 1973).

Purely fermionic systems in one dimension were considered with RG methods even before Wilson's Nobel prize in 1982 by Solyom (1979). Originally taken up by mathematical physicists (see references in Salmhofer 1999), the RG was subsequently applied to interacting Fermi systems also in higher dimensions (for a review see Shankar 1994, Metzner 1998, and Salmhofer 1999). The existence of a Fermi surface greatly enriches the analysis as the fermion propagator becomes unbounded on a $(d - 1)$ -dimensional hypersurface to be compared with the much simpler situation for bosons where the propagator becomes large only at one point (the origin) of momentum space. Rigorous proofs involving phase space arguments and the curvature of the Fermi-surface have established the RG as a mathematically well defined starting point for practical computations. Therein, the low energy projection of the vertices onto the Fermi surface involves *flowing functions* to parametrize *transversal* momentum dependences parallel to the Fermi surface which remain relevant until the very end of the flow (Zanchi 2000, Halboth 2000, Honerkamp 2001). For this reason, the Fermi surface is partitioned into patches and mapped onto a grid in momentum space. The vertex function is then parametrized by several thousand variables and the flow equations are solved numerically.

Flowing functions can be dealt with conveniently within modern functional renormalization group formulations (Polchinski 1984, Wetterich 1993, Salmhofer 2001, for a review see Berges 2002, Metzner 2005). Three formally exact flow equations have been devised: (i) the Polchinski (1984) scheme for the generating functional of connected amputated vertex functions (\mathcal{V}) utilized by Zanchi (2000), (ii) the Wick-ordered scheme (Salmhofer 1999) where the vertex functions are the expansion coefficients when expanding \mathcal{V} in Wick-ordered polynomials of the source-field utilized by Halboth (2000), and (iii) the *one-particle irreducible* (1PI) scheme (Wetterich 1993, Salmhofer 2001) for the generating functional of the 1PI-vertex functions utilized by Honerkamp (2001) and in a variety of contexts in Berges (2002).

In the next chapter, we thoroughly present the most popular, the 1PI-scheme of the functional RG. A particular strength of this scheme is the natural inclusion of self-energy corrections as all internal lines are fully dressed. Further, coupled fermion-boson theories and spontaneous symmetry-breaking can be treated easily within this scheme. We will apply this scheme for the computations in Part II of this thesis.

Functional renormalization group

In this chapter, we introduce the main computational tools employed in this thesis. First, we set up a unifying framework for fermionic and bosonic models by defining superfields whose fermionic and bosonic components are distinguished by a statistics index. Second, we define the one-particle irreducible generating functional, the effective action. Third, the functional flow equation for the effective action is derived. Finally, we explain how to devise truncations with non-zero expectation values of field variables to account for spontaneous symmetry-breaking.

3.1 Functional integral for quantum many-particle systems

We consider interacting Fermi systems described by the *bare* action,

$$\Gamma_0[\bar{\psi}, \psi] = - \int_K \bar{\psi}_K G_{f0}^{-1}(K) \psi_K + \int_{K, K', Q} V_{K, K', Q}^f \bar{\psi}_K \bar{\psi}_{K'+Q} \psi_{K'} \psi_{K+Q} , \quad (3.1)$$

where $\bar{\psi}$ and ψ are Grassmann-valued fields, the index ($K = (k_0, \mathbf{k}, \sigma)$) and its corresponding integration \int_K comprises frequency, momentum and internal states such as, for example, the spin projection, and $G_{f0}^{-1}(K) = ik_0 - \xi_{\mathbf{k}}$ is the bare inverse Green function. The Fermi surface is defined as the $(d - 1)$ -dimensional manifold $\xi_{\mathbf{k}} = 0$. $V_{K, K', Q}^f$ denotes an arbitrary and in general momentum- and spin-dependent many-body interaction of the lowest non-trivial (quartic) order ¹. In many circumstances, correlations

¹ *Models of the form Eq. (3.1) have attracted attention for decades: in one-dimensional systems, various phases such as the Luttinger liquid (Solyom 1979, Voit 1994) occur; in the context of gauge theories, in vacuum and with more elaborate internal degrees of freedom, Eq. (3.1) may describe the Thirring or Gross-Neveu Model (Hands 1993); on the lattice in two and higher dimensions, Eq. (3.1) includes the attractive or repulsive (depending on the sign of the in that case momentum-independent interaction) Hubbard model often employed in contemporary condensed matter physics (Micnas 1990, Baeriswyl 1995).*

induce fermion-pairing phenomena and one finds the description in terms of the order parameter useful. The simplest bosonic action is the ϕ^4 -model

$$\Gamma_0[\phi] = - \int_Q \phi_Q^* G_{b0}^{-1}(Q) \phi_Q + \int_{K,K',Q} V_{K,K',Q}^b \phi_{K-Q}^* \phi_{K'+Q}^* \phi_{K'} \phi_K, \quad (3.2)$$

where ϕ is here a complex-valued field but may in general contain N components referred to as $O(N)$ -models (Amit 1995). $G_{b0}^{-1}(q) = -(q_0^2 + \omega_{\mathbf{q}} + m_b^2)$ is the bosonic Green's function with $\omega_{\mathbf{q}}$ being the dispersion, usually but not always quadratic in momenta, and $m_b^2 = \xi^{-2}$ the mass or inverse correlation length. The frequency term is also not always quadratic; for the non-relativistic Bose gas one has a complex linear term $\sim iq_0$ and for certain quantum-critical systems Landau-damping entails $|q_0|$ or even $|q_0|/|\mathbf{q}|$ (Hertz 1976, Millis 1993).

Finally, models with both, fermionic and bosonic fields, may be the subject of analysis. In addition to the kinetic terms with $G_{b0}^{-1}(Q)$ and $G_{f0}^{-1}(K)$, to lowest order we then have to consider the fermion-boson vertex

$$\Gamma_0[\phi, \bar{\psi}, \psi] = \int_{K,Q} g_{K,Q} (\phi_Q^* \psi_{-K+Q} \psi_K + \phi_Q \bar{\psi}_{K+Q} \bar{\psi}_{-K}). \quad (3.3)$$

3.1.1 Superfield formulation for fermionic and bosonic models

To develop a unifying framework, we combine fermionic and bosonic fields in a superfield \mathcal{S} , where fermions and bosons are distinguished by a statistics index $s = b, f$, that is,

$$\mathcal{S}_b = \Phi, \quad \mathcal{S}_f = \Psi. \quad (3.4)$$

To account for matrix propagators necessary to describe phases with broken symmetry such as, for example, superfluidity, we here use the fermionic Nambu fields

$$\Psi_k = \begin{pmatrix} \psi_{k\uparrow} \\ \bar{\psi}_{-k\downarrow} \end{pmatrix}, \quad \bar{\Psi}_k = (\bar{\psi}_{k\uparrow}, \psi_{-k\downarrow}) \quad (3.5)$$

and bosonic Nambu fields

$$\Phi_q = \begin{pmatrix} \phi_q \\ \phi_{-q}^* \end{pmatrix}, \quad \bar{\Phi}_q = (\phi_q^*, \phi_{-q}). \quad (3.6)$$

The fermionic and bosonic matrix propagators are then given by $\mathbf{G}_f(k) = -\langle \Psi_k \bar{\Psi}_k \rangle$ and $\mathbf{G}_b(q) = -\langle \Phi_q \bar{\Phi}_q \rangle$, respectively. The superpropagator $\mathbf{G}(q) = -\langle \mathcal{S}_q \bar{\mathcal{S}}_q \rangle$ is diagonal in the statistics index.

Note that the specific choice of the fermionic and bosonic Nambu fields depends on the physical situation under investigation and can be adjusted straightforwardly.

3.1.2 One-particle irreducible generating functional

Functional integration of the bare action containing fermionic and bosonic fields, $\Gamma_0[S, \bar{S}]$, and subsequent functional differentiation with respect to source fields S' and \bar{S}' linearly coupled to S and \bar{S} yields the connected m-particle Green functions (Negele 1987)

$$\begin{aligned} G_m(K'_1, \dots, K'_m; K_1, \dots, K_m) &= -\langle S_{K'_1} \dots S_{K'_m} \bar{S}_{K_m} \dots \bar{S}_{K_1} \rangle_c \\ &= \frac{\partial^m}{\partial S'_{K'_1} \dots \partial S'_{K'_m}} \frac{\partial^m}{\partial \bar{S}'_{K_m} \dots \partial \bar{S}'_{K_1}} G[S', \bar{S}'] \Big|_{S'=\bar{S}'=0}, \end{aligned} \quad (3.7)$$

where $\langle \dots \rangle_c$ denotes the connected average and the generating functional is obtained from the logarithm of the partition function

$$G[S', \bar{S}'] = -\log \int D S D \bar{S} e^{-\Gamma_0[S, \bar{S}] + (S', \bar{S}) + (S, \bar{S}')}, \quad (3.8)$$

where the bracket $(., .)$ is a shorthand notation for the inner product for superfields. The Legendre transform of $G[S', \bar{S}']$ is the effective action

$$\Gamma[S, \bar{S}] = \mathcal{L}G[S', \bar{S}'] = G[S', \bar{S}'] - (S', \bar{S}) - (S, \bar{S}'), \quad (3.9)$$

where the conjugated field variables are

$$S = \frac{\partial G[S', \bar{S}']}{\partial \bar{S}'}, \quad \bar{S} = \frac{\partial G[S', \bar{S}']}{\partial S'}. \quad (3.10)$$

$\Gamma[S, \bar{S}]$ generates the one-particle-irreducible (1PI) Green functions. Topologically, all diagrams are generated where cutting *one line*, irrespective if fermionic or bosonic, does not separate the diagram into two disconnected parts (Negele 1987, Amit 2005).

3.2 Flow equations

In this section, we derive the exact flow equation (Wetterich 1993, Salmhofer 2001, Berges 2002, Metzner 2005, Enss 2005) for the effective action, that is, the 1PI generating functional, adapted to superfields.

3.2.1 Exact flow equation

The exact flow equation is a reformulation of the functional integral as a functional differential equation. It describes the evolution of the effective action as a function of a flow parameter Λ , usually a cutoff. The cutoff can be implemented by adding the regulator term quadratic in the fields

$$\mathcal{R}^\Lambda = (\bar{S}, \mathbf{R}^\Lambda S) = \frac{1}{2} \int_q \bar{\Phi}_q \mathbf{R}_b^\Lambda(q) \Phi_q + \int_k \bar{\Psi}_k \mathbf{R}_f^\Lambda(k) \Psi_k \quad (3.11)$$

to the bare action. The purpose of the cutoff is twofold. First, it regularizes fermionic and bosonic infrared divergences when dealing with, for example, a massless Goldstone boson or zero-temperature fermions whose propagator becomes unbounded in the vicinity of the Fermi surface. Second, \mathbf{R}^Λ incorporates the continuous flow parameter along which the functional integration is performed: as a function of decreasing cutoff, Γ^Λ interpolates smoothly between the bare action Γ_0 for $\Lambda = \infty$ and the full effective action Γ , recovered in the limit $\Lambda \rightarrow 0$.

To *regularize* and *interpolate*, the matrix elements of \mathbf{R}^Λ have to fulfill the following properties:

$$\begin{aligned} (i) \quad & R^\Lambda(Q) \geq 0 \\ (ii) \quad & \lim_{\Lambda \rightarrow 0} R^\Lambda(Q) = 0 \\ (iii) \quad & \lim_{\Lambda \rightarrow \infty} R^\Lambda(Q) = \infty . \end{aligned} \quad (3.12)$$

Integrating $e^{-\Gamma_0 - \mathcal{R}^\Lambda}$ in the presence of source fields coupling linearly to S and \bar{S} yields the cutoff-dependent generating functional for connected Green functions

$$G^\Lambda[S', \bar{S}'] = -\log \int DSD\bar{S} e^{-\Gamma_0[S, \bar{S}] - \mathcal{R}^\Lambda[S, \bar{S}] + (S', \bar{S}) + (S, \bar{S}')} . \quad (3.13)$$

The cutoff-dependent effective action Γ^Λ is defined as

$$\Gamma^\Lambda[S, \bar{S}] = \mathcal{L}G^\Lambda[S', \bar{S}'] - \mathcal{R}^\Lambda[S, \bar{S}] , \quad (3.14)$$

where $\mathcal{L}G^\Lambda$ is the Legendre transform of G^Λ as specified without a cutoff in Eq. (3.9).

Executing a scale-derivative on both sides of Eq. (3.14) and using Eq. (3.11), we obtain

$$\partial_\Lambda \Gamma^\Lambda[S, \bar{S}] = \partial_\Lambda G^\Lambda[S', \bar{S}'] - (\bar{S}, \dot{\mathbf{R}}^\Lambda S) , \quad (3.15)$$

where $\dot{\mathbf{R}}^\Lambda = \partial_\Lambda \mathbf{R}^\Lambda$ and we further compute

$$\begin{aligned} \partial_\Lambda G^\Lambda[S', \bar{S}'] &= -e^{G^\Lambda[S', \bar{S}']} \partial_\Lambda e^{-G^\Lambda[S', \bar{S}']} \\ &= e^{G^\Lambda[S', \bar{S}']} \int DSD\bar{S} (\bar{S}, \dot{\mathbf{R}}^\Lambda S) e^{-\Gamma_0[S, \bar{S}] - \mathcal{R}^\Lambda[S, \bar{S}] + (S', \bar{S}) + (S, \bar{S}')} \\ &= e^{G^\Lambda[S', \bar{S}']} (\partial_{S'}, \dot{\mathbf{R}}^\Lambda \partial_{\bar{S}'} e^{-G^\Lambda[S', \bar{S}']}) \\ &= \left(\frac{\partial G^\Lambda[S', \bar{S}']}{\partial S'}, \dot{\mathbf{R}}^\Lambda \frac{\partial G^\Lambda[S', \bar{S}']}{\partial \bar{S}'} \right) + \text{Str } \dot{\mathbf{R}}^\Lambda \frac{\partial^2 G^\Lambda[S', \bar{S}']}{\partial S' \partial \bar{S}'} \\ &= (\bar{S}, \dot{\mathbf{R}}^\Lambda S) + \text{Str } \dot{\mathbf{R}}^\Lambda \left(\frac{\partial^2 (\Gamma^\Lambda[S, \bar{S}] + \mathcal{R}^\Lambda[S, \bar{S}])}{\partial S \partial \bar{S}} \right)^{-1} , \end{aligned} \quad (3.16)$$

where the supertrace Str traces over all indices with a plus sign for bosons and a minus sign for fermions. For the first term in the last line, we have used Eq. (3.10) and for the second term in the last line we have used the relation $\partial^2 G / \partial S' \partial \bar{S}' = (\partial^2 \Gamma / \partial S \partial \bar{S})^{-1}$ augmented with the cutoff term from Eq. (3.14). Denoting

$$\mathbf{\Gamma}^{(2)\Lambda}[\mathcal{S}, \bar{\mathcal{S}}] = \frac{\partial^2 \Gamma^\Lambda[\mathcal{S}, \bar{\mathcal{S}}]}{\partial S \partial \bar{S}} , \quad (3.17)$$

and assembling Eqs. (3.16, 3.15), we obtain the exact flow equation for the effective action

$$\frac{d}{d\Lambda} \Gamma^\Lambda[\mathcal{S}, \bar{\mathcal{S}}] = \text{Str} \frac{\dot{\mathbf{R}}^\Lambda}{\mathbf{\Gamma}^{(2)\Lambda}[\mathcal{S}, \bar{\mathcal{S}}] + \mathbf{R}^\Lambda} . \quad (3.18)$$

Note that the definitions of Γ^Λ vary slightly in the literature. In particular, Γ^Λ is frequently defined as the Legendre transform of G^Λ without subtracting the regulator term \mathcal{R}^Λ , which leads to a simple additional term in the flow equation.

To expand the functional flow equation (3.18) in powers of the fields, we write the Hessian of Γ^Λ as

$$\mathbf{\Gamma}^{(2)\Lambda}[\mathcal{S}, \bar{\mathcal{S}}] = -(\mathbf{G}^\Lambda)^{-1} + \tilde{\mathbf{\Gamma}}^{(2)\Lambda}[\mathcal{S}, \bar{\mathcal{S}}] , \quad (3.19)$$

where $\tilde{\mathbf{\Gamma}}^{(2)\Lambda}[\mathcal{S}, \bar{\mathcal{S}}]$ comes from terms which are at least quadratic in the fields. Defining $\mathbf{G}_R^\Lambda = [(\mathbf{G}^\Lambda)^{-1} - \mathbf{R}^\Lambda]^{-1}$ and expanding in powers of $\tilde{\mathbf{\Gamma}}^{(2)\Lambda}$ yields

$$\frac{d}{d\Lambda} \Gamma^\Lambda = -\text{Str}(\dot{\mathbf{R}}^\Lambda \mathbf{G}_R^\Lambda) - \text{Str} \left[\mathbf{G}_R'^\Lambda (\tilde{\mathbf{\Gamma}}^{(2)\Lambda} + \tilde{\mathbf{\Gamma}}^{(2)\Lambda} \mathbf{G}_R^\Lambda \tilde{\mathbf{\Gamma}}^{(2)\Lambda} + \dots) \right] , \quad (3.20)$$

where

$$\mathbf{G}_R'^\Lambda = \mathbf{G}_R^\Lambda \dot{\mathbf{R}}^\Lambda \mathbf{G}_R^\Lambda . \quad (3.21)$$

For a sharp cutoff, Eq. (3.21) denotes the so-called single-scale propagator (Salmhofer 2001, Metzner 2005) as it then has support only for energies $= \Lambda$ due to a δ -function. In general, $\mathbf{G}_R'^\Lambda$ is smoothened and may thus have support on more energies, typically in an energy window around energies $\approx \Lambda$.

Expanding both sides of Eq. (3.20) in powers of the fields and comparing coefficients yields an (infinite) hierarchy of flow equations for the vertex functions. The zero-point vertex, $\gamma^{(0)\Lambda}$, see also the first line of Fig. 3.1 equals the effective potential with the analytic flow equation from the first term in Eq. (3.20):

$$\frac{d}{d\Lambda} U^\Lambda = -\text{Str}(\dot{\mathbf{R}}^\Lambda \mathbf{G}_R^\Lambda) . \quad (3.22)$$

Flow equations for thermodynamic properties of the system such as the specific heat or the entropy follow from derivatives with respect to the temperature of Eq. (3.22).

3.2.2 Spontaneous symmetry-breaking

The low energy regimes of the models described in Eqs. (3.1, 3.2) are often dominated by phases with broken symmetry, that is, states where interaction effects spontaneously break one, or multiple, of the symmetries present in the original bare action. The physical properties in such a phase are vastly different from the phase where the original symmetry is preserved.

In terms of our superfields, the symmetry-breaking is associated with a non-vanishing expectation value of one of the bosonic components of \mathcal{S} , referred to as the order parameter. While in the symmetric phase the flow equations are expanded around $\phi = 0$, in the symmetry-broken regime we expand around a generally non-zero value of the $q = 0$ component of the bosonic field, that is, we expand $\Gamma^\Lambda[\psi, \bar{\psi}, \alpha^\Lambda + \phi]$ in powers of $\psi, \bar{\psi}, \phi, \phi^*$, where α^Λ may be non-zero (see also Delamotte 2004, Schütz 2006).

We now illustrate how this expansion works. For this purpose, we restrict ourselves to the case of a real-valued scalar field and consider only local terms of the effective action. The ansatz for the bosonic components of the left-hand-side of Eq. (3.20) is

$$\Gamma^\Lambda[\phi] = \int \sum_{n=0}^{\infty} \frac{1}{n!} \gamma^{(n)\Lambda} (\phi - \alpha^\Lambda)^n, \quad (3.23)$$

where the integration symbol denotes the standard position space integration. Performing a scale-derivative on both sides of Eq. (3.23) yields

$$\partial_\Lambda \Gamma^\Lambda[\phi] = \int \sum_{n=0}^{\infty} \frac{1}{n!} \dot{\gamma}^{(n)\Lambda} (\phi - \alpha^\Lambda)^n - \frac{\dot{\alpha}^\Lambda}{(n-1)!} \gamma^{(n)\Lambda} (\phi - \alpha^\Lambda)^{n-1}, \quad (3.24)$$

Comparing powers of $(\phi - \alpha^\Lambda)$ between Eq. (3.24) and the right-hand-side of Eq. (3.20) yields the following prescription for the flow equation for the n-point vertex

$$\dot{\gamma}^{(n)\Lambda} = \dot{\mathbf{R}}^\Lambda \partial_{\mathbf{R}} \left(\text{all 1-loop 1PI diagrams generated by } \mathbf{G}_R^\Lambda \text{ with } n \text{ external legs} \right) + \dot{\alpha}^\Lambda \gamma^{(n+1)\Lambda}. \quad (3.25)$$

The expansion point α^Λ will be chosen such that the bosonic 1-point function $\gamma^{(1)\Lambda} = 0$ for all Λ :

$$\partial_\Lambda \gamma^{(1)\Lambda} = \text{tadpole diagram} + \dots + \dot{\alpha}^\Lambda \gamma^{(2)\Lambda} := 0, \quad \Rightarrow \quad \partial_\Lambda \alpha^\Lambda = \frac{-1}{\gamma^{(2)\Lambda}} \left(\text{tadpole diagram} + \dots \right). \quad (3.26)$$

In this way tadpole contributions are absorbed into the flow of α . The vanishing of

$$\begin{aligned}
\partial_\Lambda \gamma^{(0)\Lambda} &= \text{[dashed circle]} = \partial_\Lambda U^\Lambda \\
\partial_\Lambda \gamma^{(1)\Lambda} &= \text{[dashed line with downward triangle]} + \text{[dashed line with cross]} := 0 \\
\text{[cross]} &= \frac{-1}{\gamma^{(2)\Lambda}} \left(\text{[dashed line with downward triangle]} \right) \\
\partial_\Lambda \gamma^{(2)\Lambda} &= \text{[dashed line with square]} + \text{[dashed line with circle and two triangles]} + \text{[dashed line with triangle and cross]} \\
\partial_\Lambda \gamma^{(3)\Lambda} &= \text{[dashed line with triangle and square]} + \text{[dashed line with cross and square]} \\
\partial_\Lambda \gamma^{(4)\Lambda} &= \text{[dashed line with square and circle]} + \text{[dashed line with square and triangle]}
\end{aligned}$$

Fig. 3.1. Truncated hierarchy of 1PI vertex functions up to quartic order in the fields for phases with spontaneously broken symmetry. The cross denotes the flow of the order parameter $\partial_\Lambda \alpha^\Lambda$. Usually, the presence of vertices with an odd number of legs is peculiar to phases with broken symmetry. It is important to note that for the general case of mixed Fermi-Bose theories, many more diagrams with normal and anomalous propagators as well as normal and anomalous vertices appear; see Chapter 8.

the bosonic one-point function is equivalent to the condition that the minimum of the effective potential coincides with its first field derivative for all Λ : $U'[\phi]|_{\phi=\alpha} = 0$ (Berges 2002).

In a general polynomial truncation of Eq.(3.23) up to quartic order in the bosonic fields, the hierarchy for the n-point vertices can be represented in terms of Feynman diagrams, see Fig. (3.1).

One aspect of the practicability of the 1PI-formulation of the functional RG lies in its intimate kinship to conventional perturbation theory (Negele 1987). Eq. (3.25) contains precisely the diagrammatic corrections that would show up in a 1PI-expansion of perturbation theory. Technically, a computation of the flow equations therefore involves the determination of prefactors and signs of the various Feynman diagrams. One way to achieve this is to compare coefficients in Eq. (3.20). However, in symmetry-broken phases, the Nambu structure of the fields leads to at least 4×4 -matrices for \mathbf{G}_R^A and $\tilde{\mathbf{I}}^{(2)A}$, thus complicating the trace operation on matrix products with several of these matrices, and necessitating systematic use of software packages, for example Mathematica.

In this thesis, we determine the prefactors and signs by use of Wick's theorem and Feynman rules directly (see chapter 2.3, Negele 1987; chapter 4.4, Peskin 1995; chapter 6, Weinberg 2005).

Summary Part I

In chapter 2, some scenarios going beyond the conventional Fermi liquid description for interacting Fermi systems were discussed. After recapitulating the Fermi liquid fixed point in the functional integral formalism in section 2.1, prominent competing and conspiring ordering tendencies of two-dimensional lattice fermions were introduced. We have argued that the fermionic functional RG is a useful tool to treat these cases but for computations within symmetry-broken phases a description in terms of the collective bosonic degrees of freedom seems more practicable. In section 2.2, the mechanism of spontaneous symmetry-breaking is introduced in detail. We zoomed in on the phenomenology of Goldstone bosons which are emitted in interacting Fermi systems with broken continuous symmetry for example with magnetic or superfluid order. Critical points that separate phases with different symmetry properties were brought into play in section 2.3. The standard phase diagram in the vicinity of quantum critical point was exhibited in Fig. 2.2 and the conventional Hertz-Millis approach to theoretically describe quantum critical behavior was outlined briefly. Essential renormalization group ideas and references are summarized in section 2.4.

In chapter 3, the functional RG framework was presented as a promising tool to transform the before-mentioned theoretical concepts into real computations for systems containing both fermionic and bosonic degrees of freedom. We defined the effective action, that is, the functional which generates the one-particle irreducible vertex functions for superfields in section 3.1.2. The exact flow equation for the effective action is derived in section 3.2.1. The central result of this chapter is contained in subsection 3.2.2: the prescription how to include scale-dependent expectation values into the hierarchy of vertex functions to account for spontaneous symmetry-breaking is pictorially shown in Fig. 3.1.

In the following Part II, we merge the theoretical concepts with the functional RG framework and apply it in four cases. The chapters are sequenced in order of increasing truncation complexity, consecutively build on and extend the previous one, but may yet be read independently.

Part II

Applications

Hertz-Millis theory with discrete symmetry-breaking

5.1 Introduction

Quantum phase transitions in itinerant electron systems continue to ignite considerable interest (Sachdev 1999, Belitz 2005, Loehneysen 2007). In many physical situations, a line of finite temperature second order phase transitions in the phase diagram terminates at a quantum critical point at $T = 0$. In such cases quantum fluctuations influence the system also at finite temperatures altering physical quantities such as the shape of the phase boundary. Consequently, in a complete description of the system at finite T , quantum and thermal fluctuations have to be accounted for simultaneously.

The conventional renormalization group (RG) approach to quantum criticality in itinerant electron systems (Hertz 1976, Millis 1993), see also section 2.3, relies on the assumption that it is sensible to integrate out fermionic degrees of freedom from the functional integral representation of the partition function and then to expand the resulting effective action in powers of the order parameter alone. This approach has been questioned for magnetic phase transitions associated with spontaneous breaking of continuous spin rotation invariance, since integrating the fermions leads to singular interactions of the order parameter field (Belitz 2005, Loehneysen 2007).

In this chapter, we focus on quantum phase transitions to phases with broken *discrete* symmetry. We analyze quantum and classical fluctuations in the *symmetry-broken* phase with an Ising-like order parameter near a quantum critical point. Our calculations are based on a set of coupled flow equations obtained by approximating the exact flow equations of the one-particle irreducible version of the functional RG. Quantum and classical (thermal) fluctuations are treated on equal footing. The functional RG has been applied extensively to classical critical phenomena (Berges 2002), where it provides a unified description of $O(N)$ -symmetric scalar models, including two-dimensional systems. The classical Ising universality class has been analyzed in Refs. 9-11. In our approach, we can compute the RG flow in any region of the phase

diagram, including the region governed by non-Gaussian critical fluctuations. This allows comparison between the true transition line and the Ginzburg line, which so far has been used as an estimate of the former (Loehneysen 2007, Millis 1993). Specifically, we capture the strong-coupling behavior emergent in the vicinity of the transition line as well as the correct classical fixed point for T_c , including the anomalous dimension of the order parameter field.

Our results may be applied to Pomeranchuk transitions (Metzner 2003, Dell’Anna 2006, Wölfle 2007) which spontaneously break the discrete point group lattice symmetry, and to the Quantum Ising model (Sachdev 1999). An example of a fermionic model displaying a genuine quantum critical point already on mean-field level is the so-called f-model, where forward-scattering processes tend to deform the Fermi surface leading to Pomeranchuk transitions (Yamase 2005, Dell’Anna 2006). The control parameter here is the density/chemical potential.

In Section 5.2 we introduce Hertz’s (1976) action and the effective action for the Quantum Ising model, adapted to the symmetry-broken phase, which serves as a starting point for the subsequent analysis. In Section 5.3 we describe the functional RG method and its application in the present context, and subsequently derive the RG flow equations. In Section 5.4 we present a solution of the theory in the case $T = 0$. Section 5.5 contains numerical results for the finite T phase diagram in the region with broken symmetry. Different cases are discussed, distinguished by the dimensionality d and the dynamical exponent z . For Pomeranchuk transitions $z = 3$ and for the Quantum Ising model $z = 1$. In particular, we compare the T_c line with the Ginzburg line, thus providing an estimate of the critical region size. In Section 5.6 we summarize and discuss the results.

5.2 Bosonic action

The starting point of the standard RG approach to quantum critical phenomena in itinerant electron systems is the Hertz action (Hertz 1976, Millis 1993). It can be derived from a microscopic Hamiltonian by applying a Hubbard-Stratonovich transformation to the path-integral representation of the partition function and subsequently integrating out the fermionic degrees of freedom. The resulting action is then expanded in powers of the order parameter field, usually to quartic order.

The validity of this expansion is dubious in several physically interesting cases, in particular for magnetic transitions with $SU(2)$ -symmetry, since the integration over gapless fermionic modes can lead to singular effective interactions of the order parameter field, which may invalidate the conventional power counting (Belitz 2005, Loehneysen 2006, Abanov 2004). Such complications do probably not affect transitions in the charge channel and magnetic transitions with Ising symmetry. There

are several indications that singularities cancel in that case, namely the cancellation of singularities in effective interactions upon symmetrization of fermion loops (Neumayr 1998, Kopper 2001), and the cancellation of non-analyticities in susceptibilities (Rech 2006).

We therefore rely on the usual expansion of the action to quartic order in the order parameter field and also on the conventional parametrization of momentum and frequency dependences, which leads to the Hertz action (Hertz 1976, Millis 1993)

$$S_H[\phi] = \frac{T}{2} \sum_{\omega_n} \int \frac{d^d p}{(2\pi)^d} \phi_p \left(\frac{|\omega_n|}{|\mathbf{p}|^{z-2}} + \mathbf{p}^2 \right) \phi_{-p} + U[\phi] . \quad (5.1)$$

Here ϕ is the scalar order parameter field and ϕ_p with $p = (\mathbf{p}, \omega_n)$ its momentum representation; $\omega_n = 2\pi nT$ with integer n denotes the (bosonic) Matsubara frequencies. Momentum and energy units are chosen such that the prefactors in front of $\frac{|\omega_n|}{|\mathbf{p}|^{z-2}}$ and \mathbf{p}^2 are equal to unity. The Hertz action is regularized in the ultraviolet by restricting momenta to $|\mathbf{p}| \leq \Lambda_0$. The value of the dynamical exponent is restricted to $z \geq 2$. The case $z = 3$ for Pomeranchuk transitions is of our main interest. Formally, the results obtained with $S_H[\phi]$ as our starting point may be applied to systems with arbitrary $z \geq 2$.¹

Other interesting cases include spin systems such as the Quantum Ising model for which $z = 1$ and the associated continuum action reads (Sachdev 1999)

$$S_{\text{QI}}[\phi] = \frac{T}{2} \sum_{\omega_n} \int \frac{d^d p}{(2\pi)^d} \phi_p (\omega_n^2 + \mathbf{p}^2) \phi_{-p} + U[\phi] , \quad (5.2)$$

where the frequency term enters with the same power as the momentum term.

In the symmetric phase the potential $U[\phi]$ is minimal at $\phi = 0$, and is usually parametrized by a positive quadratic and a positive quartic term (Hertz 1976, Millis 1993). Since we approach the quantum critical point from the symmetry-broken region of the phase diagram, we assume a potential $U[\phi]$ with a minimum at a non-zero order parameter ϕ_0 :

$$\begin{aligned} U[\phi] &= \frac{u}{4!} \int_0^{1/T} d\tau \int d^d x (\phi^2 - \phi_0^2)^2 \\ &= \int_0^{1/T} d\tau \int d^d x \left[u \frac{\phi'^4}{4!} + \sqrt{3} u \delta \frac{\phi'^3}{3!} + \delta \frac{\phi'^2}{2!} \right] , \end{aligned} \quad (5.3)$$

where ϕ and ϕ' are functions of x and τ with $\phi = \phi_0 + \phi'$. The parameter

¹ A comprehensive discussion of the origin of the ω_n dependence of the action is given by Millis (1993). Eq. (5.1) is valid in the limit $\frac{|\omega_n|}{|\mathbf{p}|^{z-2}} \ll 1$ which is relevant here since the dominant fluctuations occur only in this regime.

$$\delta = \frac{u \phi_0^2}{3} = \frac{2u \rho_0}{3}, \quad (5.4)$$

controls the distance from criticality. Approaching the phase boundary in the (δ, T) -plane from the symmetry-broken phase gives rise to the three-point vertex $\sqrt{3u\delta}$, which generates an anomalous dimension of the order parameter field already at one-loop level.

Although formally correct as a result of integrating out the fermions, the Hertz action (5.1) is not a good starting point for symmetry-broken phases with a fermionic gap, such as charge density wave phases or antiferromagnets. A fermionic gap leads to a suppression of the dynamical term (linear in frequency) in the action, since it suppresses low energy particle-hole excitations. If not treated by a suitable resummation in the beginning, this effect is hidden in high orders of perturbation theory (Rosch 2001). We do not deal with this complication in the present chapter as our main interest lies in systems with Pomeranchuk deformed Fermi surfaces where the particle-hole continuum remains gapless in the phase with broken symmetry. However, our results for the transition temperature should not be affected by a gap in the symmetry-broken phase, since it vanishes continuously at T_c .

5.3 Method

To analyze the quantum field theory defined by $S[\phi]$ we compute the flow of the effective action $\Gamma^\Lambda[\phi]$ with approximate flow equations derived from an exact functional RG flow equation (Wetterich 1993, Berges 2002, Delamotte 2004, Gies 2006). The exact flow equation and the vertex expansion including symmetry-breaking was derived and discussed in detail in chapter 3. The effective action $\Gamma^\Lambda[\phi]$ is the generating functional for one-particle irreducible vertex functions in presence of an infrared cutoff Λ . The latter is implemented by adding a regulator term of the form $\int \frac{1}{2} \phi R^\Lambda \phi$ to the bare action. The effective action interpolates smoothly between the bare action $S[\phi]$ for large Λ and the full effective action $\Gamma[\phi]$ in the limit $\Lambda \rightarrow 0$ (cutoff removed). Its flow is given by the exact functional equation (Wetterich 1993)

$$\frac{d}{d\Lambda} \Gamma^\Lambda[\phi] = \frac{1}{2} \text{Tr} \frac{\dot{R}^\Lambda}{\Gamma^{(2)}[\phi] + R^\Lambda}, \quad (5.5)$$

where $\dot{R}^\Lambda = \partial_\Lambda R^\Lambda$, and $\Gamma^{(2)}[\phi] = \delta^2 \Gamma^\Lambda[\phi] / \delta \phi^2$. In momentum representation (ϕ_p), the trace sums over momenta and frequencies: $\text{Tr} = T \sum_{\omega_n} \int \frac{d^d p}{(2\pi)^d}$. For the regulator function $R^\Lambda(\mathbf{p})$ we choose the optimized Litim cutoff (Litim 2001)

$$R^\Lambda(\mathbf{p}) = Z_p (\Lambda^2 - \mathbf{p}^2) \theta(\Lambda^2 - \mathbf{p}^2), \quad (5.6)$$

where $Z_{\mathbf{p}}$ is a renormalization factor (see below). This regulator function $R^\Lambda(\mathbf{p})$ replaces $Z_{\mathbf{p}}\mathbf{p}^2$ with $Z_{\mathbf{p}}\Lambda^2$ for $|\mathbf{p}| < \Lambda$. Following (Berges 2002) we neglect $\dot{Z}_{\mathbf{p}}$ in $\dot{R}^\Lambda(\mathbf{p})$, such that $\dot{R}^\Lambda(\mathbf{p}) = 2Z_{\mathbf{p}}\Lambda\Theta(\Lambda^2 - \mathbf{p}^2)$. The scale-derivative of the Z-factor leads to additional terms on the right-hand-side of the flow equations proportional to the anomalous dimension η defined in below in Eq. (5.17). These terms are neglected here as they are of higher order in the vertices.

5.3.1 Truncation

The RG flow of the local potential of the form Eq. (5.3) will be followed by cutoff-dependent parameters u and ϕ_0 (or, alternatively, δ).

The quadratic part of the effective action for the Hertz action contains two renormalization factors, one for the frequency and one for the momentum dependence:

$$\Gamma_{\phi\phi,\text{H}} = \int_p \frac{1}{2} \phi_{-p} \left(Z_\omega \frac{|\omega_n|}{|\mathbf{p}|^{z-2}} + Z_{\mathbf{p}}\mathbf{p}^2 + \delta \right) \phi_p, \quad (5.7)$$

where \int_p comprises frequency integration (Matsubara summation) and momentum integration at zero (finite) temperature. As it will turn out below, the frequency renormalization for the Hertz action does not play a role, in contrast to the Quantum Ising model, where we have

$$\Gamma_{\phi\phi,\text{QI}} = \int_p \frac{1}{2} \phi_{-p} (Z_\omega \omega_n^2 + Z_{\mathbf{p}}\mathbf{p}^2 + \delta) \phi_p. \quad (5.8)$$

The inverse propagator exhibits relativistic invariance and Z_ω is equally important to $Z_{\mathbf{p}}$ at zero temperature.

The Green function for the Hertz action endowed with the regulator reads accordingly,

$$G_R(p) = -\langle \phi_{-p} \phi_p \rangle = \frac{-1}{Z_\omega \frac{|\omega_n|}{|\mathbf{p}|^{z-2}} + Z_{\mathbf{p}}\mathbf{p}^2 + \delta + R^\Lambda(\mathbf{p})}, \quad (5.9)$$

and similarly for the Quantum Ising model with the frequency term replacement $Z_\omega \frac{|\omega_n|}{|\mathbf{p}|^{z-2}} \rightarrow Z_\omega \omega_n^2$. In all expressions with the frequency term of the Hertz action, Eq. (5.7), the corresponding terms for the Quantum Ising model are obtained by the just described replacement of frequency terms.

We emphasize that we have used a relatively simple parametrization of the effective action $\Gamma^\Lambda[\phi]$. In particular, we kept only the dominant terms in the derivative expansion (Berges 2002) and neglected the field dependence of the Z-factors. Furthermore, the simple parametrization of the effective potential Eq. (5.3) allowed us to substitute the partial differential equation (5.10) governing the flow of $U[\phi]$ by

the two ordinary differential equations (5.32) and (5.33). The latter approximation is equivalent to neglecting all higher order vertices generated during the flow. More sophisticated truncations have been applied, among others, in the context of the classical Ising universality class, where they lead to improved results for the critical exponents (Ballhausen 2004).

5.3.2 Flow equations

We derive our flow equations keeping the notation general so as to account for zero and finite temperature. Evaluating Eq. (5.5) for a momentum-independent field ϕ yields the flow of the effective potential $U[\phi]$

$$\partial_\Lambda U[\phi] = \frac{1}{2} \text{Tr} \frac{\dot{R}^\Lambda(\mathbf{p})}{Z_\omega \frac{|\omega_n|}{|\mathbf{p}|^{z-2}} + Z_\mathbf{p} \mathbf{p}^2 + R^\Lambda(\mathbf{p}) + U''[\phi]}, \quad (5.10)$$

from which we derive the flows of the parameters ϕ_0 and u , following the procedure in (Berges 2002). Viewing U as a function of $\rho = \frac{1}{2}\phi^2$ and using $U'[\rho_0] = 0$, we can write

$$0 = \frac{d}{d\Lambda} U'[\rho_0] = \partial_\Lambda U'[\rho_0] + U''[\rho_0] \partial_\Lambda \rho_0. \quad (5.11)$$

Inserting $\partial_\Lambda U'[\rho_0]$ as obtained by differentiating Eq. (5.10) with respect to ρ at $\rho = \rho_0$, and using $U''[\rho_0] = \frac{2}{3}u$, one obtains the flow equation for ρ_0

$$\partial_\Lambda \rho_0 = \frac{3}{2} \text{Tr} \frac{\dot{R}^\Lambda(\mathbf{p})}{\left[Z_\omega \frac{|\omega_n|}{|\mathbf{p}|^{z-2}} + Z_\mathbf{p} \mathbf{p}^2 + R^\Lambda(\mathbf{p}) + \frac{2}{3}u\rho_0 \right]^2}. \quad (5.12)$$

The flow of u is obtained by differentiating Eq. (5.10) twice with respect to ρ :

$$\partial_\Lambda u = 3u^2 \text{Tr} \frac{\dot{R}^\Lambda(\mathbf{p})}{\left[Z_\omega \frac{|\omega_n|}{|\mathbf{p}|^{z-2}} + Z_\mathbf{p} \mathbf{p}^2 + R^\Lambda(\mathbf{p}) + \frac{2}{3}u\rho_0 \right]^3}. \quad (5.13)$$

Inserting the above flow equations into the Λ -derivative of $\delta = \frac{2}{3}u\rho_0$, we obtain the flow of δ . To complete the system of flow equations one still needs to derive the evolution of $Z_\mathbf{p}$ and Z_ω , which parametrize the momentum and frequency dependence of the propagator. Taking the second functional derivative of Eq. (5.5), we obtain the flow equation for the propagator

$$\partial_\Lambda G_R^{-1}(p) = 3u\delta \text{Tr} \left[\dot{R}^\Lambda G_R^2(q) G_R(q+p) \right], \quad (5.14)$$

where $G_R(q)$ is given by Eq. (5.9). Here we skipped the contribution from the tadpole diagram, since it involves no dependence on momentum and frequency, and therefore

does not contribute to the flow of the Z -factors. The momentum renormalization factor is then given by

$$Z_{\mathbf{p}} = \frac{1}{2d} \partial_{\mathbf{p}}^2 [G_R^{-1}(\mathbf{p}, \omega_n = 0)] \Big|_{\mathbf{p}=0}, \quad (5.15)$$

where $\partial_{\mathbf{p}}^2$ is the Laplace operator evaluated at constant cutoff function, that is, $\partial_{\mathbf{p}}^2$ does not act on $R^\Lambda(\mathbf{p})$. We now turn to the renormalization of Z_ω . We first consider the case $z = 2$, where at finite temperatures Z_ω can be related to the propagator by

$$Z_\omega = \frac{1}{2\pi T} \left[G_R^{-1}(\mathbf{p} = 0, 2\pi T) - G_R^{-1}(\mathbf{p} = 0, 0) \right]. \quad (5.16)$$

But we shall later show that Z_ω renormalizes only very weakly at finite temperatures for $z = 2$ and therefore even more weakly for Pomeranchuk transitions where $z = 3$. At $T = 0$, the derivatives become continuous and for the Quantum Ising model $z = 1$, Z_ω renormalizes as strongly as $Z_{\mathbf{p}}$. In the following, we will often employ the anomalous momentum scaling exponent defined as:

$$\eta = -\frac{d \log Z_{\mathbf{p}}}{d \log \Lambda}, \quad (5.17)$$

and similarly for η_ω . The contributions to the flow of δ , u , Z_ω and $Z_{\mathbf{p}}$ are illustrated in terms of Feynman diagrams in Fig. 5.1.

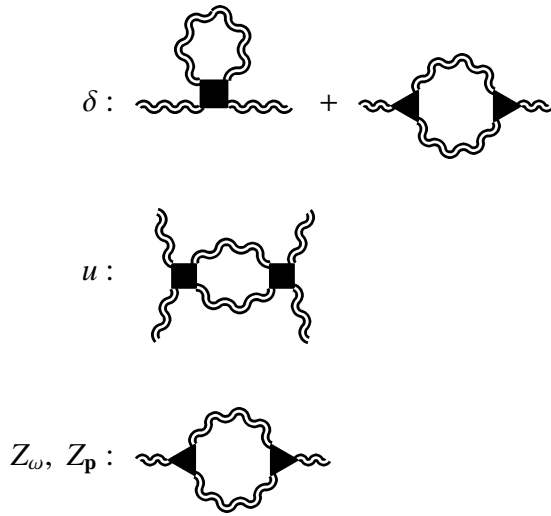


Fig. 5.1. Feynman diagrams representing the contributions to the flow equations (5.12, 5.13, 5.14).

5.4 Zero-temperature solution at the quantum critical point

In this section we present a solution of the flow equations (5.12, 5.13, 5.14) at zero temperature. For $z \geq 2$, we can linearize the flow equations around the Gaussian fixed in $d = 2$ and we provide an analytic expression for the value of the control parameter δ_0 corresponding to the quantum critical point.

For $z = 1$, the two-dimensional QCP is described by a non-Gaussian fixed point and we resort to a numerical solution of our equations.

5.4.1 $z \geq 2$

Convenient handling of the flow equations is achieved by introducing the variables

$$\begin{aligned}\tilde{v} &= \frac{A_d}{4\pi Z_p Z_\omega \Lambda^{4-(d+z)}} u \\ \tilde{\delta} &= \frac{\delta}{Z_p \Lambda^2}.\end{aligned}\tag{5.18}$$

For the Hertz action, the resulting flow equations are

$$\begin{aligned}\frac{d\tilde{\delta}}{d\log\Lambda} &= (\eta - 2)\tilde{\delta} + \frac{12\tilde{\delta}\tilde{v}}{(1+\tilde{\delta})^2} \frac{1}{d+z-2} + \frac{8\tilde{v}}{1+\tilde{\delta}} \frac{1}{d+z-2}, \\ \frac{d\tilde{v}}{d\log\Lambda} &= (d+z-4+2\eta)\tilde{v} + \frac{12\tilde{v}^2}{(1+\tilde{\delta})^2} \frac{1}{d+z-2}, \\ \eta &= \frac{6}{d} \frac{\tilde{\delta}\tilde{v}}{(1+\tilde{\delta})^4} \left[\frac{4}{3}(1+\tilde{\delta}) - \frac{(d-2)(z-2)}{3(d+z-4)}(1+\tilde{\delta})^2 - \frac{4}{d+z} \right].\end{aligned}\tag{5.19}$$

The flow equations (5.19) reveal that \tilde{v} is an irrelevant variable for $d+z > 4$ as pointed out earlier by Hertz (Hertz 1976). In this case Eqs. (5.19) have a stable Gaussian fixed point in $\tilde{v} = 0$, $\tilde{\delta} = 0$, $\eta = 0$. Linearizing the flow equations around the fixed point, one obtains the solution

$$\begin{aligned}\tilde{\delta}(\Lambda) &= \left[\tilde{\delta} + \frac{8\tilde{v}}{(d+z-2)^2} ((\Lambda/\Lambda_0)^{d+z-2} - 1) \right] (\Lambda/\Lambda_0)^{-2}, \\ \tilde{v}(\Lambda) &= (\Lambda/\Lambda_0)^{d+z-4} \tilde{v}, \\ \eta(\Lambda) &= 0,\end{aligned}\tag{5.20}$$

where $\tilde{\delta}$ and \tilde{v} on the right hand sides are the initial values of the parameters at $\Lambda = \Lambda_0$. In the marginal case $d+z = 4$ one finds logarithmic convergence of \tilde{v} and $\tilde{\delta}$ to zero. Expressing the order parameter ϕ_0 in terms of $\tilde{\delta}$ and \tilde{v} , substituting the above solution, and taking the limit $\Lambda \rightarrow 0$ yields

$$\phi_0 \propto \sqrt{\delta - \delta_0},\tag{5.21}$$

where

$$\delta_0 = \frac{2A_d}{\pi} \frac{\Lambda_0^{d+z-2}}{(d+z-2)^2} u\tag{5.22}$$

is the quantum critical point's coordinate. From Eq. (5.21) we read off the value of the exponent $\beta = \frac{1}{2}$, consistent with mean-field theory. From Eq. (5.20) one also straightforwardly evaluates the correlation length ξ , using $\xi^{-2} = \lim_{\Lambda \rightarrow 0} \delta(\Lambda) = \lim_{\Lambda \rightarrow 0} Z_p \Lambda^2 \tilde{\delta}$, which yields

$$\xi = (\delta - \delta_0)^{-1/2} , \quad (5.23)$$

as expected within mean field theory.

We have recovered the well-known fact that quantum phase transitions have properties similar to their classical counterparts in effective dimensionality $\mathcal{D} = d + z$ (Sachdev 1999). In the case studied here $\mathcal{D} \geq 4$ and one obtains mean-field behavior governed by a Gaussian fixed point.

5.4.2 $z = 1$

We now deal with the case where $\mathcal{D} = d + z$ is smaller than four and thus even at zero temperature the QCP falls into a non-Gaussian universality class for $1 < d < 3$. Although this case is covered by the quantum-classical mapping and the zero-temperature quantum theory matches that of the classical theory in $d+1$, it is worthwhile to inspect the zero-temperature flow equations in hindsight to a subsequent comparison with the finite-temperature equations in the following chapter.

We put $Z_\omega = Z_q$ as there is nothing that breaks the relativistic invariance except for our regulator function which cuts off momenta but leaves the frequencies untouched. In addition to η defined in Eq. (5.17), we here employ the rescaled variables

$$\begin{aligned} \tilde{\rho} &= \frac{\rho d Z_p}{2 \Lambda^{d-1} K_d} \\ \tilde{u} &= \frac{2u K_d}{d Z_p^2 \Lambda^{3-d}} . \end{aligned} \quad (5.24)$$

The frequency integrations can be performed analytically yielding the flow equations

$$\begin{aligned} \frac{d\tilde{\rho}}{d \log \Lambda} &= (1 - d - \eta) \tilde{\rho} + \frac{3}{2} \frac{1}{4 \left(1 + \frac{2\tilde{u}\tilde{\rho}}{3}\right)^{3/2}} \\ \frac{d\tilde{u}}{d \log \Lambda} &= (d - 3 + 2\eta) \tilde{u} + 3\tilde{u}^2 \left(\frac{3}{16 \left(1 + \frac{2\tilde{u}\tilde{\rho}}{3}\right)^{5/2}} \right) , \end{aligned} \quad (5.25)$$

and for the anomalous dimension:

$$\eta = 2\tilde{u}^2 \tilde{\rho} \frac{135 \sqrt{3} (3 + 12d + 8(d+2)\tilde{u}\tilde{\rho})}{128 (d+2) (3 + 2\tilde{u}\tilde{\rho})^{9/2}} . \quad (5.26)$$

We solve these equations numerically at the fixed point for $1 < d < 3$. The anomalous dimension comes out as $\eta = 0.126$ for $d = 2$. This can be compared with the best known estimates for the three-dimensional classical $O(1)$ -model, where $\eta \approx 0.04$ from seven-loop perturbation theory and ϵ -expansions (Berges 2002). It is a general feature of functional RG computations in simple truncations that the anomalous dimension is overestimated. Improving the truncation by including a field-dependent effective

potential and higher-order terms in the derivative expansion leads to accurate critical exponents (Berges 2002).

A thorough discussion and flows versus the cutoff-parameter follow in subsection 5.5.3.

5.5 Finite temperatures

Temperature provides for an additional scale in our problem that significantly enriches the analysis. There are now *two* relevant parameters, the first being the control parameter and the second the temperature. In the (δ, T) -plane there is now line of fixed points ending at the QCP $(\delta_{\text{crit}}, 0)$. Notably, for *any*, however small T , the critical behavior at $\Lambda \rightarrow 0$ is classical. Yet, we shall see below that the shape of the T_c -line is dominated by quantum fluctuations.

At finite temperatures, the continuous frequency integrations are substituted by discrete Matsubara sums. These sums in the flow equations (5.12) and (5.13) can be expressed in terms of polygamma functions $\Psi_n(x)$, defined recursively by $\Psi_{n+1}(x) = \Psi'_n(x)$ for $n = 0, 1, 2, \dots$, and $\Psi_0(x) = \Gamma'(x)/\Gamma(x)$, where $\Gamma(x)$ is the gamma function. From the Weierstrass representation, $\Gamma(x)^{-1} = xe^{\gamma x} \prod_{n=1}^{\infty} (1 + \frac{x}{n})e^{-x/n}$, where γ is the Euler constant, one can derive the relation

$$\sum_{n=-\infty}^{\infty} \frac{1}{(|n| + x)^2} = \frac{1}{x^2} + 2\Psi_1(x + 1) . \quad (5.27)$$

Taking derivatives with respect to x yields expressions for sums involving higher negative powers of $(|n| + x)$ in terms of polygamma functions of higher order. The d -dimensional momentum integrals on the right hand side of the flow equations can be reduced to one-dimensional integrals, since the integrands depend only on the modulus of \mathbf{p} .

Explicit dependences on Λ , Z -factors, and lengthy numerical prefactors in the flow equations can be eliminated by using the following rescaled variables:

$$\tilde{p} = |\mathbf{p}|/\Lambda , \quad (5.28)$$

$$\tilde{T} = \frac{2\pi Z_{\omega}}{Z_{\mathbf{p}} \Lambda^z} T , \quad (5.29)$$

$$\tilde{\delta} = \frac{\delta}{Z_{\mathbf{p}} \Lambda^2} , \quad (5.30)$$

$$\tilde{u} = \frac{A_d T}{2Z_{\mathbf{p}}^2 \Lambda^{4-d}} u , \quad (5.31)$$

with $A_d = (2\pi)^{-d} S_{d-1}$, where $S_{d-1} = 2\pi^{d/2}/\Gamma(d/2)$ is the area of the $(d-1)$ -dimensional unit sphere.

5.5.1 $z = 3$

For the case $z = 3$, the flow equations for $\tilde{\delta}$ and \tilde{u} are obtained as

$$\begin{aligned} \frac{d\tilde{\delta}}{d\log\Lambda} = (\eta - 2)\tilde{\delta} + 4\tilde{u} \left[\frac{1}{d} \frac{1}{(1+\tilde{\delta})^2} + \frac{1}{\tilde{T}^2} \int_0^1 d\tilde{p} \tilde{p}^{d+2z-5} \Psi_1(x) \right] \\ + 12\tilde{u}\tilde{\delta} \left[\frac{1}{d} \frac{1}{(1+\tilde{\delta})^3} - \frac{1}{\tilde{T}^3} \int_0^1 d\tilde{p} \tilde{p}^{d+3z-7} \Psi_2(x) \right], \end{aligned} \quad (5.32)$$

$$\frac{d\tilde{u}}{d\log\Lambda} = (d - 4 + 2\eta)\tilde{u} + 12\tilde{u}^2 \left[\frac{1}{d} \frac{1}{(1+\tilde{\delta})^3} - \frac{1}{\tilde{T}^3} \int_0^1 d\tilde{p} \tilde{p}^{d+3z-7} \Psi_2(x) \right], \quad (5.33)$$

where $x = 1 + \tilde{T}^{-1}(1 + \tilde{\delta})\tilde{p}^{z-2}$. Inserting Eqs. (5.14) and (5.15) into Eq. (5.17), and performing the frequency sum, one obtains for the anomalous dimension

$$\begin{aligned} \eta = \frac{6}{d} \frac{\tilde{u}\tilde{\delta}}{(1+\tilde{\delta})^5} \left[2(1+\tilde{\delta}) - \frac{8}{d+2} \right] - \frac{\tilde{u}\tilde{\delta}}{d} \tilde{T}^{-5} \int_0^1 d\tilde{p} \tilde{p}^{d+3z-13} \\ \left[-6\tilde{p}^4(z-2)(d+z-4)\tilde{T}^2\Psi_2(x) - 2\tilde{p}^{2+z} \left(2(8-d) \right. \right. \\ \left. \left. (1+\tilde{\delta} - \tilde{p}^2) + [(d-14)(1+\tilde{\delta}) + 8\tilde{p}^2]z + 3(1+\tilde{\delta})z^2 \right) \right. \\ \left. \tilde{T}\Psi_3(x) - \tilde{p}^{2z}[2(\tilde{p}^2 - 1) + \tilde{\delta}(z-2) + z]^2\Psi_4(x) \right]. \end{aligned} \quad (5.34)$$

Taking the logarithmic derivative with respect to Λ , inserting Eq. (5.14), and performing the trace yields for η_ω for the case $z = 2$

$$\eta_\omega = \frac{12}{d} \tilde{u}\tilde{\delta}\tilde{T}^{-1} \left[\frac{\tilde{T} - (1+\tilde{\delta})}{\tilde{T}(1+\tilde{\delta})^3} + \tilde{T}^{-3}\Psi_2 \left(1 + \frac{1+\tilde{\delta}}{\tilde{T}} \right) \right]. \quad (5.35)$$

From the numerical solution of the flow equation we observe that η_ω is small at all scales and vanishes for $\Lambda \rightarrow 0$. For example, in two dimensions η_ω varies between -0.033 and 0.005 for $u = 1$ at $T = e^{-4}$ and has practically no influence on the phase diagram. In three dimensions the values are at least one order of magnitude lower. For $z > 2$ one expects an even smaller η_ω , since a larger z reduces the strength of fluctuations near the quantum critical point. Therefore we set $\eta_\omega = 0$ and $Z_\omega = 1$ from now on. The scaling variable \tilde{T} then obeys the flow equation

$$\frac{d\tilde{T}}{d\log\Lambda} = (\eta - z)\tilde{T}. \quad (5.36)$$

In the flow equations (5.32,5.33,5.34) one identifies the classical mean-field (involving only one power of $\tilde{\delta}$ or \tilde{u}), classical non-Gaussian and quantum (involving \tilde{T})

terms. The quantum contributions vanish as the infrared cutoff tends to zero at constant non-zero temperature ($\tilde{T}^{-1} \ll 1$). On the other hand the quantum terms dominate the high energy part of the flow, where $\tilde{T}^{-1} \gg 1$. Our framework allows for a continuous connection of these two regimes of the flow. The scale Λ_{cl} below which quantum fluctuations become irrelevant depends on temperature. It vanishes at $T = 0$. In the absence of a sizable anomalous dimension η in the quantum regime of the flow, one has

$$\Lambda_{cl} \propto T^{1/z}, \quad (5.37)$$

as follows directly the definition of \tilde{T} . It turns out that η is indeed negligible down to the scale Λ_{cl} , except in the case $z = 2$ in two dimensions (see Sec. 5.5).

Below, we numerically solve the full RG flow equations (5.32,5.33,5.34) for finite temperatures. As already announced, the analysis is focused on the region of the phase diagram where symmetry-breaking occurs. In our notation this corresponds to sufficiently large values of the control parameter δ . First we treat the case $z = 3$ (in $d = 2, 3$) to which Eqs. (5.32,5.33,5.34) are applied directly. In all numerical results we choose an initial cutoff $\Lambda_0 = 1$, and an initial coupling constant $u = 1$.

We first solve the coupled flow equations (5.32,5.33,5.34) with the aim of determining the phase boundary $T_c(\delta)$, or, equivalently $\delta_c(T)$. To this end, for each given temperature we tune the initial value of δ such that at the end of the flow (for $\Lambda \rightarrow 0$) one obtains the critical state with $\delta(\Lambda) \rightarrow 0$. The tuned initial value is then identified as $\delta_c(T)$. Inverting the function $\delta_c(T)$ yields $T_c(\delta)$. In the variables $\tilde{\delta}$, \tilde{u} this corresponds to seeking for such values of the initial δ , that both $\tilde{\delta}(\Lambda)$ and $\tilde{u}(\Lambda)$ reach a fixed point as the cutoff is removed.

The flow of η and \tilde{u} as a function of the logarithmic scale variable $s = -\log(\Lambda/\Lambda_0)$ is shown in two exemplary plots in Fig. 5.2, respectively. The flow is shown for various temperatures T , with δ tuned to values very close to $\delta_c(T)$. The plateaus in Fig. 5.2 correspond to non-Gaussian fixed point values of the flowing parameters. From Fig. 5.2 where $d = 2$, one reads off the value of the anomalous dimension $\eta \approx 0.5$. The exact value from the Onsager solution to the Ising model is $\frac{1}{4}$. For the case $d = 3$ we find $\eta \approx 0.1$ within our truncation, which is also about twice as large as the best estimates for the exact value (Goldenfeld 1992). To obtain scaling behavior in the range of a few orders of magnitude one needs to fine-tune the initial conditions with an accuracy of around 15 digits. The breakdown of scaling behavior observed for very small Λ is due to insufficient accuracy of the initial value of δ and numerical errors. The plateaus are more extended as we go on fine-tuning the initial condition. Only exactly *at* the critical point true scale invariance manifested by plateaus of infinite size is expected.

The figures also reveal the Ginzburg scale Λ_G at which non-Gaussian fluctuations become dominant, such that the exponent η attains a non-zero value. By fitting a

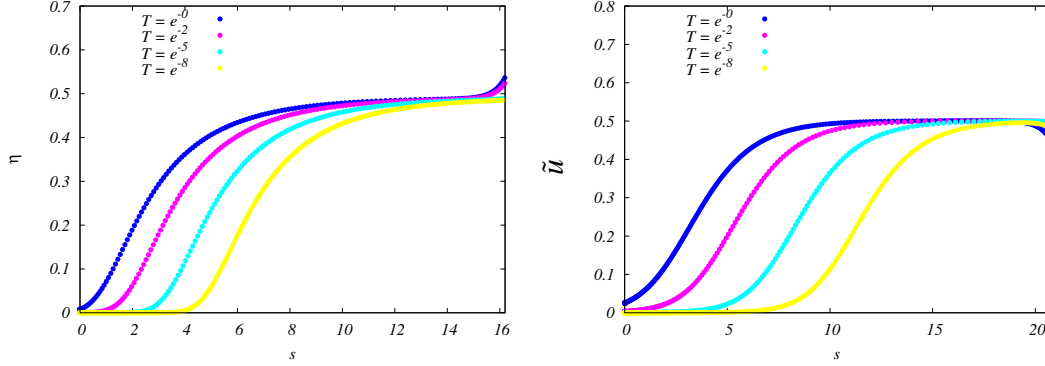


Fig. 5.2. Left: Anomalous dimension $\eta(\Lambda)$ plotted as function of $s = -\log(\Lambda/\Lambda_0)$ for different values of temperature in the case $z = 3$ and $d = 2$. The function $\eta(s)$ exhibits crossover from the mean-field value $\eta = 0$, to the non-Gaussian result $\eta \approx 0.5$. The crossover scale Λ_G is shifted towards smaller values (larger s) as temperature is reduced. Right: Quartic coupling $\tilde{u}(\Lambda)$ plotted as function of $s = -\log(\Lambda/\Lambda_0)$ for different values of temperature in the case $z = 3$ and $d = 3$.

power-law we observe $\Lambda_G \propto T_c$ for $d = 3$ and $\Lambda_G \propto \sqrt{T_c}$ for $d = 2$ with non-universal proportionality factors. As expected, Λ_G vanishes at the quantum critical point, because at $T = 0$ the effective dimensionality $\mathcal{D} = d + z$ is above the upper critical dimension $d_c = 4$. At finite temperatures, Λ_G is the scale at which \tilde{u} is promoted from initially small values (of order T) to values of order one. From the linearized flow equations one obtains

$$\Lambda_G \propto T_c^{\frac{1}{4-d}} \quad (5.38)$$

in agreement with the numerical results for $d = 2$ and $d = 3$. Note that $\Lambda_G \ll \Lambda_{cl}$, since $\Lambda_{cl} \propto T_c^{1/3}$ for $z = 3$, see Eq. (5.37). Hence anomalous scaling (finite η) is indeed absent in the regime where quantum fluctuations contribute, and non-Gaussian fluctuations appear only in the classical regime. As already mentioned, the quantum contributions influence the flow only at relatively large Λ for $T > 0$. In particular, they do not alter any fixed point values. However, at the beginning of the flow they dominate over the classical part and therefore are crucial for a correct computation of the initial value of δ leading to a scaling solution in the infrared limit.

Results for the transition line $T_c(\delta)$ for $d = 2$ and $d = 3$ are shown in Fig. 5.3. In both cases we recover the shape of the transition line as derived by Millis (1993), who used the Ginzburg temperature in the symmetric phase as an estimate for T_c . Namely, we find

$$(\delta - \delta_0) \propto T_c \log T_c \quad (5.39)$$

for $d = 2$, and

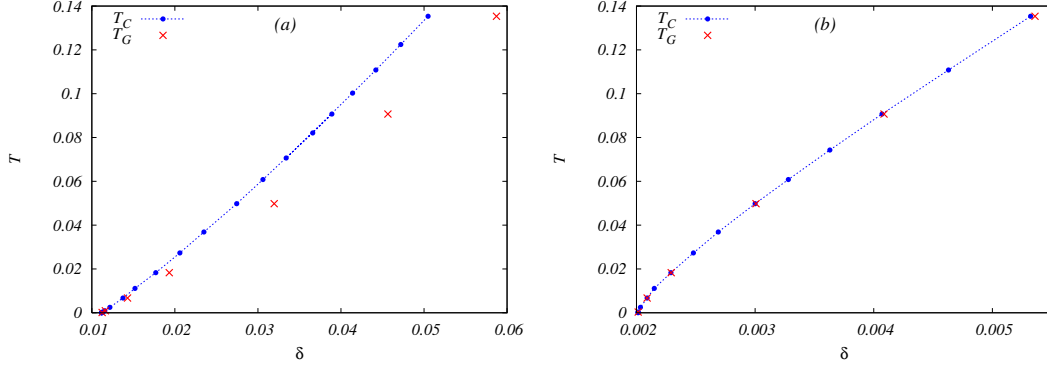


Fig. 5.3. The transition lines $T_c(\delta)$ obtained for $z = 3$, $d = 2$ (a) and $z = 3$, $d = 3$ (b). The phase with broken symmetry is located below the line. The phase boundary $T_c(\delta)$ obeys $(\delta - \delta_0) \propto T_c \log T_c$ for $d = 2$ and $T_c \propto (\delta - \delta_0)^{0.75}$ in agreement with the result by Millis (1993). The crosses indicate the Ginzburg temperature T_G for various choices of δ .

$$T_c \propto (\delta - \delta_0)^{0.75} \quad (5.40)$$

for $d = 3$. The exponent $3/4$ in the three-dimensional case matches with the general formula for the shift exponent

$$\psi = \frac{z}{d + z - 2} \quad (5.41)$$

for arbitrary z in dimensions $d > 2$ as long as $d + z > 4$. Generally, we see from this formula that *increasing* z has qualitatively (neglecting possible log-corrections) the same effect as *decreasing* d . Note that the phase boundary $T_c(\delta)$ approaches the quantum critical point with vanishing first derivative for $d = 2$ and with singular first derivative in the case $d = 3$.

An advantage of the present approach is that one can also follow the RG flow into the strong coupling regime, where non-Gaussian critical behavior occurs. This in turn allows an estimate of the critical region's size as a function of temperature or the control parameter δ . To evaluate the Ginzburg line in the symmetry-broken phase one solves the flow equations (5.32,5.33,5.34) for fixed T and at different values of $\delta > \delta_c(T)$, observing the behavior of fixed point values of the average order parameter ϕ_0 (or, alternatively, the correlation length ξ) as δ approaches δ_c . Typical results are plotted in Fig. 5.4 from which we read off the value of the exponent β describing the decay of the order parameter upon approaching the transition line $\phi_0 \propto (\delta - \delta_c)^\beta$. In the truly critical region (for $\delta - \delta_c$ small enough) one obtains $\beta \approx 0.11$ for $d = 2$ and $\beta \approx 0.30$ for $d = 3$. These results come out close to the correct classical values 0.125 and 0.31, respectively. This is unlike the other critical exponents (η and the correlation

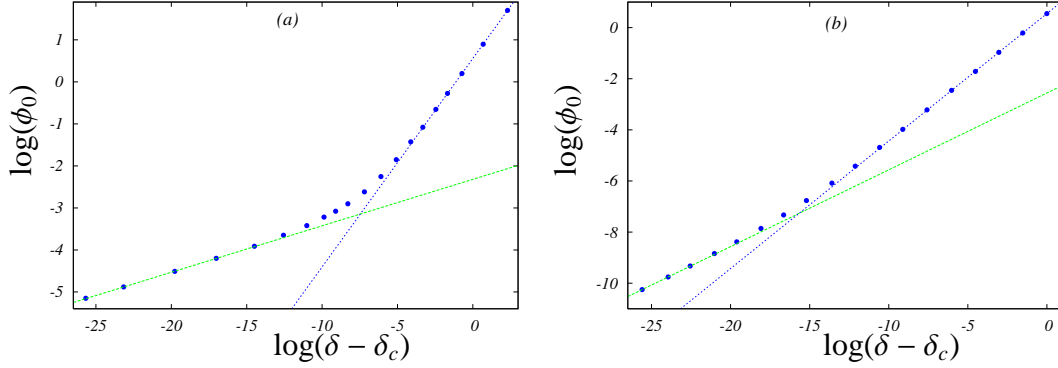


Fig. 5.4. Order parameter ϕ_0 as a function of $(\delta - \delta_c)$ at $T = e^{-5}$ for $z = 3$, $d = 2$ (a), and $z = 3$, $d = 3$ (b). The exponent β governing the decay of ϕ_0 upon approaching δ_c exhibits a crossover from a mean-field value $\beta = 0.5$ to a non-Gaussian $\beta \approx 0.11$ for $d = 2$, and $\beta \approx 0.30$ for $d = 3$.

length exponent ν) which within our truncation differ by factors close to 2 from their correct values.

Indeed, as discussed in (Ballhausen 2004), to obtain accurate values of the critical exponents in the Ising universality class, and in particular in $d = 2$, one not only needs to consider the full partial differential equation governing the RG flow of the effective potential $U[\phi]$, but also the field dependence of the wave function renormalization and higher orders in the derivative expansion of the effective action (Berges 2002).

From Fig. 5.4 we can extract the Ginzburg value δ_G below which true critical behavior is found at the chosen temperature T . Around δ_G , the exponent β exhibits a crossover from its mean-field value $\beta = 0.5$ to a non-Gaussian value. In other words, δ_G marks the boundary of the non-Gaussian critical region at a given T . At zero temperature, δ_G coincides with the quantum phase transition point δ_0 , since there the fluctuations are effectively $d + z > 4$ dimensional, leading to mean-field behavior. Several Ginzburg points in the $\delta - T$ plane are plotted as $T_G(\delta)$ in Fig. 5.3, where they can be compared to the phase transition line. In three dimensions T_G and T_c almost coincide, such that T_G provides an accurate estimate for T_c . In two dimensions a sizable region between T_G and T_c appears in the phase diagram. In that region non-Gaussian classical fluctuations are present.

We stress that accounting for the anomalous exponent η is necessary to describe the classical scaling regime, that is to obtain the plateaus in Fig. 5.2. Upon putting $\eta = 0$ the scaling plateaus do not form. On the other hand, the shapes of the phase boundaries and the Ginzburg curves become very similar at $T \rightarrow 0$ in the present cases, where $d + z \geq 4$.

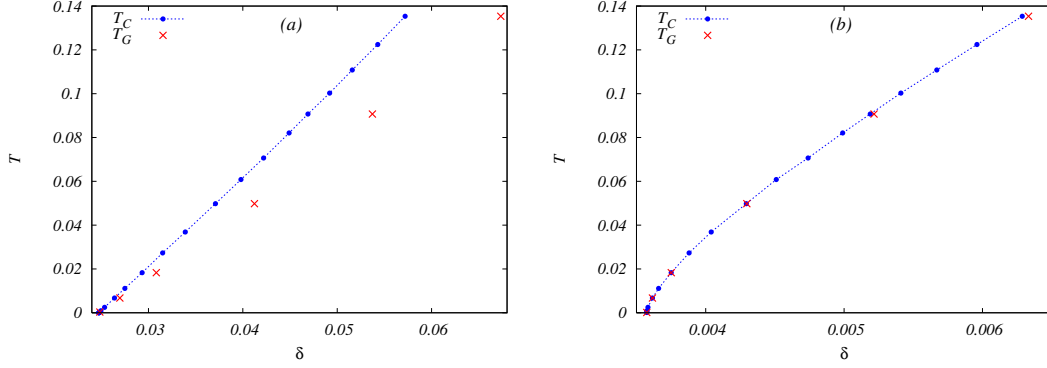


Fig. 5.5. The transition lines $T_c(\delta)$ obtained for $z = 2$, $d = 2$ (a) and $z = 2$, $d = 3$ (b). The phase with broken symmetry is located below the line. For $d = 2$ the phase boundary $T_c(\delta)$ is consistent with the relation $(\delta - \delta_0) \propto T_c \log \log T_c / \log T_c$ derived by Millis (1993). For $d = 3$ it follows the expected power law $T_c(\delta) \propto (\delta - \delta_0)^\psi$ with $\psi = 2/3$. The crosses indicate the Ginzburg temperature T_G for various choices of δ .

5.5.2 $z = 2$

In the case $z = 2$ the flow equations (5.32,5.33,5.34) are significantly simplified, as all the integrals can be evaluated analytically. One obtains

$$\begin{aligned} \frac{d\tilde{\delta}}{d \log \Lambda} &= (\eta - 2) \tilde{\delta} + 2\tilde{u} \left[\frac{2}{d} \frac{1}{(1 + \tilde{\delta})^2} + \frac{4}{d} \tilde{T}^{-2} \Psi_1(y) \right] + 3\tilde{u}\tilde{\delta} \left[\frac{4}{d} \frac{1}{(1 + \tilde{\delta})^3} - \frac{4}{d} \tilde{T}^{-3} \Psi_2(y) \right] \\ \frac{d\tilde{u}}{d \log \Lambda} &= (d - 4 + 2\eta) \tilde{u} + 3\tilde{u}^2 \left[\frac{4}{d} \frac{1}{(1 + \tilde{\delta})^3} - \frac{4}{d} \tilde{T}^{-3} \Psi_2(y) \right], \end{aligned} \quad (5.42)$$

and for the anomalous dimension,

$$\eta = \frac{6}{d} \frac{\tilde{u}\tilde{\delta}}{(1 + \tilde{\delta})^5} \left[2(1 + \tilde{\delta}) - \frac{8}{d+2} \right] + \frac{4\tilde{u}\tilde{\delta}}{d} \tilde{T}^{-5} \left[\tilde{T} \Psi_3(y) + \frac{1}{d+2} \Psi_4(y) \right], \quad (5.43)$$

where the argument of the polygamma functions is given by $y = 1 + (1 + \tilde{\delta})/\tilde{T}$.

The procedure to evaluate the phase diagram and the Ginzburg line is the same as in the previously discussed case $z = 3$. In Fig. 5.5 we show results for the transition line $T_c(\delta)$ in two and three dimensions. We also show the Ginzburg temperature T_G for various choices of δ .

In two dimensions, the transition line is consistent with the almost linear behavior $(\delta - \delta_0) \propto T_c \log \log T_c / \log T_c$, derived previously for the Ginzburg temperature (Millis 1993). However, a sizable region with non-Gaussian fluctuations opens between T_c and T_G . In three dimensions, $T_c(\delta)$ obeys the expected (Millis 1993) power law $T_c(\delta) \propto (\delta - \delta_0)^\psi$ with shift exponent $\psi = 2/3$, and the Ginzburg temperature is very close to T_c for any δ .

5.5.3 $z = 1$

We now consider the Quantum Ising model at finite temperatures. This case has not been considered before in $d < 3$ and also not by Millis (1993). The Millis analysis relies on the fact that the QCP is described by a Gaussian fixed point which is *not* applicable here. The zero-temperature equations (5.25, 5.26) are generalized to finite temperatures. We first define the variables:

$$\begin{aligned}\tilde{\rho} &= \frac{Ad\rho}{2K_d T \Lambda^{d-2}} \\ \tilde{u} &= \frac{2K_d T u}{dA^2 \Lambda^{4-d}} \\ \tilde{T} &= \frac{2\pi T}{\Lambda A} ,\end{aligned}\tag{5.44}$$

to write the flow equations as

$$\begin{aligned}\frac{d\tilde{\rho}}{d\log\Lambda} &= (2 - d - \eta)\tilde{\rho} + \frac{3}{2} \left[\frac{1}{\left(1 + \frac{2\tilde{u}\tilde{\rho}}{3}\right)^2} + 2 \sum_{n=1}^{\infty} \frac{1}{\left((n\tilde{T})^2 + 1 + \frac{2\tilde{u}\tilde{\rho}}{3}\right)^2} \right] \\ \frac{d\tilde{u}}{d\log\Lambda} &= (d - 4 + 2\eta)\tilde{u} + 3\tilde{u}^2 \left[\frac{1}{\left(1 + \frac{2\tilde{u}\tilde{\rho}}{3}\right)^3} + 2 \sum_{n=1}^{\infty} \frac{1}{\left((n\tilde{T})^2 + 1 + \frac{2\tilde{u}\tilde{\rho}}{3}\right)^3} \right] .\end{aligned}\tag{5.45}$$

The anomalous dimension is determined by

$$\eta = 2\tilde{u}^2\tilde{\rho} \left[\frac{1}{\left(1 + \frac{2\tilde{u}\tilde{\rho}}{3}\right)^4} - \frac{2}{(d+2)\left(1 + \frac{2\tilde{u}\tilde{\rho}}{3}\right)^5} + 2 \sum_{n=1}^{\infty} \frac{1}{\left((n\tilde{T})^2 + 1 + \frac{2\tilde{u}\tilde{\rho}}{3}\right)^4} - \frac{2}{(d+2)\left((n\tilde{T})^2 + 1 + \frac{2\tilde{u}\tilde{\rho}}{3}\right)^5} \right] ,\tag{5.46}$$

and the effective temperature scales as

$$\frac{d\tilde{T}}{d\log\Lambda} = (\eta - 1)\tilde{T} .\tag{5.47}$$

The Matsubara summation can be performed analytically, which we have done for a computationally cheaper numerical solution, but they do not deliver analytic insights here.

We discuss the numerical solution of the finite temperature flow equations (5.45, 5.46) and we compare it to the zero-temperature flow equations of subsection 5.4.2. Note that now $d + z = 3 < 4$, and this case has not been covered previously (Hertz 1976, Millis 1993). Non-Gaussian fluctuations persist even at zero temperature which is illustrated in a qualitative comparison of the Ginzburg line with the T_c -line in Fig. 5.6.

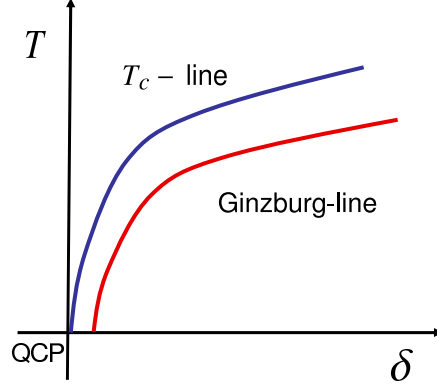


Fig. 5.6. Schematic comparison of the Ginzburg line with the T_c -line for $d = 2$, $z = 1$. The critical region extends down to zero temperature.

In Fig. 5.7, the zero-temperature flow is juxtaposed with finite-temperature flows. Clearly, there is no continuous crossover from the finite-temperature behavior to the zero-temperature one. Hence, taking the limit $T \rightarrow 0$ is a *discontinuous* process. Both, the finite- T and the $T = 0$ find a description in terms of two distinct non-Gaussian fixed points.² From Fig. 5.7 (b), we deduce the Ginzburg-scale to vary with temperature as

$$\Lambda_G \propto T_c^{1/2}, \quad (5.48)$$

fitting the formula derived for $d + z > 4$, $\Lambda_G \propto T_c^{1/(4-d)}$. As expected, the QCP-value for η shown in Fig. 5.8 (a) is smaller than its classical counterpart as the QCP is effectively $d + 1$ -dimensional thus taming critical fluctuations. The phase boundary in double-logarithmic plot is shown in Fig. 5.8 (b). The points do not lie on a straight line, indicating log-corrections correcting the power-law behavior. ψ attains effective values in the range: $\psi \approx 0.5 - 0.7$ over six (!) orders of magnitude in good agreement with

$$T_c \sim 9.28 \frac{\sqrt{\delta - \delta_c}}{|\ln(\delta - \delta_c)|} \quad (5.49)$$

which, as anticipated, does not fit the Millis formula, Eq. (5.41), which was derived under the assumption $d + z > 4$. However, the existence of these log-corrections remains inconclusive. Interestingly, ψ is *reduced* compared to its two-dimensional

² As a counterexample, consider the merger of the non-Gaussian Wilson-Fisher-type fixed point with the Gaussian fixed point when taking the limit $d \rightarrow d_c^+$, with d_c^+ the upper critical dimension, in standard ϕ^4 -theory (Goldenfeld 1992).

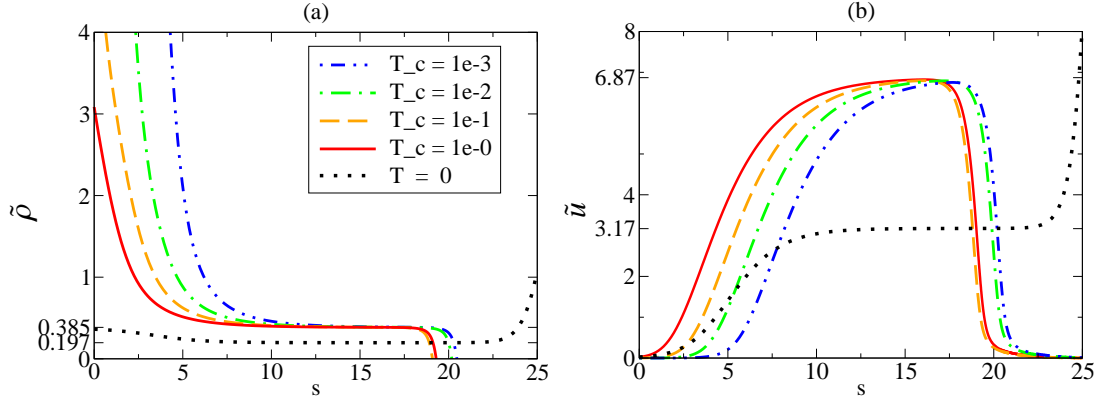


Fig. 5.7. Flows for the *Quantum Ising model* ($z = 1$) in $d = 2$. (a): Flows of $\tilde{\rho}$ as a function of logarithmic cutoff-scale $s = -\log[\Lambda/\Lambda_0]$ for various temperatures and at $T = 0$. The values of the classical fixed point ($\tilde{\rho} = 0.385$) and the QCP ($\tilde{\rho} = 0.197$) are marked on the vertical axis. We set $\Lambda_0 = 1$. The infrared (ultraviolet) is to the right (left) of the graphs. (b): Corresponding flows of \tilde{u} . The values of the classical fixed point ($\tilde{u} = 6.87$) and the QCP ($\tilde{u} = 3.17$) are marked on the vertical axis.

analogs when $z > 1$ although the strength of non-Gaussian classical fluctuations is *increased* when reducing z . This underpins the importance of Gaussian quantum fluctuations which on the other hand *decrease* when reducing z .

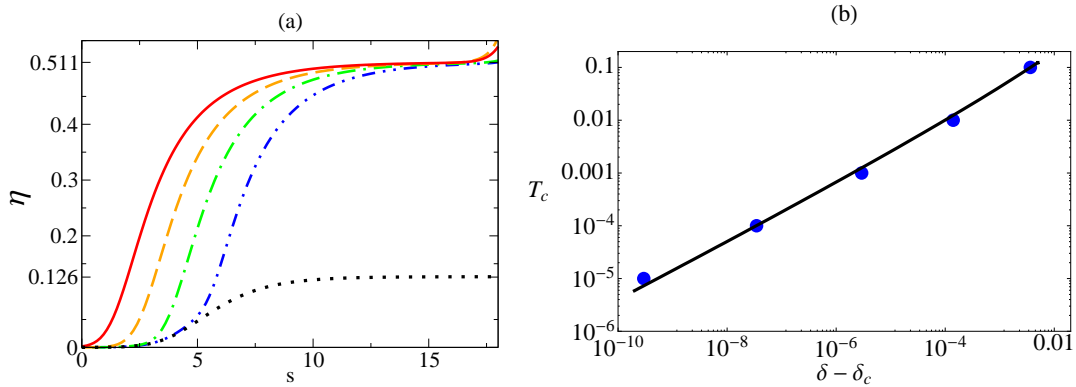


Fig. 5.8. Results for the *Quantum Ising model* ($z = 1$) in $d = 2$. (a): Cutoff-scale dependences of the anomalous dimension for the same temperatures as in Fig. 5.7. The value of the anomalous dimension at the classical fixed point ($\eta = 0.511$) and the QCP ($\eta = 0.126$) are marked on the vertical axis. (b): Double logarithmic plot of the phase boundary fitted to Eq. (5.49).

5.6 Conclusion

We have analyzed classical and quantum fluctuations in the symmetry-broken phase near a quantum phase transition in an itinerant electron system and in the Quantum Ising model. The analysis is restricted to the case of *discrete* symmetry breaking, where no Goldstone modes appear. Following Hertz (1976) and Millis (1993), we use an effective bosonic action for the order parameter fluctuations as a starting point. For the Quantum Ising model, the effective continuum action is also of the ϕ^4 -type but with dynamical critical exponent $z = 1$. The renormalization of the Hertz action and the Quantum Ising model by fluctuations is obtained from a system of coupled flow equations, which are derived as an approximation to the exact flow equation for one-particle irreducible vertex functions in the functional RG framework. In addition to the renormalization of the effective mass and the four-point coupling, we also take the anomalous dimension η of the order parameter fields into account. In the symmetry-broken phase, contributions to η appear already at one-loop level. Quantum and thermal fluctuations are captured on equal footing. The flow equations are applicable also in the immediate vicinity of the transition line at finite temperature, where fluctuations deviate strongly from Gaussian behavior.

We have computed the transition temperature T_c as a function of the control parameter δ near the quantum critical point, approaching the transition line from the symmetry-broken phase. Explicit results were presented for dynamical exponents $z = 3$ and $z = 1$ in two and three dimensions corresponding to Pomeranchuk transitions and the Quantum Ising model, respectively. For $z = 3$, $T_c(\delta)$ agrees with the behavior of the Ginzburg temperature above T_c derived previously by Millis (1993). For $z = 1$ in two dimensions, even the zero-temperature theory is characterized by a non-Gaussian fixed point. This case is not covered in the Hertz-Millis theory. We computed the phase boundary and found logarithmic corrections to power-law behavior. The effective shift-exponent, $\psi(d = 2, z = 1) \approx 0.5 - 0.7$ is smaller than the two-dimensional Hertz-Millis value, $\psi(d = 2, z \geq 2) = 1$.

We have also computed the Ginzburg temperature T_G below T_c , above which non-Gaussian fluctuations become important. Although T_G and T_c almost coincide in three dimensions, a sizable region between T_G and T_c opens in two dimensions. While for $z \geq 2$ this critical region shrinks to zero for $T_c \rightarrow 0$, a finite difference between the Ginzburg and critical coordinates persists even at zero-temperature for $z = 1$.

It will be interesting to extend the present approach to the case of continuous symmetry breaking. Then, symmetry-breaking at finite temperature is suppressed completely for $d \leq 2$ by Goldstone fluctuations. We consider the fluctuation effects of Goldstone modes on the quantum critical behavior at zero and at finite temperature in the next chapter.

Quantum critical points with Goldstone modes

6.1 Introduction

A quantum critical point may separate a phase with broken continuous symmetry from a normal phase (see Fig. 6.1) as is the case for example in quantum magnets, superfluids (Belitz 2005, Loehneysen 2007), or continuum systems with Pomeranchuk Fermi surface deformations (Oganesyan 2001, Wölfle 2007, Quintanilla 2008). The distinct signature of phases with broken continuous symmetry is the occurrence of Goldstone modes. In a recent experiment on quantum magnets with pressure as non-thermal control parameter (Rüegg 2008), inelastic neutron scattering data reconfirmed the vanishing mass for the Goldstone mode in the magnetic phase and provided information about the magnitude of the longitudinal mass in the vicinity of the QCP. Theoretically, it is largely unexplored how Goldstone modes affect the zero and finite temperature properties on the ordered side of the quantum phase transition (Wetterich 2008).

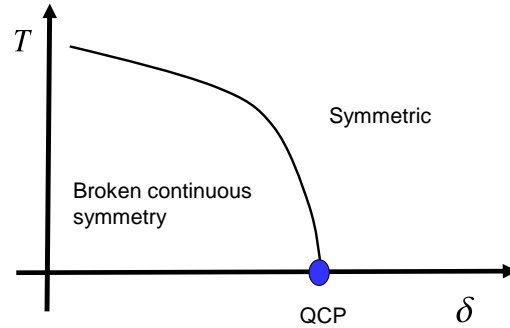


Fig. 6.1. Phase diagram of the QCP with Goldstone modes for $d > 2$. At $d = 2$ thermal fluctuations destroy the order and suppress the T_c -line to zero temperature according to the Mermin-Wagner theorem.

For classical bosonic $O(N)$ -models with Goldstone and longitudinal fluctuations, the functional RG provided a unifying picture (Berges 2002). In the present chapter, we compute RG flows in the vicinity of a QCP accounting for transversal and longitudinal fluctuations of the order parameter restricting ourselves to Goldstone modes dispersing linearly in momentum ($\Omega \sim |\mathbf{q}|$) as is the case in superfluids and antiferromagnets (Belitz 2005).

At finite temperatures, we extend our computation of the phase boundary for discrete symmetry-breaking (see chapter 5, Jakubczyk 2008) to account for Goldstone modes. We compute the shift-exponent ψ which characterizes how the T_c -line varies as a function of control parameter (Loehneysen 2007) in three dimensions. We also clarify the singularity structure of the theory and establish the infrared asymptotics away from the phase boundary.

We start by presenting the σ - Π model for phases with broken continuous symmetry in section 6.2. We clearly distinguish longitudinal fluctuations (σ) from the Goldstone modes (Π) both dispersing relativistically with dynamical exponent $z = 1$. In section 6.3, we describe our functional RG set-up. In section 6.4, we compute the shift-exponent characterizing the shape of the phase boundary at finite temperatures for $d = 3$. In section 6.5, we extend our calculation to regions away from the phase boundary and we analytically establish the infrared properties of both, the Goldstone and longitudinal propagator, as well as the bosonic self-interaction. Summary and conclusions follow in section 6.6.

6.2 σ - Π Model for continuous symmetry-breaking

We are interested in the effective action for N -component real-valued bosonic fields Φ in phases with spontaneously broken continuous symmetry ($N \geq 2$). The most general action to fourth order in the fields that respects the $O(N)$ -symmetry and contains no more than two derivatives reads (Wetterich 1991, Tetradis 1994):

$$\Gamma[\Phi] = \int \left[\frac{Z}{2} (\partial\Phi)^2 + \frac{Y}{8} (\Phi\partial\Phi)^2 \right] + U^{\text{loc}}[\Phi] , \quad (6.1)$$

where Z and Y are renormalization factors, ∂ denotes the standard derivative operator, and the integration symbol \int denotes the standard space integration. Including the field component index a and the dimensionality index μ , the products in the derivative terms are defined as: $(\partial\Phi)^2 = \partial_\mu \Phi^a \partial^\mu \Phi_a$, and $(\Phi\partial\Phi)^2 = (\Phi^a \partial_\mu \Phi_a) (\Phi^b \partial^\mu \Phi_b)$ where $a, b = 1, \dots, N$ and $\mu = 1, \dots, d+1$. Local interaction terms are retained in the effective potential:

$$U^{\text{loc}}[\Phi] = \frac{u}{8} \int (\Phi^2 - |\alpha|^2)^2 , \quad (6.2)$$

where the effective potential has a minimum at $\Phi = (\alpha, 0, 0, \dots)$ with α real and positive. It is convenient to decompose Φ into a longitudinal component σ and $(N-1)$ transverse components Π via

$$\Phi = (\sigma, 0, 0, \dots) + (0, \Pi) . \quad (6.3)$$

Substituting $\Phi \rightarrow (\alpha + \sigma, \Pi)$ in Eq. (6.1) yields various interaction terms (see below) and two distinct quadratic parts:

$$\begin{aligned} \Gamma_{\sigma\sigma} &= \frac{1}{2} \int_q \sigma_{-q} \left((Z + Y|\alpha|^2) q^2 + u|\alpha|^2 \right) \sigma_q \\ \Gamma_{\pi\pi} &= \frac{1}{2} \int_q \Pi_{-q} (Zq^2) \Pi_q, \end{aligned} \quad (6.4)$$

where $q = (q_0, \mathbf{q})$ collects the frequency and momenta and $\int_q = \int \frac{dq_0}{2\pi} \int \frac{d^d q}{(2\pi)^d}$ comprises the corresponding integrations. The components of the Π -field are massless as these are the Goldstone modes. The propagators for the σ - and Π -field have the form

$$\begin{aligned} G_\sigma(\Omega, \mathbf{q}) &= -\langle \sigma_q \sigma_{-q} \rangle = \frac{-1}{Z_\sigma q^2 + m_\sigma^2} \\ G_\pi(\Omega, \mathbf{q}) &= -\langle \Pi_q \Pi_{-q} \rangle = \frac{-1}{Z_\pi q^2}, \end{aligned} \quad (6.5)$$

with $\rho = |\alpha|^2$, $Z_\pi = Z$, and

$$\begin{aligned} Z_\sigma &= Z + Y\rho \\ m_\sigma^2 &= u\rho. \end{aligned} \quad (6.6)$$

For the interaction terms, we obtain:

$$\begin{aligned} \Gamma_{\sigma^4} &= \int_{q,q',p} \gamma_{\sigma^4} \sigma_{-q-p} \sigma_{-q'+p} \sigma_{q'} \sigma_q, \\ \Gamma_{\pi^4} &= \int_{q,q',p} \gamma_{\pi^4} \Pi_{-q-p} \Pi_{-q'+p} \Pi_{q'} \Pi_q, \\ \Gamma_{\sigma^2\pi^2} &= \int_{q,q',p} \gamma_{\sigma^2\pi^2} \sigma_{-q-p} \sigma_{-q'+p} \Pi_{q'} \Pi_q, \\ \Gamma_{\sigma^3} &= \int_{q,p} \gamma_{\sigma^3} \sigma_{-q-p} \sigma_p \sigma_q, \\ \Gamma_{\sigma\pi^2} &= \int_{q,p} \gamma_{\sigma\pi^2} \sigma_{-q-p} \Pi_p \Pi_q, \end{aligned} \quad (6.7)$$

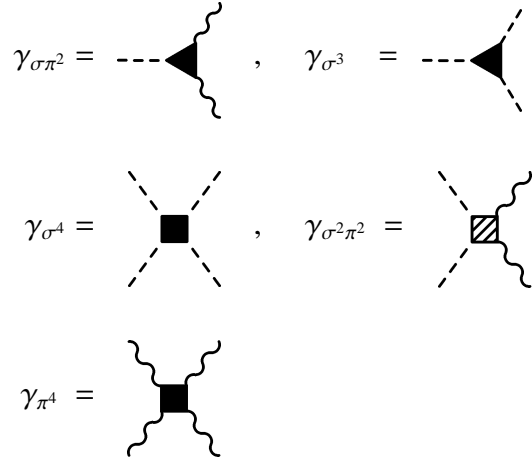


Fig. 6.2. Interaction vertices and propagators of the σ - Π model for continuous symmetry-breaking.

with $\gamma_{\sigma^4} = \gamma_{\pi^4} = (u + Y\rho^2)/8$, $\gamma_{\sigma^2\pi^2} = (u + Y\rho^2)/4$, and $\gamma_{\sigma^3} = \gamma_{\sigma\pi^2} = (u + Y\rho^2)\alpha/2$ as depicted in Fig. 6.2. In total, the $\sigma - \Pi$ model contains four independent parameters: α , u , Z , and Y .

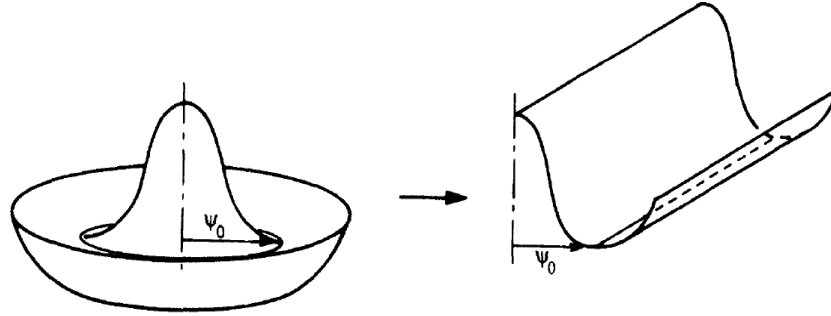


Fig. 6.3. Linearly realized $O(N)$ -symmetry. Here, $\psi_0 = \alpha$ is the order-parameter and the trough is understood to be $N - 1$ dimensional. From Weichman (1988).

A comment on the choice of field basis in Eq. (6.3) is in place. The rotational $O(N)$ -symmetry in internal space is realized only *linearly*. The periodicity of the Goldstone field is deformed to a linear trough of infinite extension, see. Fig. 6.3. Consequently, periodic field configurations such as vortices are hard to capture in this basis.

Alternative choices are the phase-amplitude representation (schematic): $\Phi \sim \rho_0 e^{i\Sigma\Theta}$, with Σ the $N - 1$ group generators, Θ the conjugate Goldstone modes, and ρ_0 the amplitude of the order-parameter. This phase-amplitude representation manifestly preserves the rotational symmetry and allows, for example, a convenient description of the non-linear sigma model when the mass of the radial boson is sufficiently large so that Goldstone bosons remain the only fluctuating fields (Amit 2005). An analytic treatment of some aspects of the Kosterlitz-Thouless phase for $N = 2$ is also easily accessible (Goldenfeld 1992).

At criticality, however, when the effective potential is flat in the center and the order-parameter is still small, the phase-amplitude basis has a parametric singularity at the origin for $\rho_0 \gtrsim 0$. And at higher energies, in the symmetric phase, neither Eq. (6.3) nor the phase-amplitude representation is appropriate: then, the particle representation in terms of the Φ -field is most transparent.

We are therefore confronted with the situation that different choices of basis in field space are useful only in limited regions of the phase diagram. This problem has been the subject of an extensive body of literature (Popov 1987, Nepomnashchy 1992 and references therein, Pistolesi 1997, Diener 2008, Strack 2008). A derivation of Ward identities for the σ - Π model can be found in Amit (2005).

A promising RG approach employing the linear basis in Eq. (6.3) but additionally invoking constraints from Ward identities has recently been put forward in (Pistolesi 1997, 2004). How one might smoothly connect the linear basis with the phase-amplitude basis via scale-dependent transformations is shown in Diener (2008).

6.3 Method

In this section, we present the functional RG method and our truncation for the symmetry-broken phase. We have explained in subsection 3.2.2 in detail how to account for spontaneous symmetry-breaking with the exact flow equation for the effective action (Wetterich 1993, Berges 2002, Salmhofer 2001, Metzner 2005):

$$\frac{d}{d\Lambda} \Gamma^\Lambda[\Phi] = \text{Tr} \frac{\dot{\mathbf{R}}^\Lambda}{\mathbf{\Gamma}^{(2)\Lambda}[\Phi] + \mathbf{R}^\Lambda}, \quad (6.8)$$

where $\mathbf{\Gamma}^{(2)\Lambda} = \partial^2 \Gamma^\Lambda[\Phi] / \partial \Phi^2$ is the second functional derivative with respect to the order parameter field and the trace (Tr) traces over all indices (see section 3.2 for a detailed derivation). When expanding this equation around a non-vanishing minimum α of the effective action, additional terms will arise in the flow equations for the n -point vertex involving the scale-derivative of the order-parameter, $\dot{\alpha}$, and the $n+1$ -point vertex, see Fig. 3.1.

The objective is now to compute the flow of the independent parameters α , u , Z , and Y of the $\sigma - \Pi$ model. A convenient cutoff function \mathbf{R}^Λ that respects the $O(N)$ -symmetry is a self-energy independent sharp cutoff for space-like momenta:

$$\mathbf{R}^\Lambda(k) = [\mathbf{G}_0(k)]^{-1} - [\chi^\Lambda(\mathbf{k}) \mathbf{G}_0(k)]^{-1} \quad (6.9)$$

where $\chi^\Lambda(\mathbf{k}) = \Theta(|\mathbf{k}| - \Lambda)$. This term replaces the bare propagator \mathbf{G}_0 by $\mathbf{G}_0^\Lambda = \chi^\Lambda \mathbf{G}_0$.

For a sharp momentum cutoff the momentum variable running around the loop is pinned by $\mathbf{G}'_R(\mathbf{k})$ to $|\mathbf{k}| = \Lambda$ as the so-called single-scale propagator \mathbf{G}'_R^Λ has support only for momenta at the cutoff, that is, for $|\mathbf{k}| = \Lambda$. Hence the momentum integral can be performed analytically. The problem that the integrand contains also step functions $\chi^\Lambda(\mathbf{k}) = \Theta(|\mathbf{k}| - \Lambda)$ can be treated by using the identity

$$\int dx \delta(x - x_0) f[x, \Theta(x - x_0)] = \int_0^1 du f(x_0, u), \quad (6.10)$$

which is valid for any continuous function f . More specifically, in the present case the one-loop diagrams are evaluated for vanishing external momenta and depend only on the modulus $|\mathbf{k}|$, such that all internal propagators carry the same momentum and one can use the identity

$$n \int \frac{d^d k}{(2\pi)^d} \mathbf{G}'_R(k) \mathbf{A} [\mathbf{G}_R(k) \mathbf{A}]^{n-1} = \Lambda^{d-1} K_d [\mathbf{G}(k) \mathbf{A}]^n|_{|\mathbf{k}|=\Lambda}, \quad (6.11)$$

valid for any matrix \mathbf{A} and with K_d being defined by $\int \frac{d^d k}{(2\pi)^d} = K_d \int d|k| |k|^{d-1}$. The factor n corresponds to the n possible choices of positioning \mathbf{G}'_R in a loop with n lines. For loop integrals in the flow equations, we use the short-hand notation

$$\int_{k|\Lambda} = \int \frac{dk_0}{(2\pi)} \int \frac{d^d k}{(2\pi)^d} \delta(|\mathbf{k}| - \Lambda) . \quad (6.12)$$

At finite temperatures, the continuous frequency integration becomes a discrete Matsubara sum: $\int \frac{dk_0}{2\pi} \rightarrow T \sum_{\Omega_n}$, with $\Omega_n = 2\pi nT$.

6.4 Finite temperature phase boundary in three dimensions

The primary objective of this section is to extend the finite temperature work presented in chapter 5 to systems with Goldstone modes. Most importantly, we compute the shift-exponent ψ of the finite temperature phase boundary in $d = 3$.

On the phase boundary at T_c , the effective potential is flat and there exists only one bosonic excitation. Following Tetradis and Wetterich (1994), we set $Y = 0$ in this section and therefore: $Z_\sigma = Z_\pi = Z$. This truncation gives the best results for critical exponents and correctly reflects that the phase transition becomes mean-field like with vanishing anomalous dimension in the large N limit. For an extended discussion we refer to section 9 of Tetradis (1994).

6.4.1 Flow equations

As demanded by the condition of a vanishing bosonic one-point vertex for all scales, see Eq. (3.26), the square of the order parameter obeys the flow equation

$$\partial_\Lambda \rho = - \int_{q|\Lambda} 3G_\sigma(q) + (N-1)G_\pi(q) , \quad (6.13)$$

The bosonic self-interaction is driven by

$$\partial_\Lambda u = u^2 \int_{q|\Lambda} 9G_\sigma^2(q) + (N-1)G_\pi^2(q) . \quad (6.14)$$

Lastly, the bosonic field renormalization is determined by the expression

$$\partial_\Lambda Z = u^2 \rho \int_{q|\Lambda} \frac{\partial_{\mathbf{k}}^2}{2} [G_\pi(q+k)G_\sigma(q)]_{k=0} , \quad (6.15)$$

where $\partial_{\mathbf{k}}^2 = \frac{1}{d} \sum_{i=1}^d \partial_{k_i}^2$. The flow equations (6.13-6.15) are shown in terms of Feynman diagrams in Fig. 6.4.

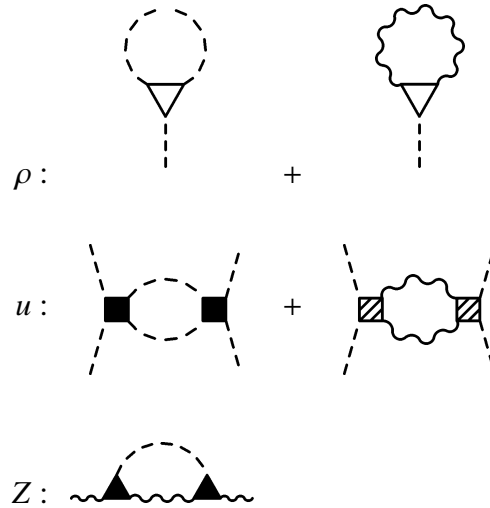


Fig. 6.4. Feynman diagrams for the flow equations (6.13-6.15).

We split the Matsubara summations into their classical and quantum parts

$$T \sum_{\Omega_n} f(\Omega_n) = T f(\Omega_n = 0) + T \sum_{\Omega_n \neq 0}^{(\text{quant})} f(\Omega_n), \quad (6.16)$$

and utilize the following variables,

$$\begin{aligned} \tilde{\rho} &= \frac{Z \rho}{\Lambda^{d-2} T K_d} \\ \tilde{u} &= \frac{K_d T u}{Z^2 \Lambda^{4-d}}, \end{aligned} \quad (6.17)$$

as well as a rescaled temperature and anomalous dimension

$$\begin{aligned} \tilde{T} &= \frac{2\pi T}{\Lambda} \\ \eta &= -\frac{d \log Z}{d \log \Lambda}. \end{aligned} \quad (6.18)$$

We therewith obtain for the squared order-parameter and the quartic coupling:

$$\begin{aligned} \frac{d\tilde{\rho}}{d \log \Lambda} &= (2 - d - \eta) \tilde{\rho} + \frac{3}{(1 + \tilde{u}\tilde{\rho})} + (N - 1) + 2 \sum_{n=1}^{\infty} \frac{3}{\left((n\tilde{T})^2 + 1 + \tilde{u}\tilde{\rho} \right)^2} + \\ &\quad \frac{N - 1}{\left((n\tilde{T})^2 + 1 \right)^2} \\ \frac{d\tilde{u}}{d \log \Lambda} &= (d - 4 + 2\eta) \tilde{u} + \tilde{u}^2 \left[\frac{9}{(1 + \tilde{u}\tilde{\rho})^2} + (N - 1) + 2 \sum_{n=1}^{\infty} \frac{9}{\left((n\tilde{T})^2 + 1 + \tilde{u}\tilde{\rho} \right)^2} + \right. \\ &\quad \left. \frac{N - 1}{\left((n\tilde{T})^2 + 1 \right)^2} \right]. \end{aligned} \quad (6.19)$$

Terms proportional to $N - 1$ outside the summation stem from classical Goldstone fluctuations. But the Goldstone mode also yields new quantum terms proportional to $N - 1$ inside the summation. The anomalous dimension is determined by

$$\eta = \tilde{u}^2 \tilde{\rho} \left[\frac{1}{(1 + \tilde{u}\tilde{\rho})} + 2 \sum_{n=1}^{\infty} \frac{1}{(n\tilde{T})^2 + 1 + \tilde{u}\tilde{\rho}} \frac{1}{\left((n\tilde{T})^2 + 1 \right)^2} \right] \quad (6.20)$$

The Matsubara summations can be performed analytically yielding hyperbolic trigonometric functions. The rather complex expressions do not deliver any additional insights.

6.4.2 Classical fixed point

In the classical limit, considering only the zeroth Matsubara frequency/neglecting the summation terms, our equations (6.19, 6.20) describe the correct classical critical behavior of the Heisenberg universality class for $N = 3$. Inspection of the first term of $\frac{d\bar{\rho}}{d\Lambda}$ in Eq. (6.19) yields the lower critical dimension $d_c^- = 2$ for $N > 1$ in agreement with the Mermin-Wagner theorem. The flow equations therefore correctly account for the fact that Goldstone fluctuations suppress T_c to zero in two dimensions. The upper critical dimension is $d_c^+ = 4$ from the first term in $\frac{d\bar{u}}{d\Lambda}$, as expected. The fixed point value for the anomalous exponent in three dimensions comes out as: $\eta = 0.058$ to be compared with the known value $\eta = 0.036$ from other methods (Berges 2002).

6.4.3 Shift exponent ψ

The shift exponent determines how the critical temperature varies with control parameter in the immediate vicinity of the QCP:

$$T_c \propto (\delta - \delta_{\text{crit}})^\psi . \quad (6.21)$$

We compute ψ employing the same procedure as explained below Eq. (5.37) in chapter 5. The numerical flows look identical to those of the previous section in Fig. 5.7 except that the scaling plateaus form at the fixed point values of the Heisenberg universality class for $N = 3$. We find that the Ginzburg scale decreases with decreasing T_c as:

$$\Lambda_G \propto T_c , \quad (6.22)$$

fitting the formula $\Lambda_G \propto T_c^{1/(4-d)}$ derived in the previous chapter, c.f. Eq. (5.38) for $d = 3$. For the shift exponent, we find

$$\psi \approx 1/2 , \quad (6.23)$$

which matches the formula derived by Millis (1993): $\psi = \frac{z}{d+z-2}$ for $d = 3$ and $z = 1$. We have verified that for any value of N , the shift-exponent attains the Millis value $1/2$ derived in the symmetric phase without accounting for Goldstone bosons.

Therefore, the shift-exponent for three dimensional QCPs where a bosonic description is appropriate does not depend on the number of Goldstone bosons. This is the main result of this section.

6.5 Infrared asymptotics in the symmetry-broken phase

Away from the QCP and the phase boundary, the system is characterized by a finite minimum in the effective potential. In this section, we clarify the singularity structure of the $\sigma - \Pi$ model in the limit of vanishing cutoff $\Lambda \rightarrow 0$ in the presence of a finite order parameter ρ . We will compute at zero temperature but the obtained results for the infrared properties may be transferred to finite temperature by increasing spatial dimensionality by one. We establish the scaling properties of the various parameters and show that the Goldstone propagator and longitudinal propagator exhibit very different momentum scaling, in stark contrast to the phase boundary where both modes become degenerate.

Technically, it is crucial to consider the Y -term which distinguishes the Goldstone field renormalization Z_π from that of the longitudinal mode Z_σ , see Eq. (6.6).

6.5.1 Flow equations

The flow equations for ρ and u remain unchanged from Eqs. (6.13,6.14). The flow equation for $G_\sigma^{-1}(k)$ contains terms from the four diagrams shown in Fig. 6.5 and has the form:

$$\begin{aligned} \partial_\Lambda G_\sigma^{-1}(k) = & \frac{\rho}{2} \int_{q|\Lambda} (u + Yq^2)^2 [9G_\sigma(q+k)G_\sigma(q) + (N-1)G_\pi(q+k)G_\pi(q)] \\ & + \int_{q|\Lambda} \frac{Yq^2}{2} [(N-1)G_\pi(q+k) + 3G_\sigma(q+k)] . \end{aligned} \quad (6.24)$$

The flow equation for $G_\pi^{-1}(k)$ corresponding to the three diagrams in the second line of Fig. 6.5 reads:

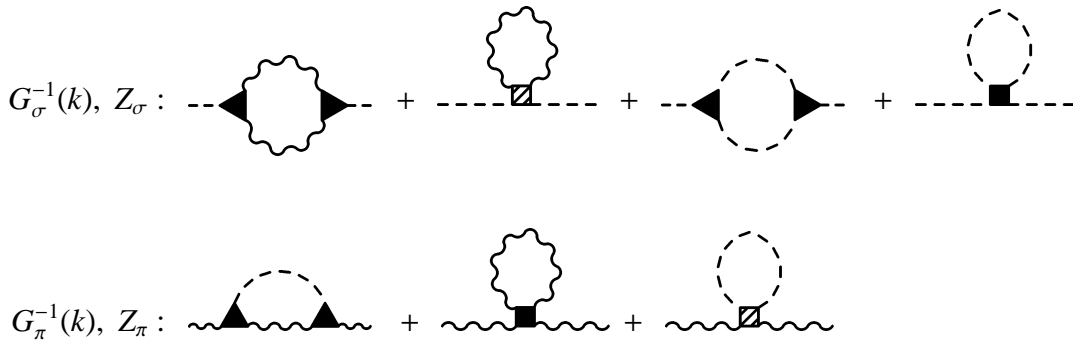


Fig. 6.5. Feynman diagrams for Eqs. (6.24,6.25).

$$\partial_\Lambda G_\pi^{-1}(k) = \int_{q|\Lambda} \left(\frac{\rho}{2} \left(\frac{u + Yq^2}{2} \right)^2 3G_\sigma(q) + 3\frac{Yq^2}{2} \right) G_\pi(q+k) + \int_{q|\Lambda} \frac{Yq^2}{2} G_\sigma(q+k) , \quad (6.25)$$

where the factor of three in front of $G_\sigma(q)$ in the first term arises from three different contractions of the first diagram in the second line of Fig. 6.5 as drawn in Eq. (4.36) of Pistoiesi, et al. (2004). One obtains the flow for Z_σ and Z_π by applying the Laplacian $\partial_{\mathbf{k}}^2/2$ evaluated at $|\mathbf{k}| = 0$ to both sides of Eqs. (6.24, 6.25), respectively. The flow of Y follows then from the scale derivative of the relation:

$$Y = \frac{Z_\sigma - Z_\pi}{\rho} . \quad (6.26)$$

6.5.2 Analytical results

We now identify the leading singularities in the flow equations for u , Z_σ , and Z_π to determine their scaling behavior in the infrared, that is, in the limit of vanishing cutoff $\Lambda \rightarrow 0$. The order parameter ρ is finite and does not scale to zero as we are now in the symmetry-broken phase away from the phase boundary and the QCP.

For the quartic coupling u , the diagram with two Goldstone propagators in Fig. 6.4 is the most singular, leading to the expression:

$$\partial_\Lambda u = u^2 \int_{q|\Lambda} (N-1) G_\pi^2(q) . \quad (6.27)$$

This equation can be integrated analytically and yields in $d = 2$ at zero temperature:

$$u \rightarrow Z_\pi^2 \Lambda , \quad (6.28)$$

provided $N > 1$. As the longitudinal mass is proportional to the quartic coupling, see Eq. (6.6), it also vanishes linearly as a function of scale. In three dimensions, the linear behavior becomes logarithmic.

For Z_σ , the first diagram in the first line of Fig. 6.5 contains the leading singularity:

$$\partial_\Lambda Z_\sigma = \frac{u^2 \rho}{2} (N-1) \int_{q|\Lambda} \frac{\partial_{\mathbf{k}}^2}{2} [G_\pi(q+k)G_\pi(q)]_{k=0} , \quad (6.29)$$

Upon inserting Eq. (6.28), we obtain in two dimensions

$$Z_\sigma \rightarrow \frac{Z_\pi^2 \rho}{\Lambda} . \quad (6.30)$$

In three dimensions Z_σ diverges only logarithmically. As we will demonstrate below, Z_π remains finite and therefore by virtue of Eq. (6.26), we obtain for the Y -term:

$$Y \sim \frac{Z_\sigma}{\rho} \rightarrow \frac{Z_\pi^2}{\Lambda}, \quad (6.31)$$

where we have used Eq. (6.30). What remains to be shown is that all singularities for the Goldstone propagator cancel such that Z_π is rendered finite. The leading term for the Goldstone propagator from Eq. (6.25) can be written:

$$\partial_\Lambda G_\pi^{-1}(k) = \int_{q|\Lambda} \gamma_{\pi^4}^{\text{eff}}(q) G_\pi(q+k), \quad (6.32)$$

where the effective momentum-dependent self-interaction among the Goldstone bosons contains two terms:

$$\gamma_{\pi^4}^{\text{eff}}(q) = \tilde{\gamma}_{\pi^4}(q) + \tilde{\gamma}_{\sigma\pi^2}^2 G_\sigma(q), \quad (6.33)$$

with $\tilde{\gamma}_{\pi^4}(q) = \frac{3}{2} Y q^2$ and $\tilde{\gamma}_{\sigma\pi^2} = \frac{3}{2} \rho \left(\frac{u+Yq^2}{2} \right)^2$. Since $G_\sigma(q)$ is negative, the interaction among Goldstone bosons from exchange of longitudinal fluctuations has the opposite sign of the direct interaction $\tilde{\gamma}_{\pi^4}$ (Pistolesi 2004). By inserting the longitudinal propagator from Eq. (6.5) and the obtained scale dependences of Eqs. (6.28, 6.30, 6.31) into Eq. (6.33), we obtain as the central result of this section:

$$\gamma_{\pi^4}^{\text{eff}}(q) \rightarrow 0, \quad (6.34)$$

therefore liberating the corrections to the Goldstone propagator from singularities and ensuring the finiteness of Z_π for $d > 1$ ($d > 2$) at zero (finite) temperature. In the important work by Pistolesi, Castellani, et al. (2004), this proof has been extended to arbitrary loop order for the case of an interacting Bose gas.

We have established the following infrared ($\Lambda \rightarrow 0$) behavior for the longitudinal propagator at zero temperature:

$$\begin{aligned} G_\sigma(\Lambda) &\propto \frac{-1}{\Lambda} \quad \text{for } d = 2 \\ G_\sigma(\Lambda) &\propto \log \Lambda \quad \text{for } d = 3, \end{aligned} \quad (6.35)$$

while the Goldstone propagator remains quadratic:

$$G_\pi(\Lambda) \propto \frac{-1}{\Lambda^2} \quad \text{for } d = 2, 3, \quad (6.36)$$

and the bosonic self-interaction scales as:

$$\begin{aligned} u(\Lambda) &\propto \Lambda \quad \text{for } d = 2 \\ u(\Lambda) &\propto -\frac{1}{\log \Lambda} \quad \text{for } d = 3. \end{aligned} \quad (6.37)$$

These results may be transferred to finite temperatures by incrementing spatial dimensionality d by one.

6.6 Conclusion

This chapter was devoted to an analysis of the effects of Goldstone modes in the vicinity of quantum critical points where a description in terms of bosonic fields is appropriate. Within the functional RG framework, we derived flow equations for the relativistic $\sigma - \Pi$ model with dynamical exponent $z = 1$ suitable for the ordered phase at zero and finite temperature.

First, we computed the shift-exponent ψ characterizing the shape of the phase boundary at finite temperature in three dimensions and found that ψ is independent of the number of Goldstone bosons in three dimensions.

We then clarified the infrared properties of the Goldstone and longitudinal propagator as well as the bosonic self-interaction away from the phase boundary. We showed that the longitudinal propagator and the self-interaction are strongly renormalized. The Goldstone propagator, on the other hand, remains quadratic in momenta as the effective interaction among Goldstone bosons flows to zero due to symmetries.

In the future, it would be worthwhile to apply an extended version of the flow equations devised in this chapter to quantum criticality in the Kosterlitz-Thouless universality class (see also Outlook 9.3.2) and to compute, for example, the shift-exponent for the Kosterlitz-Thouless temperature.

Fermi-Bose renormalization group for quantum critical fermion systems

7.1 Introduction

As noticed already more than 30 years ago by Hertz (1976), quantum phase transitions in correlated fermion systems may be described in terms of the order parameter field alone when one integrates out fermions from the path integral in one stroke and subsequently deals with an exclusively bosonic theory. The resultant effective action is expanded in powers of the bosonic field ϕ and often truncated after the ϕ^4 -term. Although an analysis in terms of ϕ^4 -type theories seems mundane, the presence of *two* relevant energy scales, one given by temperature and the other given by a non-thermal control parameter acting as a mass term in the bosonic propagator, gives rise to a rich finite temperature phase diagram (Millis 1993).

The Hertz-Millis approach relies on integrating out fermions first. In general, however, the zero temperature fermion propagator is gapless and consequently may lead to singular coefficients in the effective bosonic action (Belitz 2005, Loehneysen 2007). In such cases, it is obligatory to keep the gapless fermions in the theory and consider them on equal footing to the bosons as performed in several works with (resummed) perturbation theory (Altshuler 1995, Abanov 2000, Abanov 2003, Rech 2006).

Recently, various quantum critical exponents for U(1) gauge theories with Dirac fermions and complex-valued bosonic fields in two spatial dimensions were computed in the limit of a large number of fermion and boson species N_f and N_b (Kaul 2008). However, the complicated interplay of two singular propagators promotes a controlled perturbative treatment to a formidable task (Rech 2006) and represents a clear calling for the renormalization group (RG).

When computing RG flows for coupled fermion-boson theories, where the propagator of the zero temperature fermions becomes unbounded for momenta on the Fermi surface and the propagator for massless bosons is singular at the origin of momentum space, it is crucial to *synchronize* the evolution of correlation functions so that both singularities are reached simultaneously at the end of the flow.

Within the functional RG framework formulated for fermionic and bosonic fields (Berges 2002, Baier 2004, Schütz 2005, Strack 2008), this poses no particular problem as the regulator functions for fermions and bosons can be chosen to synchronize both types of fluctuations. The mutual feedback of gapless fermions coupled to massless bosons has been studied already with functional flow equations in Quantum Electrodynamics (Gies 2004), non-abelian gauge theories (Pawlowski 2004), and the Gross-Neveu model (Rosa 2001).

In the present chapter, we study a model of attractive Dirac fermions relevant for neutral Graphene and cold atoms in the half-filled honeycomb lattice (Zhao 2006, Castro Neto 2007, Castro Neto 2008) exhibiting a quantum phase transition from a semimetal to a superfluid as shown in Fig. 7.1. The flow equations are analytically transparent and a simple truncation yields the complete set of quantum critical exponents. As a central result, the fermion and order parameter two-point correlation functions develop non-analytic dependences on frequency and momentum at the QCP.

In section 7.2, we introduce the *Dirac cone model* and show that the mean-field theory of this model leads to a semimetal-to-superfluid quantum phase transition at a critical interaction strength U_c . In section 7.3, the RG method, truncation and flow equations are presented. Results for the quantum critical behavior follow in section 7.4. We finally summarize and conclude in section 7.5.

7.2 Dirac cone model

We consider an attractively interacting Dirac fermion system with the *bare action*

$$\Gamma_0[\psi, \bar{\psi}] = - \int_{k\sigma} \bar{\psi}_{k\sigma}(ik_0 - \xi_{\mathbf{k}}) \psi_{k\sigma} + \int_{k,k',q} U \bar{\psi}_{-k+\frac{q}{2}\downarrow} \bar{\psi}_{k+\frac{q}{2}\uparrow} \psi_{k'+\frac{q}{2}\uparrow} \psi_{-k'+\frac{q}{2}\downarrow}, \quad (7.1)$$

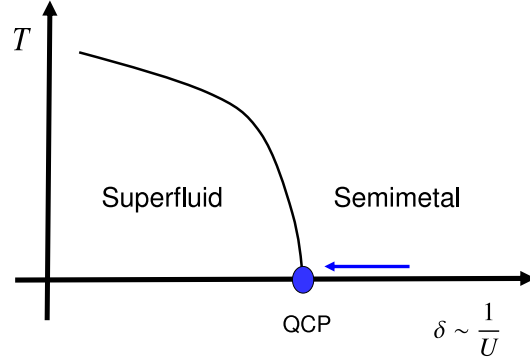


Fig. 7.1. Schematic phase diagram of attractive Dirac fermions. The QCP at a critical interaction strength U_c separates the semimetal from the superfluid. In the present chapter, we approach the QCP at $T = 0$ from the semimetallic phase indicated with an arrow.

where the variables $k = (k_0, \mathbf{k})$ and $q = (q_0, \mathbf{q})$ collect the zero temperature Matsubara energies and momenta, and we use the short-hand notation $\int_k = \int_{k_0} \int_{\mathbf{k}} = \int_{-\infty}^{\infty} \frac{dk_0}{2\pi} \int \frac{d^d \mathbf{k}}{(2\pi)^d}$ for momentum and energy integrals, and $\int_{k\sigma}$ includes also a spin sum. The dispersion for Dirac fermions with the chemical potential directly at the Dirac point (see Fig. 7.2) is given by:

$$\xi_{\mathbf{k}} = \pm v_f |\mathbf{k}|, \quad (7.2)$$

with $+v_f$ for the empty cone and $-v_f$ for the filled cone. Energy integrations over $\xi_{\mathbf{k}}$ are cut off in the ultraviolet and restricted to the band $\{\min \xi_{\mathbf{k}} = -\Lambda_0, \max \xi_{\mathbf{k}} = +\Lambda_0\}$. For attractive interactions the coupling constant U is negative and drives spontaneous breaking of the global $U(1)$ gauge symmetry. Therefore, we decouple the Hubbard interaction in the s-wave spin-singlet pairing channel by introducing a complex bosonic Hubbard-Stratonovich field ϕ_q conjugate to the bilinear composite of fermionic fields (Popov 1987)

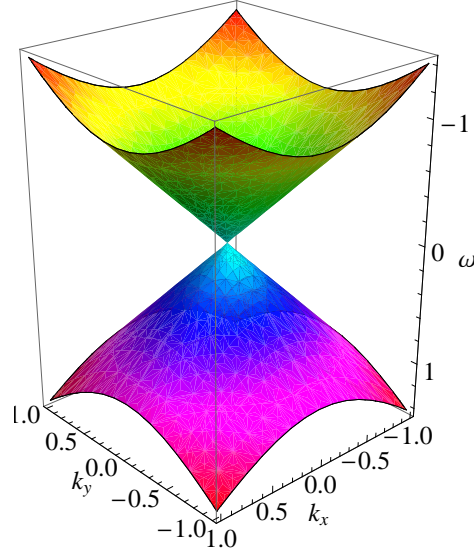


Fig. 7.2. Energy spectrum of two-dimensional Dirac fermions.

$$\tilde{\phi}_q = U \int_k \psi_{k+\frac{q}{2}\uparrow} \psi_{-k+\frac{q}{2}\downarrow}. \quad (7.3)$$

This yields a functional integral over ψ , $\bar{\psi}$ and ϕ with the new bare action

$$\begin{aligned} \Gamma_0[\psi, \bar{\psi}, \phi] = & - \int_{k\sigma} \bar{\psi}_{k\sigma} (ik_0 - \xi_{\mathbf{k}}) \psi_{k\sigma} - \int_q \phi_q^* \frac{1}{U} \phi_q \\ & + \int_{k,q} \left(\bar{\psi}_{-k+\frac{q}{2}\downarrow} \bar{\psi}_{k+\frac{q}{2}\uparrow} \phi_q + \psi_{k+\frac{q}{2}\uparrow} \psi_{-k+\frac{q}{2}\downarrow} \phi_q^* \right). \end{aligned} \quad (7.4)$$

where ϕ^* is the complex conjugate of ϕ , while ψ and $\bar{\psi}$ are algebraically independent Grassmann variables.

7.2.1 Mean-field theory

When neglecting bosonic fluctuations by replacing ϕ_q with its expectation value $\phi_{q=0}$, the saddle-point approximation exactly solves the functional integral of Eq. (7.4) and leads to the standard BCS gap equation (Popov 1987):

$$\phi_0 = -U \int_k \frac{\phi_0}{k_0^2 + \xi_{\mathbf{k}}^2 + \phi_0^2}, \quad (7.5)$$

with U and ϕ_0 independent of momenta. To compute the critical interaction strength U_c at which the gap equation has a solution with non-zero ϕ_0 , we rearrange Eq. (7.5):

$$\frac{-1}{U_c} = \int \frac{dk_0}{2\pi} \int_{-\Lambda_0}^{\Lambda_0} d\xi_{\mathbf{k}} N(\xi_{\mathbf{k}}) \frac{1}{k_0^2 + \xi_{\mathbf{k}}^2}, \quad (7.6)$$

where the density of states has the form:

$$N(\xi) = \frac{|\xi|^{d-1} K_d}{v_f^d}, \quad (7.7)$$

with K_d being defined by $\int \frac{d^d k}{(2\pi)^d} = K_d \int d|k| |k|^{d-1}$. The expression in Eq. (7.6) is equivalent to the Thouless criterion for superconductivity which involves summing the particle-particle ladder in the normal phase to infinite order and determining the divergence of the effective interaction. Since the density of states vanishes –linearly in two dimensions– at the Dirac point, the zero temperature system is stable against formation of a superfluid for any weak attraction. Instead, a finite attraction larger than a certain threshold is necessary to cause superfluidity at zero temperature. Performing the integrations in Eq. (7.6), we obtain the mean-field position of the quantum phase transition in Fig. 7.1. The control parameter provides a mass term for the boson propagator in Eq. (7.4) and is therefore inversely related to the four-fermion attraction. For the physical case of two dimensions, we have:

$$\frac{1}{\delta_{\text{MFT}}} = -U_{c, \text{MFT}} = \frac{2\pi v_f^2}{\Lambda_0}, \quad (7.8)$$

where here v_f has units of energy. For electrons in the honeycomb lattice, the Fermi velocity in the vicinity of the Dirac points is proportional to the nearest-neighbor hopping matrix element t (Castro Neto 2007). Upon setting $v_f = \Lambda_0 = 1$, the numerical value for the mean-field control parameter value is $\delta_{\text{MFT}} = 0.159$. Note that the position of the QCP is non-universal and depends on microscopic parameters such as the ultraviolet band cutoff Λ_0 and the Fermi velocity.

In the following, we will conduct a renormalization group study which enables us not only to compute the *non-universal* renormalized position of the QCP but also yields the complete set of *universal* quantum critical exponents at and in the vicinity of the QCP.

7.3 Method

We derive flow equations for the scale-dependent effective action $\Gamma_\Lambda [\psi, \bar{\psi}, \phi]$ within the functional RG framework for fermionic and bosonic degrees of freedom in its

one-particle irreducible representation (Berges 2002, Baier 2004, Schütz 2005, Strack 2008). Starting from the bare fermion-boson action $\Gamma_{\Lambda=\Lambda_0}[\psi, \bar{\psi}, \phi]$ in Eq. (7.4), fermionic and bosonic fluctuations are integrated along the continuous flow parameter Λ *simultaneously*. In the infrared limit $\Lambda \rightarrow 0$, the renormalized, effective action $\Gamma_{\Lambda \rightarrow 0}[\psi, \bar{\psi}, \phi]$ is obtained from which physical properties can be extracted. Its RG flow is governed by the exact functional flow equation

$$\frac{d}{d\Lambda} \Gamma^\Lambda[\mathcal{S}, \bar{\mathcal{S}}] = \text{Str} \frac{\dot{\mathbf{R}}^\Lambda}{\mathbf{\Gamma}^{(2)\Lambda}[\mathcal{S}, \bar{\mathcal{S}}] + \mathbf{R}^\Lambda}, \quad (7.9)$$

where we have collected fermionic and bosonic fields in superfields $\bar{\mathcal{S}}, \mathcal{S}$ defined in subsection 3.1.1 and $\mathbf{\Gamma}^{(2)\Lambda} = \partial^2 \Gamma^\Lambda[\mathcal{S}, \bar{\mathcal{S}}] / \partial \mathcal{S} \partial \bar{\mathcal{S}}$ denotes the second functional derivative with respect to the superfields and the supertrace (Str) traces over all indices with an additional minus sign for fermionic contractions. We refer to Section 3.2 for a detailed derivation and discussion of the 1PI functional RG framework for both fermionic and bosonic fields.

7.3.1 Truncation

When evolving Γ^Λ towards $\Lambda \rightarrow 0$, infinitely many terms involving fermionic and/or bosonic fields with possibly complicated dependences on frequency and momenta are generated necessitating a truncation of the effective action. The purpose of this subsection is to explain how the effective action for the model Eq. (7.4) is truncated with the objective to capture the most relevant quantum critical renormalization effects.

Fermion propagator

To account for a renormalization of the single-particle, fermionic properties by order parameter fluctuations, the quadratic fermionic term in the action is modified by a field renormalization factor,

$$\Gamma_{\bar{\psi}\psi} = - \int_{k\sigma} \bar{\psi}_{k\sigma} Z_f (ik_0 - \xi_{\mathbf{k}}) \psi_{k\sigma}, \quad (7.10)$$

yielding the fermion propagator

$$G_f(k) = -\langle \psi_k \bar{\psi}_k \rangle = \frac{Z_f^{-1}}{ik_0 - \xi_{\mathbf{k}}}. \quad (7.11)$$

A diverging Z_f suppresses the quasi-particle weight to zero. If it diverges as a power law, $Z_f \sim 1/\Lambda^{\eta_f}$, the fermion self-energy becomes a non-analytic function of frequency ($k_0 = \omega$) with

$$\Sigma_f(\omega) \sim \omega^{1-\eta_f} \quad (7.12)$$

upon identifying the cutoff scale Λ with ω . As already mentioned above, the Fermi velocity is not renormalized separately but kept fixed at unity for the following reasons. The flow equations for the frequency- and momentum renormalization factors are obtained by derivatives of expressions corresponding to 1PI-diagrams. The flow equation for an independently parametrized v_f would come from one derivative of the diagram involving G_f and G_b , shown in the first line of Fig. 7.4, with respect to the deviation of momenta from the Dirac point. In parallel, the flow equation for Z_f also comes from one derivative with respect to frequency of the same expression. Hence, both expressions are almost identical for a linearized fermion dispersion and keeping v_f does not yield additional information. The initial condition for Z_f is $Z_f = 1$.

Boson propagator

The bosonic quadratic part of the bare action, Eq. (7.4), consists only of a local mass term. Upon integrating out fluctuations, the effective four-fermion interaction mediated by boson exchange will become momentum- and frequency-dependent. To capture this propagating order parameter field, we deploy a renormalization factor Z_b multiplying the lowest order frequency and momentum terms in a derivative expansion of the fermionic particle-particle bubble. The real part of the particle-particle bubble spanned by fermion propagators endowed with the regulator \mathbf{R}^Λ is a quadratic function of external frequencies and momenta leading to the bosonic quadratic part of the action:

$$\Gamma_{\phi^*\phi} = \int_q \phi_q^* (Z_b (q_0^2 + \mathbf{q}^2) + \delta) \phi_q . \quad (7.13)$$

Note that there is no complex linear term in frequency here, as we consider the half-filled band and the imaginary linear frequency part of the particle-particle bubble and hence the boson propagator vanishes exactly. The control parameter term δ controls the distance to the continuous quantum phase transition and is also renormalized by fluctuations. If the initial value of δ is fine-tuned so that $\delta \rightarrow 0$ for vanishing cutoff $\Lambda \rightarrow 0$, we are in the quantum critical state with infinite susceptibility, $\chi \sim \frac{1}{\delta}|_{\Lambda \rightarrow 0}$. The boson propagator, parametrized by two RG parameters, reads

$$G_b(q) = -\langle \phi_q \phi_q^* \rangle = \frac{-1}{Z_b (q_0^2 + \mathbf{q}^2) + \delta} . \quad (7.14)$$

Recall that this initial ansatz for the boson propagator is motivated by the *intermediate* energy behavior of the particle-particle bubble as the low energy regime is excluded from the spectrum by the regulator \mathbf{R}^Λ . The *low energy* regime is controllably accessed subsequently in the coupled Fermi-Bose RG flow when \mathbf{R}^Λ , $\Lambda \rightarrow 0$. We will see below that, although we have started with a differentiable function of frequencies and momenta for the boson propagator at intermediate energies, at criticality in

the low energy regime a diverging Z_b -factor induces strong analyticities in the boson propagator –the order parameter field attains an anomalous dimension. The initial condition for Z_b is $Z_b = 0$ and for the control parameter $\delta = 1/U$.

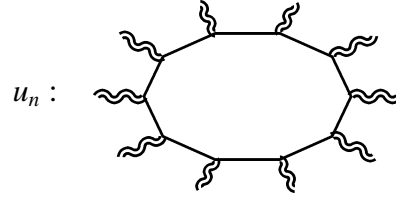
Order parameter self interactions

We now demonstrate how to account for direct self-interactions of the order parameter field within our coupled Fermi-Bose scheme. Recollect that in the conventional Hertz-Millis theory of quantum criticality (Hertz 1976, Millis 1993, Loehneysen 2006) one expands the purely bosonic action in (even) powers of the bosonic fields:

$$\gamma[\phi] = \sum_{n \geq 4, \text{ even}} \frac{u_n}{2 \left(\frac{n}{2}\right)! \left(\frac{n}{2}\right)!} (\phi^* \phi)^{n/2}, \quad (7.15)$$

where the coefficients u_n are generated by fermion loops with n fermion propagators and n external bosonic legs as shown in Fig. 7.3. At finite temperatures and when the fermions are gapped, such expressions are possibly large but finite. With the bare, gapless fermion propagator at zero temperature defined in Eq. (7.11), however, these coefficients are singular for small momenta:

$$u_n \sim \int d^{d+1}k \frac{1}{k^n} \sim \frac{1}{k^{n-(d+1)}}, \quad (7.16)$$



leading for instance to a power law singularity for the ϕ^4 coefficient $u_4 \equiv u \sim 1/k$ in $d = 2$. The presence of these singularities completely invalidates the Hertz-Millis approach of expanding the effective action in powers of the ordering field alone. Our coupled Fermi-Bose scheme is capable of renormalizing such power law singularities, as during the RG flow, fermionic fluctuations will generate order parameter self-interactions even if there is no ϕ^4 -term present in the bare action. To capture this, we keep the local fourth-order term in the effective action:

$$\Gamma_{|\phi|^4} = \frac{u}{8} \int_{q,q',p} \phi_{q+p}^* \phi_{q'-p}^* \phi_{q'} \phi_q. \quad (7.17)$$

The initial condition for u is $u = 0$. Note that the fermion-boson vertex in Eq. (7.4) is not renormalized within our truncation. The standard vertex correction one-loop diagram $\sim g^3$ vanishes by particle conservation. In the following, we keep the fermion-boson vertex at its bare value $g = 1$, which can be read off from Eq. (7.4).

Fig. 7.3. Fermion rings which generate the bosonic n -point vertex (here for $n = 10$).

7.3.2 Flow equations

In this subsection, we derive analytic expressions for our flow equations of the truncated effective action. Both Green functions, Eqs. (7.11, 7.14), display singularities for certain choices of momenta, the fermion propagator everywhere in the phase diagram, and the boson propagator at the QCP when the bosonic mass vanishes. These potential infrared singularities for $|\text{momenta}| < \Lambda$ are regularized by adding optimized momentum cutoffs (Litim 2001) for fermions (subscript f) and bosons (subscript b),

$$\begin{aligned} R_{f\Lambda}(\mathbf{k}) &= Z_f \left(-\Lambda \operatorname{sgn} [\xi_{\mathbf{k}}] + \xi_{\mathbf{k}} \right) \theta [\Lambda - |\xi_{\mathbf{k}}|] \\ R_{b\Lambda}(\mathbf{q}) &= Z_b \left(\Lambda^2 - \mathbf{q}^2 \right) \theta [\Lambda^2 - \mathbf{q}^2] \end{aligned} \quad (7.18)$$

to the inverse of the propagators in Eqs. (7.11, 7.14). The cutoff-endowed propagators are denoted with by G_{fR} and G_{bR} in the following. The scale-derivatives of the cutoffs read,

$$\begin{aligned} \partial_{\Lambda} R_{f\Lambda} &= \dot{R}_{f\Lambda} = -Z_f \operatorname{sgn} [\xi_{\mathbf{k}}] \theta [\Lambda - |\xi_{\mathbf{k}}|] \\ \dot{R}_{b\Lambda} &= 2Z_b \Lambda \theta [\Lambda^2 - \mathbf{q}^2] \ , \end{aligned} \quad (7.19)$$

where terms proportional to η_f and η_b defined below in Eq. (7.26) are neglected here. These additional terms are of higher order in the vertices and subleading. Further arguments buttressing this commonly employed procedure are given in (Berges 2002).

A comment on the choice of relative cutoff scale between fermions and bosons is in order. In principle, fermion fluctuations can be cut off at Λ_f and their bosonic counterparts at Λ_b with both cutoffs being independent functions of Λ . Without approximations, the results do not depend on the concrete choices of $\Lambda_f(\Lambda)$ and $\Lambda_b(\Lambda)$. In Eq. (7.18), we have chosen $\Lambda_f = \Lambda_b = \Lambda$; the standard choice for critical Fermi-Bose theories (Litim 2001, Gies 2004).

The recipe to obtain the flow equations is now the following: one executes a cutoff-derivative acting on $R_{f,b\Lambda}$ in the analytic expressions corresponding to all 1-loop one-particle-irreducible Feynman diagrams for the parameters Z_f, Z_b, δ, u , which can be generated with G_{fR} and G_{bR} as shown in Fig. 7.4. The subsequent trace operation is abbreviated by

$$\int_{k,R_s} = \int \frac{dk_0}{2\pi} \int \frac{d^d k}{(2\pi)^d} \sum_{s=f,b} (-\dot{R}_{s\Lambda}) \partial_{R_{s\Lambda}} . \quad (7.20)$$

The flow equation for the fermion self-energy is obtained from the Fock-type diagram in the first line of Fig. 7.4 involving G_{bR} and G_{fR} . This feedback of bosonic fluctuations on the fermionic propagator is captured via the flow equation:

$$\partial_{\Lambda} Z_f = g^2 \int_{q,R_s} \partial_{ik_0} G_{fR}(q-k) G_{bR}(q) |_{k=0} . \quad (7.21)$$

This expression vanishes for a local boson ($Z_b = 0$) from multiple poles in the upper complex frequency half-plane. This correctly reflects that for a momentum-independent four-fermion interaction, the fermionic Z_f -factor is renormalized only at the two-loop level. When reinserting the particle-particle bubble which generates Z_b in the third line of Fig. 7.4 into the bosonic propagator in the first line of Fig. 7.4, we indeed observe that effectively our flow equations capture two-loop effects by keeping the boson propagator as momentum- and frequency dependent ($Z_b \neq 0$).

For the control parameter, we evaluate the 1PI-diagrams with two external bosonic legs, and we obtain the two contributions:

$$\begin{aligned} \partial_\Lambda \delta = & g^2 \int_{k, R_f} G_{fR}(k) G_{fR}(-k) \\ & + \frac{u}{2} \int_{q, R_b} G_{bR}(q) , \end{aligned} \quad (7.22)$$

The fermionic contribution on the right-hand-side is positive leading to a reduction of δ for decreasing Λ whereas the bosonic contribution counteracts the fermions and tends to increase δ . This is the generic behavior of the bosonic fluctuations as they always tend to restore the symmetry.

The flow of the bosonic frequency renormalization is obtained as the second frequency derivative of the particle-particle bubble:

$$\partial_\Lambda Z_b = g^2 \int_{k, R_f} \frac{1}{2} \partial_{q_0}^2 G_{fR}(k+q) G_{fR}(-k) |_{q=0} . \quad (7.23)$$

The bosonic tadpole diagram does not contribute here, as the ϕ^4 -vertex u is taken as momentum- and frequency-independent.

Finally, the bosonic self-interaction flows according to:

$$\partial_\Lambda u = -4g^4 \int_{k, R_f} [G_{fR}(-k)]^2 [G_{fR}(k)]^2 + \frac{5}{4} u^2 \int_{q, R_b} [G_{bR}(q)]^2 , \quad (7.24)$$

where the first terms generates u and the second, bosonic term tends to reduce u in the course of the flow. All frequency and momentum integrations in the above

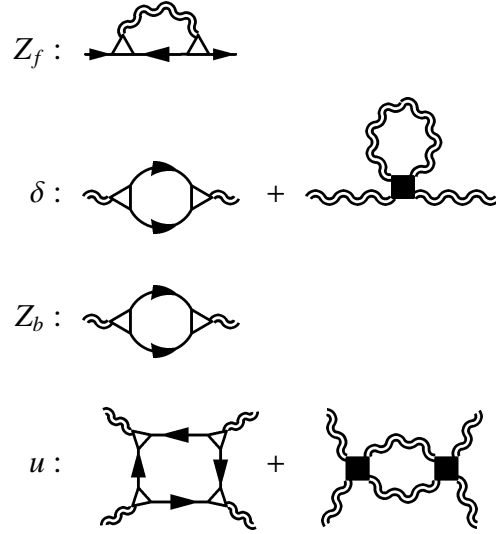


Fig. 7.4. Feynman diagrams representing the flow equations.

flow equations can be performed analytically. We now elegantly reformulate the flow equations by employing the following scaling variables:

$$\begin{aligned}\tilde{\delta} &= \frac{\delta}{\Lambda^2 Z_b} \\ \tilde{g} &= \frac{g \sqrt{K_d}}{\Lambda^{\frac{3-d}{2}} Z_f \sqrt{Z_b} \sqrt{d}} \\ \tilde{u} &= \frac{u K_d}{\Lambda^{3-d} Z_b^2 d} ,\end{aligned}\tag{7.25}$$

where K_d is defined by $\int \frac{d^d k}{(2\pi)^d} = K_d \int d|k| |k|^{d-1}$. By defining the anomalous exponents for the fermionic and bosonic Z-factor, respectively,

$$\begin{aligned}\eta_f &= -\frac{d \log Z_f}{d \log \Lambda} \\ \eta_b &= -\frac{d \log Z_b}{d \log \Lambda} ,\end{aligned}\tag{7.26}$$

the explicit dependence on the Z-factors disappears from the expressions. The flow equations for the control parameter and the bosonic self-interaction are obtained as:

$$\begin{aligned}\frac{d\tilde{\delta}}{d \log \Lambda} &= (\eta_b - 2) \tilde{\delta} + \tilde{g}^2 - \frac{\tilde{u}}{4 (1 + \tilde{\delta})^{3/2}} \\ \frac{d\tilde{u}}{d \log \Lambda} &= (d - 3 + 2\eta_b) \tilde{u} - 6 \tilde{g}^4 + \frac{15}{16} \frac{\tilde{u}^2}{(1 + \tilde{\delta})^{5/2}} .\end{aligned}\tag{7.27}$$

The rescaled fermion-boson vertex \tilde{g} obeys the equation:

$$\frac{d\tilde{g}}{d \log \Lambda} = \left(\eta_f + \frac{1}{2} \eta_b - \frac{3-d}{2} \right) \tilde{g} .\tag{7.28}$$

The equations (7.27, 7.28) have to be considered in conjunction with the fermion and boson anomalous exponents:

$$\begin{aligned}\eta_b &= \frac{3}{4} \tilde{g}^2 \\ \eta_f &= \tilde{g}^2 \left(\frac{1}{(1 + \tilde{\delta})^{3/2}} + \frac{2}{(1 + \tilde{\delta})} \right) \frac{1}{2 + \tilde{\delta} + 2 \sqrt{1 + \tilde{\delta}}} .\end{aligned}\tag{7.29}$$

We will now investigate the analytic properties of these equations and then solve them numerically.

7.4 Solution at the quantum critical point

At the quantum critical point, the system becomes scale-invariant, that is, the parameters show no dependence on the scale Λ . Translated into an algebraic condition, this becomes

$$\frac{d\tilde{\delta}}{d\log\Lambda} = \frac{d\tilde{g}}{d\log\Lambda} = \frac{d\tilde{u}}{d\log\Lambda} = 0, \quad (7.30)$$

and one has to solve Eqs. (7.27, 7.28) for fixed points together with the anomalous exponents of Eq. (7.29). It is immediately apparent that both, the fermion-boson vertex \tilde{g} and the boson self-interaction \tilde{u} are relevant couplings below three dimensions. For the $d = 2$ case possibly relevant for graphene and cold atoms in the honeycomb lattice, the RG equations for \tilde{g} and \tilde{u} have stable non-Gaussian ($\tilde{g} \neq 0$, $\tilde{u} \neq 0$) solutions with finite The anomalous scaling exponents are interrelated at the QCP:

$$\eta_f = \frac{3-d}{2} - \frac{1}{2}\eta_b, \quad (7.31)$$

anomalous exponents η_f and η_b as follows directly from Eq. (7.28). The values of the anomalous exponents from a numerical solution of Eqs. (7.27-7.29) under the constraint at the QCP, Eq. (7.30), are shown in Fig. 7.5.

At quantum criticality, the fermionic properties of the system cannot be described in terms of conventional Fermi liquid theory (Nozières 1964). A finite fermion anomalous dimension entails a fermion propagator of the form,

$$G_f(k_0, \mathbf{k}) \propto \frac{1}{(ik_0 - \xi_{\mathbf{k}})^{1-\eta_f}} \propto \frac{1}{\Lambda^{1-\eta_f}}, \quad (7.32)$$

with a non-analytic frequency-dependence of the fermion self-energy ($k_0 = \omega$):

$$\Sigma_f(\omega) \sim \omega^{1-\eta_f}, \quad (7.33)$$

where $1 - \eta_f = 0.68$ for $d = 2$ as can be read off from Fig. 7.5 (a). The quasi-particle picture breaks down. A similar quantum criticality induced breakdown of the Fermi liquid has been noted, among others, in the context of Fermi surface fluctuations near a Pomeranchuk instability (Metzner 2003, Dell'Anna 2006 and references therein).

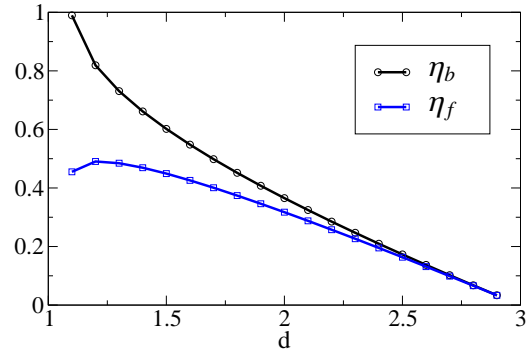


Fig. 7.5. Fermion and boson anomalous exponents at the QCP for $1 < d < 3$.

There, the frequency exponent of the fermion self-energy at the QCP is $\sim \omega^{2/3}$. The fermion propagator also develops a small Luttinger-like anomalous dimension in QED₃ (Franz 2002) and in the Gross-Neveu model (Rosa 2001, Herbut 2006).

Concerning the collective properties of the system at quantum criticality, a finite boson anomalous dimension entails an order parameter propagator of the form,

$$G_b(q_0, \mathbf{q}) \propto \frac{1}{(q_0^2 + \mathbf{q}^2)^{1-\eta_b}} \propto \frac{1}{\Lambda^{2-\eta_b}}, \quad (7.34)$$

with a non-analytic boson self-energy

$$\Sigma_b(q) \sim q^{2-\eta_b}, \quad (7.35)$$

where $2 - \eta_b = 1.63$ in two dimensions, see Fig. 7.5 (a). In a completely different context, at the antiferromagnetic QCP of the spin-fermion model in two dimensions, Chubukov *et al.* (Abanov 2000, Abanov 2003, Abanov 2004) estimated for the spin susceptibility the momentum scaling $\sim |\mathbf{q}|^{1.75}$ within a perturbative $1/N$ calculation where N is the number of hot spots on the Fermi surface. The physical origin of the anomalous momentum exponent for the spin-fermion model is different from that of the present work. There, peculiarities from antiferromagnetic scattering processes cause all ϕ^n -vertices to be marginal in $d = 2$. Summing these logarithms, Chubukov *et al.* then obtain the power law for the quantum critical bosonic self-energy alluded to above. This non-analyticity thus vanishes for $d > 2$ as the logarithms are special to $d = 2$. The present work most closely resembles the Gross-Neveu model with two fermion flavors where the boson anomalous dimension is however expected to be rather large $\eta_{b,\text{Gross-Neveu}} \approx 0.7$ (Rosa 2001, Herbut 2006).

By comparing the exponents for the quantum critical fermion and order parameter self-energies of attractive Dirac fermions to other physical contexts, we offer that some of the overarching *qualitative* features generic to various QCPs found with various methods are elegantly accessible within our coupled Fermi-Bose RG framework.

7.4.1 Quantum critical flows in two dimensions

We now establish a direct continuous link between the microscopic bare action in Eq. (7.4) and the infrared properties of the *effective action* at the QCP. For this purpose, we solve the flow equations (7.27-7.29) numerically as function of the flow parameter Λ in two dimensions. The initial conditions of our parameters are chosen to precisely match the bare action in Eq. (7.4): $u = 0$, $Z_b = 0$, $Z_f = 1$, and $g = 1$. As in the mean-field calculation of subsection 7.2.1, the Fermi velocity and the ultraviolet cutoff are set to unity $\Lambda_0 = v_f = 1$. To reach the quantum critical state, the initial value of δ is fine-tuned so that at the end of the flow, for $\Lambda \rightarrow 0$, $\delta \rightarrow 0$.

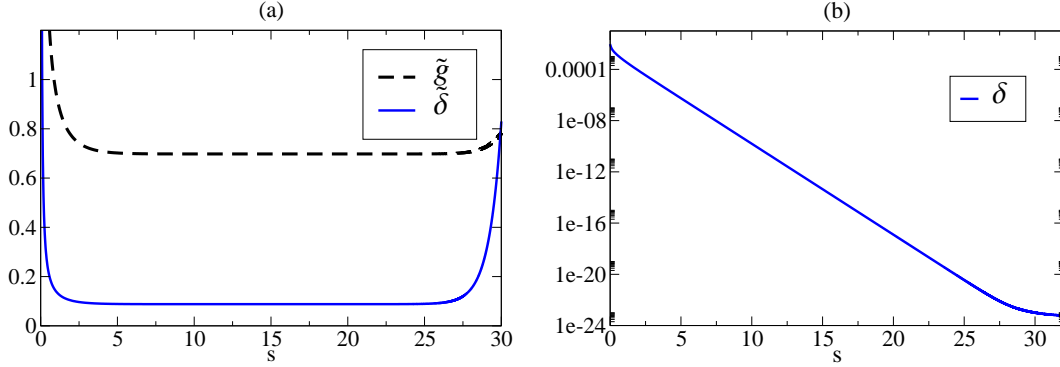


Fig. 7.6. (a) Flows of the rescaled control parameter and fermion-boson vertex versus $s = -\log[\Lambda/\Lambda_0]$. The ultraviolet (infrared) regime is on the left (right) side of the plots. (b): Flow of the control parameter δ at the QCP.

In Fig. 7.6 (b), we exhibit such a characteristic flow of the control parameter at the QCP versus cutoff scale in a double logarithmic plot. We observe scaling behavior over more than 20 (!) orders of magnitude limited only by numerical accuracy (note the small values of δ on the vertical axis). The slope is the value of the exponent with which the control parameter decreases:

$$\delta \sim \Lambda^{2-\eta_b} , \quad (7.36)$$

illustrated by the fixed point plateaus of the *rescaled* control parameter $\tilde{\delta}$ and also the rescaled fermion-boson vertex shown in Fig. 7.6 (a). The point we make here is, that we can verify whether the effective action is really *attracted* toward the quantum critical fixed point when one starts from the microscopic model and whether this behavior is numerically *stable*. Beyond doubt, this is indeed the case here.

In Fig. 7.7, we present flows for the fermionic and bosonic frequency- and momentum renormalization factors Z_f and Z_b as well as the associated anomalous dimensions η_f and η_b . In Fig. 7.7 (b), we observe that although Z_b is zero initially, it is generated for small s (large Λ) and subsequently diverges as a power law with slope η_b : $Z_b \sim 1/\Lambda^{\eta_b}$, which is underlined by fixed point plateaus of η_b shown in Fig. 7.7 (a). The fermionic Z_f is initially equal to unity and then also diverges as a power law

$$Z_f \sim \frac{1}{\Lambda^{\eta_f}} , \quad (7.37)$$

with a slightly smaller slope than Z_b to be read off from the fixed point plateau of η_f in Fig. 7.7 (a). The numerical solution for both Z-factors exactly fulfills the interrelation condition Eq. (7.31) and the fixed point values precisely match those of Fig. 7.5 at $d = 2$. We show flows of the ϕ^4 -vertex in Fig. 7.8. Starting from zero initial value, fermion fluctuations quickly generate u as is observed in the peak for small s in Fig.

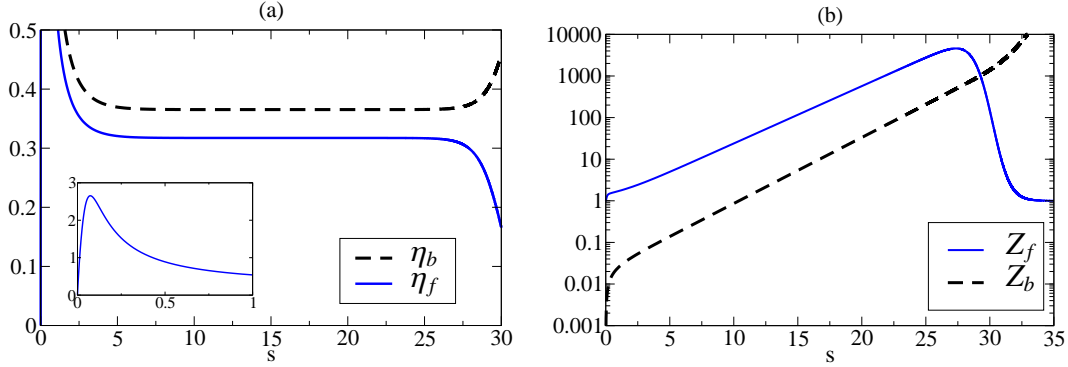


Fig. 7.7. (a): Scaling plateaus of the fermion and boson anomalous dimensions at quantum criticality versus $s = -\log[\Lambda/\Lambda_0]$. The fermion anomalous dimension starts off at zero (inset) and becomes finite as soon as $Z_b \neq 0$, see discussion below Eq. (7.21). (b): Flow of the bosonic and fermionic frequency- and momentum factors Z_f and Z_b .

7.8 (b), and then the interplay of fermionic and bosonic fluctuations leads to the power law scaling behavior

$$u \sim \Lambda^{3-d-2\eta_b}, \quad (7.38)$$

again accompanied by fixed point plateaus of \tilde{u} depicted in Fig. 7.8 (a).

We emphasize that our RG equations not only yield various scaling exponents at the QCP, but are also useful in determining *non-universal* properties of the system. The characteristic scale Λ_{QC} at which the quantum critical asymptotics sets in, for example, can be determined. From Fig. 7.7, we find that the anomalous dimensions attain their fixed point values at $s \approx 5$ and therefore $\Lambda_{\text{QC}} \approx \Lambda_0 e^{-5}$.

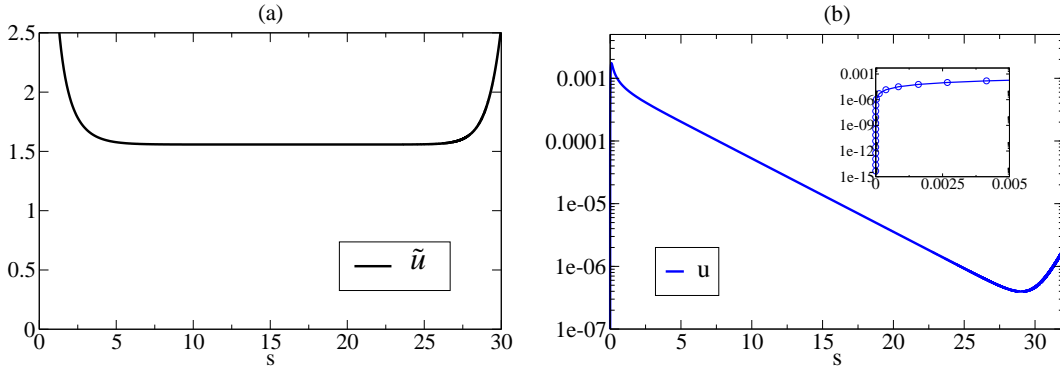


Fig. 7.8. (a): Fixed point plateau of the rescaled ϕ^4 -coupling versus $s = -\log[\Lambda/\Lambda_0]$. (b): Flow of the quartic coupling u . Inset: Small- s behavior when fermionic fluctuations generate u .

Additionally, we can compute the renormalized interaction strength U_c at which the system becomes quantum critical and compare it to the mean-field value derived in Eq. (7.8) since we have chosen the same values for the upper band cutoff ($\Lambda_0 = 1$) and the Fermi velocity ($v_f = 1$) as in the mean-field calculation. U_c is the inverse of the fine-tuned initial value of the control parameter ($\delta_{\Lambda=\Lambda_0} = 0.009032269344423279716$) such that δ vanishes at the end of the flow. We find for the ratio between mean-field and RG interaction strengths:

$$\frac{U_c}{U_{c,\text{MFT}}} \approx 17.6, \quad (7.39)$$

therewith renormalizing the mean-field position of the QCP in Fig. 7.1 to the left. Fluctuations drastically reduce the size of the superfluid phase.

7.4.2 Quantum critical exponents

When approaching a critical point along the relevant parameter axis, the susceptibility and correlation length diverge as a power law. The presence of gapless fermions places the quantum phase transition considered in this chapter outside the usual Ginzburg-Landau-Wilson paradigm, as distinctively signalled by the fermion anomalous dimension η_f (see Figs. 7.5 and 7.7) which governs the disappearance of quasi-particles when approaching the QCP from the semimetallic side. η_f influences all other critical exponents similar to the universality class of the Gross-Neveu model to which the semimetal to anti-ferromagnetic insulator QCP for *repulsively* interacting electrons in the 2d-honeycomb lattice has been proposed to belong to (Herbut 2006).

We now compute the susceptibility exponent for $d = 2$ in the vicinity of the QCP,

$$\chi \sim \frac{1}{(\delta - \delta_{\text{crit}})^\gamma}, \quad (7.40)$$

where the inverse susceptibility is identified with the (non-rescaled) mass term δ of the bosonic propagator, see Eq. (7.14). In Fig. 7.9, we present a double-logarithmic plot of the susceptibility at the end of the flow $\chi^{-1} = \delta|_{\Lambda \rightarrow 0}$ versus the difference of initial values of the control parameter, where δ_{crit} corresponds to the location of the QCP: $\chi_{\Lambda \rightarrow 0}^{-1}(\delta_{\text{crit}}) \rightarrow 0$. γ can be read off from the slope in Fig. 7.9:

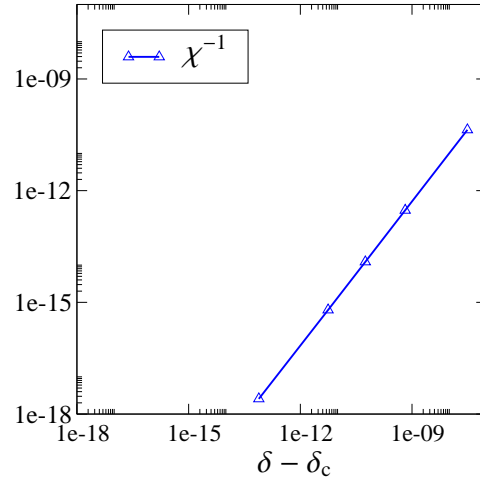


Fig. 7.9. Logarithmic plot of the inverse susceptibility versus δ in $d = 2$.

$$\gamma = 1.3 . \quad (7.41)$$

The correlation length exponent ν now follows from the scaling relation (Goldenfeld 1992, Kaul 2008): $\gamma = \nu(2 - \eta_b)$. With $\eta_b = 0.37$ in $d = 2$ from Fig. 7.7, one obtains:

$$\nu = 0.8 . \quad (7.42)$$

The critical exponents of the structurally similar Gross-Neveu model were computed with functional RG methods by Rosa et al. (2001). In a recent paper on a field theory containing bosons, fermions, and a gauge field, various quantum critical exponents were estimated in the limit of large number of fermion and boson species (Kaul 2008).

7.5 Conclusion

In this chapter, we derived coupled flow equations for fermionic and bosonic degrees of freedom in quantum critical fermion systems. These equations capture the mutual feedback of two distinct types of gapless fluctuations: the first associated with zero temperature fermions and the second with massless order parameter fluctuations. As a first application, we computed various scaling exponents for the quantum critical point between the semimetal and superfluid phase of attractive Dirac fermions. The fermion and order parameter propagators are non-analytic functions of frequency and momentum. In two dimensions, the fermionic self-energy as function of frequency scales $\sim \omega^{0.68}$ leading to a complete breakdown of the Fermi liquid. We demonstrated how to compute the susceptibility and correlation length exponents when approaching the QCP along the control parameter axis and presented first estimates thereof.

Extending the work of this chapter to finite temperatures is interesting. For example the correlation length in the quantum critical regime as a function of temperature, $\xi(T, \delta_{\text{crit}})$, when approaching the QCP vertically from the top (see Fig. 7.1), would be worthwhile to investigate within our coupled Fermi-Bose RG.

In the next chapter, we combine the bosonic truncations devised for phases with broken symmetry in chapters 5 and 6 with the normal phase analysis in terms of fermionic and bosonic fields in chapter 7 and we compute various physical properties of fermionic superfluids at $T = 0$ with a coupled fermion-boson action.

Fermionic superfluids at zero temperature

8.1 Introduction

In this chapter, we analyze the attractive Hubbard model as a prototype of a Fermi system with a superfluid low temperature phase (Micnas 1990). An experimental realization of the attractive Hubbard model is conceivable by trapping fermionic atoms in an optical lattice and tuning the interaction close to a Feshbach resonance (Hofstadter 2002, Jaksch 2005, Chin 2006).

We here theoretically focus on the superfluid ground state for which the importance of quantum fluctuations has been emphasized recently in the context of the BCS-BEC crossover (Diener 2008). Although the long-range order is not destroyed by fluctuations in dimensions $d > 1$, the order parameter correlations are nevertheless non-trivial in $d \leq 3$. The Goldstone mode leads to severe infrared divergences in perturbation theory. A detailed analysis of the infrared behavior of fermionic superfluids has appeared earlier in the mathematical literature (Feldman 1993), where the perturbative renormalizability of the singularities associated with the Goldstone mode was established rigorously. To a large extent divergences of Feynman diagrams cancel due to Ward identities, while the remaining singularities require a renormalization group treatment. Since the fermions are gapped at low energy scales, the infrared behavior of the collective, bosonic sector in fermionic superfluids is equivalent to the one of an interacting Bose gas, where the Goldstone mode of the condensed state strongly affects the longitudinal correlations, leading to drastic deviations from mean-field theory in dimensions $d \leq 3$ (Nepomnyashchy 1992, Pistolesi 2004) as already demonstrated within the functional RG setting in chapter 6.

Technically, we implement the order parameter via a Hubbard-Stratonovich field and we compute the renormalized effective action for the coupled theory of bosons and fermions by truncating the exact hierarchy of flow equations for the one-particle irreducible vertex functions (Baier 2004, Schütz 2005, Schütz 2006). A truncation of this hierarchy has been applied a few years ago to the antiferromagnetic state of the two-dimensional repulsive Hubbard model (Baier 2004). Important features of the

quantum antiferromagnet at low temperatures were captured by the flow. More recently, various aspects of superfluidity in attractively interacting Fermi systems have been studied in the fRG framework with a Hubbard-Stratonovich field for the superfluid order parameter. Approximate flow equations were discussed previously for the superfluid ground state (Krippa 2005), for the Kosterlitz-Thouless transition in two-dimensional superfluids (Krahl 2007) and for the BCS-BEC crossover in three-dimensional cold atomic Fermi gases (Diehl 2007).

The purpose of this chapter is to construct a relatively simple truncation of the exact fRG flow which is able to describe the correct infrared asymptotic behavior, and which yields reasonable estimates for the magnitude of the order parameter at least for weak and moderate interaction strength. From a numerical solution of the flow equations, which we perform in two dimensions, we obtain information on the importance of Goldstone modes and other fluctuation effects.

In Sec. 8.2, we introduce the bare fermion-boson action obtained from the attractive Hubbard model by a Hubbard-Stratonovich transformation. Neglecting bosonic fluctuations, one recovers the standard mean-field theory for fermionic superfluids, as recapitulated in Sec. 8.3. By truncating the exact fRG hierarchy, we derive approximate flow equations involving fermionic and bosonic fluctuations in Sec. 8.4. At the end of that section we reconsider mean-field theory from a flow equation perspective. Sec. 8.5 is dedicated to a discussion of results obtained by solving the flow equations. We discuss the asymptotic behavior in the infrared limit in two and three dimensions and then present numerical results for the flow in two dimensions, where fluctuation effects are most pronounced. Finally, we summarize our results in Sec. 8.6.

8.2 Bare action

As a prototype model for the formation of a superfluid ground state in an interacting Fermi system we consider the attractive Hubbard model represented by the Hamiltonian

$$H = \sum_{\mathbf{i}, \mathbf{j}} \sum_{\sigma} t_{\mathbf{ij}} c_{\mathbf{i}\sigma}^{\dagger} c_{\mathbf{j}\sigma} + U \sum_{\mathbf{i}} n_{\mathbf{i}\uparrow} n_{\mathbf{i}\downarrow} , \quad (8.1)$$

where $c_{\mathbf{i}\sigma}^{\dagger}$ and $c_{\mathbf{i}\sigma}$ are creation and annihilation operators for spin- $\frac{1}{2}$ fermions with spin orientation σ on a lattice site \mathbf{i} . For the hopping matrix we employ $t_{\mathbf{ij}} = -t$ if \mathbf{i} and \mathbf{j} are nearest neighbors on the lattice, and $t_{\mathbf{ij}} = 0$ otherwise. On a d -dimensional simple cubic lattice, this leads to a dispersion relation $\epsilon_{\mathbf{k}} = -2t \sum_{i=1}^d \cos k_i$. For the attractive Hubbard model the coupling constant U is negative.

The attractive Hubbard model has a superfluid ground state for any particle density n in $d \geq 2$ dimensions (Micnas 1990), provided the lattice is not completely

filled ($n = 2$) or empty ($n = 0$). The Fermi surface for the fiducial case of a quarter filled band is shown in Fig. 8.1. At half filling ($n = 1$) the usual U(1) global gauge symmetry becomes a subgroup of a larger SO(3) symmetry group, and the order parameter for superfluidity mixes with charge density order (Micnas 1990).

Our analysis is based on a functional integral representation of the effective action, that is, the generating functional of one-particle irreducible correlation functions. For the Hubbard model, the starting point is a functional integral over fermionic fields ψ and $\bar{\psi}$ with the *bare* action

$$\begin{aligned} \Gamma_0[\psi, \bar{\psi}] = & - \int_{k\sigma} \bar{\psi}_{k\sigma}(ik_0 - \xi_{\mathbf{k}}) \psi_{k\sigma} \\ & + \int_{k,k',q} U \bar{\psi}_{-k+\frac{q}{2}\downarrow} \bar{\psi}_{k+\frac{q}{2}\uparrow} \psi_{k'+\frac{q}{2}\uparrow} \psi_{-k'+\frac{q}{2}\downarrow}, \end{aligned} \quad (8.2)$$

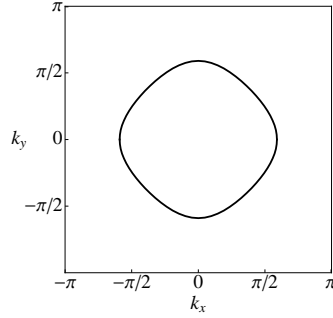


Fig. 8.1. Exemplary Fermi surface for a quarter-filled band.

where $\xi_{\mathbf{k}} = \epsilon_{\mathbf{k}} - \mu$ is the single-particle energy relative to the chemical potential. The variables $k = (k_0, \mathbf{k})$ and $q = (q_0, \mathbf{q})$ collect Matsubara energies and momenta. We use the short-hand notation $\int_k = \int_{k_0} \int_{\mathbf{k}} = \int_{-\infty}^{\infty} \frac{dk_0}{2\pi} \int_{-\pi}^{\pi} \frac{d^d \mathbf{k}}{(2\pi)^d}$ for momentum and energy integrals, and $\int_{k\sigma}$ includes also a spin sum. We consider only *ground state* properties, so that the energy variables are continuous.

The attractive interaction drives spin-singlet pairing with s-wave symmetry and a spontaneous breaking of the global U(1) gauge symmetry. Therefore, we decouple the Hubbard interaction in the s-wave spin-singlet pairing channel by introducing a complex bosonic Hubbard-Stratonovich field ϕ_q conjugate to the bilinear composite of fermionic fields (Popov 1987)

$$\tilde{\phi}_q = U \int_k \psi_{k+\frac{q}{2}\uparrow} \psi_{-k+\frac{q}{2}\downarrow}. \quad (8.3)$$

This yields a functional integral over ψ , $\bar{\psi}$ and ϕ with the new bare action

$$\begin{aligned} \Gamma_0[\psi, \bar{\psi}, \phi] = & - \int_{k\sigma} \bar{\psi}_{k\sigma}(ik_0 - \xi_{\mathbf{k}}) \psi_{k\sigma} - \int_q \phi_q^* \frac{1}{U} \phi_q \\ & + \int_{k,q} \left(\bar{\psi}_{-k+\frac{q}{2}\downarrow} \bar{\psi}_{k+\frac{q}{2}\uparrow} \phi_q + \psi_{k+\frac{q}{2}\uparrow} \psi_{-k+\frac{q}{2}\downarrow} \phi_q^* \right). \end{aligned} \quad (8.4)$$

where ϕ^* is the complex conjugate of ϕ , while ψ and $\bar{\psi}$ are algebraically independent Grassmann variables. Our aim is to compute fermionic and bosonic correlation functions with focus on the correct description of the low energy (infrared) behavior.

8.3 Mean-field theory

As a warm-up for the renormalization group treatment it is instructive to recapitulate the mean-field theory for the superfluid phase in the functional integral formalism (Popov 1987). In mean-field approximation bosonic fluctuations are neglected, that is, the bosonic field ϕ is fixed instead of being integrated over all possible configurations. The fermion fields can be integrated exactly. The (fixed) bosonic field is determined by minimizing the effective action as a functional of ϕ . For a homogeneous system, the minimizing ϕ_q can be non-zero only for $q = 0$. We denote the minimum by α . Substituting $\phi_0 \rightarrow \alpha + \phi_0$ yields

$$\begin{aligned} \Gamma_0[\psi, \bar{\psi}, \alpha + \phi] = & - \int_{k\sigma} \bar{\psi}_{k\sigma} (ik_0 - \xi_{\mathbf{k}}) \psi_{k\sigma} - \alpha^* \frac{1}{U} \alpha + \int_k (\bar{\psi}_{-k\downarrow} \bar{\psi}_{k\uparrow} \alpha + \psi_{k\uparrow} \psi_{-k\downarrow} \alpha^*) \\ & - \frac{1}{U} (\alpha^* \phi_0 + \alpha \phi_0^*) + \int_{k,q} \left(\bar{\psi}_{-k+\frac{q}{2}\downarrow} \bar{\psi}_{k+\frac{q}{2}\uparrow} \phi_q + \psi_{k+\frac{q}{2}\uparrow} \psi_{-k+\frac{q}{2}\downarrow} \phi_q^* \right) \\ & - \int_q \phi_q^* \frac{1}{U} \phi_q . \end{aligned} \quad (8.5)$$

A necessary condition for a minimum of the effective action is that its first derivative with respect to ϕ (or ϕ^*), that is, the bosonic 1-point function $\Gamma_b^{(1)}(q)$, vanishes. In other words, terms linear in ϕ (or ϕ^*) have to vanish in the effective action. For $q \neq 0$, $\Gamma_b^{(1)}(q)$ vanishes for any choice of α in a homogeneous system. For $q = 0$ and in mean-field approximation, the 1-point function is given by

$$\Gamma_b^{(1)}(0) = -\frac{1}{U} \alpha + \int_k \langle \psi_{k\uparrow} \psi_{-k\downarrow} \rangle , \quad (8.6)$$

where $\langle \dots \rangle$ denotes expectation values. The first term on the right hand side corresponds to the contribution $-\frac{1}{U} \alpha \phi_0^*$ to Γ_0 in the second line of Eq. (8.5), while the second term is generated by contracting the fermions in the contribution proportional to ϕ_q^* in the second line of Eq. (8.5). In the absence of bosonic fluctuations there is no other contribution to $\Gamma_b^{(1)}$. From the condition $\Gamma_b^{(1)}(0) = 0$ one obtains

$$\alpha = U \int_k \langle \psi_{k\uparrow} \psi_{-k\downarrow} \rangle , \quad (8.7)$$

which relates α to a fermionic expectation value. We now turn to the fermionic 2-point functions. The normal fermionic propagator $G_{f\sigma}(k) = -\langle \psi_{k\sigma} \bar{\psi}_{k\sigma} \rangle$ and the anomalous propagators $F_f(k) = -\langle \psi_{k\uparrow} \psi_{-k\downarrow} \rangle$ and $\bar{F}_f(k) = -\langle \bar{\psi}_{-k\downarrow} \bar{\psi}_{k\uparrow} \rangle$ can be conveniently collected in a Nambu matrix propagator

$$\mathbf{G}_f(k) = \begin{pmatrix} G_{f\uparrow}(k) & F_f(k) \\ \bar{F}_f(k) & -G_{f\downarrow}(-k) \end{pmatrix} . \quad (8.8)$$

The anomalous propagators satisfy the relations $\bar{F}_f(k) = F_f^*(k)$ and $F_f(-k) = F_f(k)$. In (our) case of spin rotation invariance the normal propagator does not depend on σ , and therefore, $G_{f\uparrow}(k) = G_{f\downarrow}(k) = G_f(k)$.

In mean-field theory, the fermionic 2-point vertex function $\mathbf{\Gamma}_f^{(2)} = -\mathbf{G}_f^{-1}$ can be read off directly from the bare action in the form Eq. (8.5):

$$\mathbf{\Gamma}_f^{(2)}(k) = - \begin{pmatrix} ik_0 - \xi_{\mathbf{k}} & \alpha \\ \alpha^* & ik_0 + \xi_{-\mathbf{k}} \end{pmatrix}. \quad (8.9)$$

The off-diagonal elements are due to the last bracket in the first line of Eq. (8.5). Tadpole contributions which are generated from the terms in the second and third line of Eq. (8.5) cancel exactly by virtue of the condition $\Gamma_b^{(1)} = 0$. In the absence of bosonic fluctuations there are no other contributions to $\mathbf{\Gamma}_f^{(2)}$. Inverting $\mathbf{\Gamma}_f^{(2)}$ and using $\xi_{-\mathbf{k}} = \xi_{\mathbf{k}}$ from reflection symmetry yields

$$G_f(k) = \frac{-ik_0 - \xi_{\mathbf{k}}}{k_0^2 + E_{\mathbf{k}}^2} \quad (8.10)$$

$$F_f(k) = \frac{\Delta}{k_0^2 + E_{\mathbf{k}}^2}, \quad (8.11)$$

where $E_{\mathbf{k}} = (\xi_{\mathbf{k}}^2 + |\Delta|^2)^{1/2}$ and $\Delta = \alpha$. We observe that in mean-field theory the bosonic order parameter α is equivalent to the gap Δ in the fermionic excitation spectrum. Eq. (8.6) corresponds to the BCS gap equation

$$\Delta = -U \int_k F_f(k). \quad (8.12)$$

We finally compute the bosonic 2-point functions in mean-field theory (see Keller (1999) for a more detailed explanation of the diagrammatic ingredients and the notation in the superfluid phase). The bosonic propagators $G_b(q) = -\langle \phi_q \phi_q^* \rangle$ and $F_b(q) = -\langle \phi_q \phi_{-q} \rangle = -\langle \phi_{-q}^* \phi_q^* \rangle^*$ form the matrix propagator

$$\mathbf{G}_b(q) = \begin{pmatrix} G_b(q) & F_b(q) \\ F_b^*(q) & G_b(-q) \end{pmatrix}. \quad (8.13)$$

Note that $F_b(-q) = F_b(q)$. The bosonic 2-point function $\mathbf{\Gamma}_b^{(2)}$ is equal to $-\mathbf{G}_b^{-1}$. We define a bosonic self-energy $\mathbf{\Sigma}_b$ via the Dyson equation $(\mathbf{G}_b)^{-1} = (\mathbf{G}_{b0})^{-1} - \mathbf{\Sigma}_b$, where the bare propagator corresponding to the bare action Γ_0 is given by

$$\mathbf{G}_{b0}(q) = \begin{pmatrix} U & 0 \\ 0 & U \end{pmatrix}. \quad (8.14)$$

In mean-field theory, only fermionic bubble diagrams contribute to the bosonic self-energy:

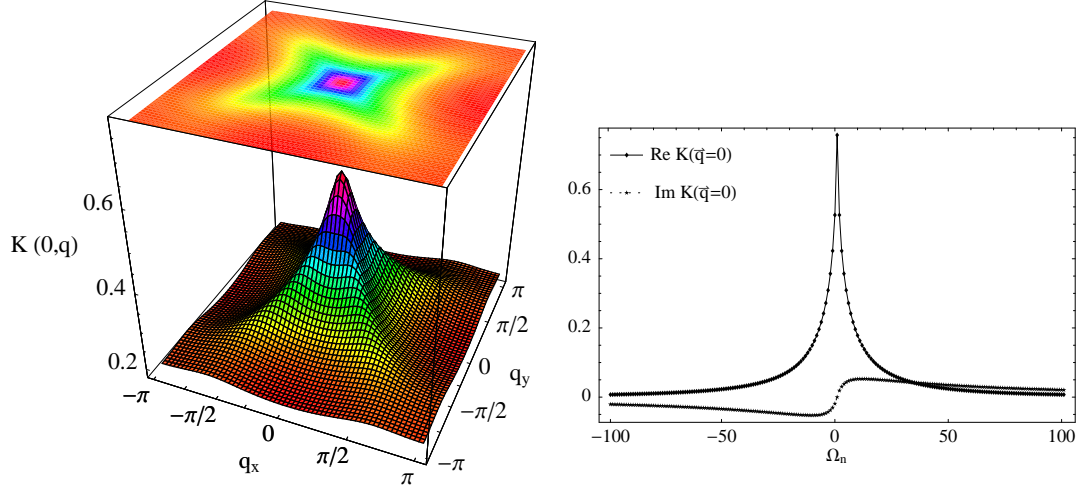


Fig. 8.2. Momentum (left) and frequency (right) dependence of $K(q)$ in the normal phase. The small linear frequency dependence in the imaginary part vanishes at half-filling and is discussed in Sec. 8.4.

$$\Sigma_b(q) = \begin{pmatrix} K(q) & L(q) \\ L^*(q) & K(-q) \end{pmatrix}, \quad (8.15)$$

where

$$K(q) = - \int_k G_f(k+q) G_f(-k) \quad (8.16)$$

$$L(q) = \int_k F_f(k+q) F_f(-k), \quad (8.17)$$

see Fig. 8.2 for an exemplary plot of $K(q)$ in the normal phase. In the absence of bosonic fluctuations, there are no other contributions to Σ_b . Tadpole diagrams cancel due to $\Gamma_b^{(1)} = 0$. Note that $K(-q) = K^*(q)$ while $L(-q) = L(q)$. Inverting the matrix $\mathbf{G}_{b0} - \Sigma_b$ one obtains the bosonic propagator in mean-field approximation

$$\mathbf{G}_b(q) = \frac{1}{d(q)} \begin{pmatrix} U^{-1} - K(-q) & L(q) \\ L^*(q) & U^{-1} - K(q) \end{pmatrix}, \quad (8.18)$$

with the determinant $d(q) = |U^{-1} - K(q)|^2 - |L(q)|^2$. Using the explicit expressions (8.10) and (8.11) for G_f and F_f , respectively, one can see that

$$U^{-1} - K(0) + |L(0)| = U^{-1} + \frac{1}{\Delta} \int_k F_f(k), \quad (8.19)$$

which vanishes if Δ is non-zero and satisfies the gap equation. Hence $d(q)$ has a zero and $\mathbf{G}_b(q)$ a pole in $q = 0$. This pole corresponds to the Goldstone mode associated with the spontaneous breaking of the U(1) symmetry of the model. For small finite \mathbf{q} and q_0 , the leading q -dependences of $|U^{-1} - K(q)|$ and $L(q)$ are of order $|\mathbf{q}|^2$ and q_0^2 . Hence the divergence of $\mathbf{G}_b(q)$ for $q \rightarrow 0$ is quadratic in \mathbf{q} and q_0 . Continuing q_0 to real frequencies one obtains a propagating mode with a linear dispersion relation. The second pole of $d(q)$ is gapped and features a quadratic momentum dispersion.

By appropriately tailoring the fRG-truncation in Sec. 8.4 to the results of this mean-field calculation in the superfluid phase, we incorporate the effects of transversal Goldstone fluctuations as well as longitudinal fluctuations into our computation.

8.4 Truncation

At the core of our analysis is the exact functional flow equation for the scale-dependent effective action Γ^Λ , which generates all 1PI correlation functions (Wetterich 1993, Berges 2002, Salmhofer 2001, Metzner 2005):

$$\frac{d}{d\Lambda} \Gamma^\Lambda[\mathcal{S}, \bar{\mathcal{S}}] = \text{Str} \frac{\mathbf{R}^\Lambda}{\mathbf{\Gamma}^{(2)\Lambda}[\mathcal{S}, \bar{\mathcal{S}}] + \mathbf{R}^\Lambda}, \quad (8.20)$$

where $\mathbf{\Gamma}^{(2)\Lambda} = \partial^2 \Gamma^\Lambda[\mathcal{S}, \bar{\mathcal{S}}] / \partial \mathcal{S} \partial \bar{\mathcal{S}}$ denotes the second functional derivative with respect to the superfields and the supertrace (str) traces over all indices with an additional minus sign for fermionic contractions. We refer to Section 3.2 for a detailed exposition of the functional RG formalism including symmetry-breaking.

Untruncated, the exact effective action contains an infinite number of terms of arbitrary order in fermionic and/or bosonic fields. We now describe which terms are kept and how they are parametrized. We keep all terms which are crucial for a qualitatively correct description of the low-energy behavior of the system. We distinguish the symmetric regime, where $\alpha = 0$, from the symmetry broken regime, where $\alpha \neq 0$. The former applies to large Λ , the latter to small Λ .

8.4.1 Symmetric regime

The bare action Eq. (8.4) contains quadratic terms for fermions and bosons, and an interaction term where bosons couple linearly to a fermion bilinear. In the effective action we keep these terms with generalized cutoff-dependent parameters and add a bosonic self-interaction of order $|\phi|^4$. The latter is generated by the flow and becomes crucial when the quadratic part of the bosonic potential changes sign. Other interactions generated by the flow are neglected. For our choice of parameters (relatively small U), the fermionic propagator receives only Fermi liquid renormalizations, leading to a slightly reduced quasi particle weight and a weakly renormalized dispersion relation. We neglect these quantitatively small effects and leave the quadratic

fermionic term in the action unrenormalized, that is,

$$\Gamma_{\bar{\psi}\psi} = - \int_{k\sigma} \bar{\psi}_{k\sigma}(ik_0 - \xi_{\mathbf{k}}) \psi_{k\sigma}, \quad (8.21)$$

corresponding to an unrenormalized fermionic propagator

$$G_f(k) = G_{f0}(k) = \frac{1}{ik_0 - \xi_{\mathbf{k}}}. \quad (8.22)$$

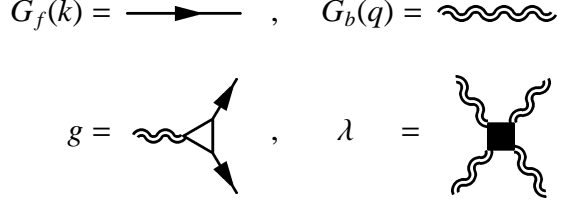


Fig. 8.3. Diagrammatic constituents of our truncation in the symmetric regime as described in Sec. 8.4.1.

In the bare action the term quadratic in bosons contains only a mass term. In the effective action this mass decreases with decreasing cutoff until it vanishes at a critical scale Λ_c , which marks the transition to the symmetry-broken regime. As the mass decreases, the momentum and frequency dependence of the bosonic 2-point function becomes important. The latter is generated in particular by fermionic fluctuations. For small \mathbf{q} , the leading \mathbf{q} -dependence is of order $|\mathbf{q}|^2$. The leading frequency-dependent contribution to the real part of the bosonic 2-point function is of order q_0^2 . The frequency-dependence of the imaginary part is generally of order q_0 but the prefactor is very small which is related to the fact that it vanishes completely in case of particle-hole symmetry. Furthermore this small imaginary part does not have any qualitative impact on the quantities we compute in the following. We therefore neglect this term and make the ansatz

$$\Gamma_{\phi^*\phi} = \frac{1}{2} \int_q \phi_q^* (m_b^2 + Z_b q_0^2 + A_b \omega_{\mathbf{q}}^2) \phi_q, \quad (8.23)$$

where $\omega_{\mathbf{q}}^2 = 2 \sum_{i=1}^d (1 - \cos q_i)$ is fixed, while m_b^2 , Z_b , and A_b are cutoff-dependent numbers. The function $\omega_{\mathbf{q}}^2$ has been chosen such that the quadratic momentum dependence for small \mathbf{q} is continued to a periodic function defined on the entire Brillouin zone. The initial conditions for the parameters in the bosonic 2-point function,

$$G_b(q) = -\frac{2}{Z_b q_0^2 + A_b \omega_{\mathbf{q}}^2 + m_b^2}, \quad (8.24)$$

can be read off from the bare action as $m_b^2 = |2/U|$ and $Z_b = A_b = 0$.

The interaction between fermions and bosons remains regular and finite near Λ_c . It can therefore be parametrized as

$$\Gamma_{\psi^2\phi^*} = g \int_{k,q} \left(\bar{\psi}_{-k+\frac{q}{2}\downarrow} \bar{\psi}_{k+\frac{q}{2}\uparrow} \phi_q + \psi_{k+\frac{q}{2}\uparrow} \psi_{-k+\frac{q}{2}\downarrow} \phi_q^* \right), \quad (8.25)$$

where the coupling constant g depends on the cutoff, but not on momentum and frequency. The initial condition for g is $g = 1$.

The flow generates a bosonic self-interaction which plays a crucial role near and in the symmetry-broken regime, that is, when the bosonic mass term becomes small and finally changes sign. The most relevant term is a local $|\phi|^4$ -interaction

$$\Gamma_{|\phi|^4} = \frac{\lambda}{8} \int_{q,q',p} \phi_{q+p}^* \phi_{q'-p}^* \phi_{q'} \phi_q , \quad (8.26)$$

where the coupling constant λ depends on the cutoff but not on momentum and frequency. The initial condition for λ is $\lambda = 0$.

The propagators and vertices are represented diagrammatically in Fig. 8.3.

8.4.2 Symmetry-broken regime

For $\Lambda < \Lambda_c$ the effective action develops a minimum at $\phi_{q=0} = \alpha \neq 0$. Due to the U(1) symmetry associated with charge conservation the minimum is degenerate with respect to the phase of α . We here employ the σ - Π model presented previously in section 6.2 consisting of the quartic coupling λ and the minimum α , see Eqs. (6.2, 6.3, 6.7). In this chapter we focus on the case $N = 2$ degrading the vector field Π to a one-component field π representing the Goldstone mode. The leading momentum and frequency dependence of the bosonic 2-point function is quadratic in \mathbf{q} and q_0 , both for the σ - and π -component. Hence we make the following ansatz for the quadratic bosonic contributions to the effective action

$$\begin{aligned} \Gamma_{\sigma\sigma} &= \frac{1}{2} \int_q \sigma_{-q} (m_\sigma^2 + Z_\sigma q_0^2 + A_\sigma \omega_{\mathbf{q}}^2) \sigma_q \\ \Gamma_{\pi\pi} &= \frac{1}{2} \int_q \pi_{-q} (Z_\pi q_0^2 + A_\pi \omega_{\mathbf{q}}^2) \pi_q . \end{aligned} \quad (8.27)$$

$G_f(k) = \text{---}\blacktriangleright\text{---} \quad , \quad F_f(k) = \text{---}\blacktriangleleft\text{---}$

$G_\sigma(k) = \text{-----} \quad , \quad G_\pi(k) = \text{~~~~~}$

$g_\sigma = \text{---}\triangleleft\text{---}$

$g_\pi = \text{~~~~~}\triangleleft\text{---}$

where m_σ , Z_σ , A_σ , Z_π , and A_π are cut-off dependent real numbers. The propagators for the σ and π fields thus have the form

$$\begin{aligned} G_\sigma(q) &= -\frac{1}{m_\sigma^2 + Z_\sigma q_0^2 + A_\sigma \omega_{\mathbf{q}}^2} \\ G_\pi(q) &= -\frac{1}{Z_\pi q_0^2 + A_\pi \omega_{\mathbf{q}}^2} . \end{aligned} \quad (8.28)$$

The longitudinal mass is determined by the $|\phi|^4$ coupling λ and the minimum α as

$$m_\sigma^2 = \lambda |\alpha|^2 . \quad (8.29)$$

Fig. 8.4. Propagators and fermion-boson vertex for our truncation in the symmetry-broken regime as specified in Sec. 8.4.2. The bosonic self-interactions are exhibited in Fig. 6.2.

The small imaginary contribution to $\Gamma_{\phi^*\phi}$ generated by fermionic fluctuations in the absence of particle-hole symmetry, mentioned already above, gives rise to an off-diagonal quadratic term $\Gamma_{\sigma\pi}$ with a contribution linear in q_0 . Since this term would complicate the analysis without having any significant effect, we will neglect it.

We now discuss terms involving fermions in the case of symmetry breaking. In addition to the normal quadratic fermionic term $\Gamma_{\bar{\psi}\psi}$ defined as before, see Eq. (8.21), the anomalous term

$$\Gamma_{\psi\psi} = \int_k (\Delta \bar{\psi}_{-k\downarrow} \bar{\psi}_{k\uparrow} + \Delta^* \psi_{k\uparrow} \psi_{-k\downarrow}) \quad (8.30)$$

is generated in the symmetry-broken regime, where $|\Delta|$ is a cutoff-dependent energy gap. The phase of Δ is inherited from the phase of α while its modulus is generally different, due to fluctuations. Since we have chosen α real and positive, Δ is real and positive, too. The normal and anomalous fermionic propagators G_f and F_f corresponding to $\Gamma_{\bar{\psi}\psi}$ and $\Gamma_{\psi\psi}$ have the standard mean-field form as in Eqs. (8.10) and (8.11), with $E_{\mathbf{k}} = (\xi_{\mathbf{k}}^2 + |\Delta|^2)^{1/2}$, but now Δ is not equal to α .

In addition to the interaction between fermions and bosons of the form Eq. (8.25), an anomalous term of the form

$$\Gamma_{\psi^2\phi} = \tilde{g} \int_{k,q} \left(\bar{\psi}_{-k+\frac{q}{2}\downarrow} \bar{\psi}_{k+\frac{q}{2}\uparrow} \phi_q^* + \psi_{k+\frac{q}{2}\uparrow} \psi_{-k+\frac{q}{2}\downarrow} \phi_q \right) \quad (8.31)$$

is generated in the symmetry-broken regime. Inserting the decomposition of ϕ in longitudinal and transverse fields into the normal and anomalous interaction terms, we obtain

$$\Gamma_{\psi^2\sigma} = g_\sigma \int_{k,q} \left(\bar{\psi}_{-k+\frac{q}{2}\downarrow} \bar{\psi}_{k+\frac{q}{2}\uparrow} \sigma_q + \psi_{k+\frac{q}{2}\uparrow} \psi_{-k+\frac{q}{2}\downarrow} \sigma_{-q} \right), \quad (8.32)$$

$$\Gamma_{\psi^2\pi} = ig_\pi \int_{k,q} \left(\bar{\psi}_{-k+\frac{q}{2}\downarrow} \bar{\psi}_{k+\frac{q}{2}\uparrow} \pi_q - \psi_{k+\frac{q}{2}\uparrow} \psi_{-k+\frac{q}{2}\downarrow} \pi_{-q} \right), \quad (8.33)$$

where $g_\sigma = g + \tilde{g}$ and $g_\pi = g - \tilde{g}$. Fermions couple with different strength to the σ - and π -field, respectively.

A diagrammatic representation of the various propagators and interaction vertices in the symmetry-broken regime is shown in Fig. 8.4.

We finally note that in a previously reported truncation (Birse 2005) of the fRG flow in a fermionic superfluid, no distinction between longitudinal and transverse fields was made for the bosonic Z-factors in the symmetry-broken regime.

8.4.3 Flow equations

Inserting the above ansatz for the truncated effective action into the exact flow equation and comparing coefficients yields a set of coupled flow equations for the cutoff dependent parameters. The various contributions can be conveniently represented by

Feynman diagrams. The prefactors and signs in the flow equations could be extracted from the expansion of the exact flow equation, Eq. (3.20). However, in practice we determine them by comparison to a conventional perturbation expansion.

All contributions to our flow equations correspond to one-loop diagrams with only one momentum and frequency integration, as dictated by the structure of the exact flow equation in the form (3.20). One of the propagators in the loop is a bosonic or fermionic component of the single-scale propagator \mathbf{G}'_R , the others (if any) are components of \mathbf{G}_R .

In this chapter, we use sharp frequency cutoffs which exclude bosonic fields with $|\text{frequency}| < \Lambda_b$ and fermionic fields with $|\text{frequency}| < \Lambda_f$ from the functional integral. Thereby both fermionic and bosonic infrared divergences are regularized.

Both cutoffs are monotonic functions of the flow parameter, $\Lambda_b(\Lambda)$ and $\Lambda_f(\Lambda)$, which vanish for $\Lambda \rightarrow 0$ and tend to infinity for $\Lambda \rightarrow \infty$. Concretely, we employ

$$\mathbf{R}_s^\Lambda(k) = [\mathbf{G}_{s0}(k)]^{-1} - [\chi_s^\Lambda(k_0) \mathbf{G}_{s0}(k)]^{-1} \quad (8.34)$$

for $s = b, f$, and $\chi_s^\Lambda(k_0) = \Theta(|k_0| - \Lambda_s)$. This term replaces the bare propagators \mathbf{G}_{s0} by $\mathbf{G}_{s0}^\Lambda = \chi_s^\Lambda \mathbf{G}_{s0}$.

For a sharp frequency cutoff the frequency variable running around the loop is pinned by $\mathbf{G}'_R(k_0)$ to $k_0 = \pm\Lambda_b$ or $k_0 = \pm\Lambda_f$ as the so-called single-scale propagator \mathbf{G}'_R has support only for frequencies at the cutoffs, that is, for $|k_0| = \Lambda_s$. Hence the frequency integral can be performed analytically. The problem that the integrand contains also step functions $\chi_s^\Lambda(k_0) = \Theta(|k_0| - \Lambda_s)$ can be treated by using the identity

$$\int dx \delta(x - x_0) f[x, \Theta(x - x_0)] = \int_0^1 du f(x_0, u), \quad (8.35)$$

which is valid for any continuous function f .

More specifically, in the present case the one-loop diagrams are evaluated for vanishing external frequencies, such that all internal propagators carry the same frequency. In loops involving only either only bosonic or only fermionic propagators, one can use the identity

$$n \int dk_0 \mathbf{G}'_{sR}(k_0) \mathbf{A} [\mathbf{G}_{sR}(k_0) \mathbf{A}]^{n-1} = \Lambda'_s \sum_{k_0=\pm\Lambda_s} [\mathbf{G}_s(k_0) \mathbf{A}]^n, \quad (8.36)$$

valid for any matrix \mathbf{A} , to replace the frequency integration by a frequency sum over $\pm\Lambda_s$ while replacing all the propagators in the loop by \mathbf{G}_s . The factor n corresponds to the n possible choices of positioning \mathbf{G}'_{sR} in a loop with n lines, and $\Lambda'_s = \partial\Lambda_s/\partial\Lambda$. For $\Lambda_b = \Lambda_f$ the above formula holds also for the superpropagator \mathbf{G}_R , such that it applies also to loops with mixed products of bosonic and fermionic propagators. For $\Lambda_b \neq \Lambda_f$, mixed loops contribute only if the single-scale propagator is associated with the larger cutoff. For example, for $\Lambda_b > \Lambda_f$, the single-scale propagator has to be bosonic, since

\mathbf{G}_b vanishes at $|k_0| = \Lambda_f$. On the other hand, for $|k_0| = \Lambda_b$ one has $\mathbf{G}_{fR}(k_0) = \mathbf{G}_f(k_0)$, and for the integration of the bosonic factors in the loop one can again use Eq. (8.36).

For loop integrals involving the frequency sum over $\pm\Lambda_s$ and the momentum integral over the Brillouin zone we use the short-hand notation

$$\int_{k|\Lambda_s} = \frac{\Lambda'_s}{2\pi} \sum_{k_0=\pm\Lambda_s} \int \frac{d^d k}{(2\pi)^d}, \quad (8.37)$$

where $\Lambda'_s = \partial\Lambda_s/\partial\Lambda$.

The frequency cutoff is convenient for fermion-boson theories at zero temperature as the singularity for both particle species is situated at the origin $|q_0| = 0$ on the frequency axis. This makes mixed diagrams particularly easy to treat as alluded to above. The downside, on the other hand, is that cutting off frequencies ruins the analyticity properties of Green functions in the complex frequency plane. In the present chapter, this issue is not important but in other parts of this thesis, when for example calculating a Z-factor for the fermion self-energy as performed in chapter 7, we resorted to other cutoffs.

Symmetric regime

Here we choose $\Lambda_b = \Lambda_f = \Lambda$. One is in principle free to choose the fermionic and bosonic cutoff independently. We have checked that the concrete choice of Λ_b and Λ_f in the symmetric regime does not change the final results for $\Lambda \rightarrow 0$ much. The diagrams contributing to the flow in the symmetric regime are shown in Fig. 8.5.

The flow of the bosonic mass is given by the bosonic self-energy at vanishing external momentum and frequency, that is,

$$\partial_\Lambda \frac{m_b^2}{2} = g^2 \int_{k|\Lambda} G_f(k) G_f(-k) + \frac{\lambda}{2} \int_{q|\Lambda} G_b(q). \quad (8.38)$$

The fermionic contribution to $\partial_\Lambda m_b^2$ is positive, leading to a reduction of m_b^2 upon decreasing Λ , while the bosonic fluctuation term is negative (since $G_b(q) < 0$). The flow of Z_b is obtained from the second frequency derivative of the bosonic self-energy as

$$\partial_\Lambda Z_b = g^2 \int_{k|\Lambda} \partial_{q_0}^2 G_f(k+q) G_f(-k) \Big|_{q=0}. \quad (8.39)$$

Similarly, the flow of A_b is obtained from a second momentum derivative of the bosonic self-energy:

$$\partial_\Lambda A_b = g^2 \int_{k|\Lambda} \partial_{\mathbf{q}}^2 G_f(k+q) G_f(-k) \Big|_{q=0}, \quad (8.40)$$

where $\partial_{\mathbf{q}}^2 = \frac{1}{d} \sum_{i=1}^d \partial_{q_i}^2$. Since the bosonic self-energy is isotropic in \mathbf{q} to leading

(quadratic) order in \mathbf{q} , the results do not depend on the direction in which the momentum derivative is taken. The bosonic tadpole diagram in Fig. 8.5 contributes only to m_b , not to Z_b and A_b , since it yields a momentum and frequency independent contribution to the self-energy.

Finally, the flow of the $|\phi|^4$ coupling is given by

$$\begin{aligned} \partial_\Lambda \lambda = & -4g^4 \int_{k|\Lambda} [G_f(k)]^2 [G_f(-k)]^2 \\ & + \frac{5}{4} \lambda^2 \int_{q|\Lambda} [G_b(q)]^2. \end{aligned} \quad (8.41)$$

Within the truncation of the effective action described in Sec. 8.4.1 there is no contribution to the flow of the interaction between fermions and bosons in the symmetric phase. The coupling g remains therefore invariant.

Symmetry broken regime

In the limit $\Lambda \rightarrow 0$ we are forced to choose $\Lambda_f \ll \Lambda_b$ to avoid an artificial strong coupling problem, as will become clear below. We therefore choose $\Lambda_f < \Lambda_b$ in the entire symmetry broken regime, which implies that the frequencies in mixed loops with bosonic and fermionic propagators are pinned at the bosonic cutoff. The precise choice of the cutoffs will be specified later.

We first derive the flow equation for the minimum of the bosonic potential α , which is derived from the condition that the bosonic 1-point vertex $\Gamma_\sigma^{(1)}$ be zero for all Λ . The flow equation for $\Gamma_\sigma^{(1)}$ reads

$$\begin{aligned} \partial_\Lambda \Gamma_\sigma^{(1)} = & m_\sigma^2 \partial_\Lambda \alpha + 2g_\sigma \int_{k|\Lambda_f} F_f(k) \\ & + \frac{\lambda \alpha}{2} \int_{q|\Lambda_b} [3G_\sigma(q) + G_\pi(q)]. \end{aligned} \quad (8.42)$$

The various contributions are represented diagrammatically in Fig. 8.6.

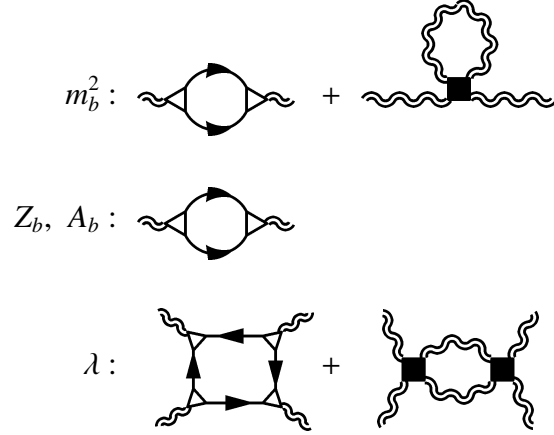


Fig. 8.5. Feynman diagrams representing the flow equations in the symmetric regime.

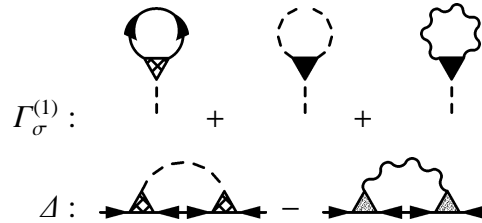


Fig. 8.6. Contributions to the bosonic 1-point vertex and fermion gap below Λ_c .

The first term is due to the cutoff-dependence of the expansion point around which the effective action is expanded in powers of the fields. The condition $\partial_\Lambda \Gamma_\sigma^{(1)} = 0$ yields

$$\partial_\Lambda \alpha = -\frac{2g_\sigma}{m_\sigma^2} \int_{k|\Lambda_f} F_f(k) - \frac{1}{2\alpha} \int_{q|\Lambda_b} [3G_\sigma(q) + G_\pi(q)] . \quad (8.43)$$

We have used Eq. (8.29) to simplify the last term. The fermionic contribution to $\partial_\Lambda \alpha$ is negative, leading to an increase of α upon decreasing Λ , while the bosonic fluctuation term is positive and therefore reduces α . The behavior of Eq. (8.43) in the vicinity of the critical scale, $\Lambda \lesssim \Lambda_c$, when α and m_σ^2 are small, is shown below in Sec. 8.5.1.

The flow of Δ is obtained from the flow of the anomalous component of the fermionic self-energy as

$$\partial_\Lambda \Delta = g_\sigma \partial_\Lambda \alpha - \int_{q|\Lambda_b} F_f(q-k) [g_\sigma^2 G_\sigma(q) - g_\pi^2 G_\pi(q)] \Big|_{k=(0,\mathbf{k}_F)} . \quad (8.44)$$

The first term, due to the cutoff-dependence of the expansion point for the effective action, links the flow of the fermionic gap to the flow of the bosonic order parameter. The second term captures a correction to the relation between α and Δ due to bosonic fluctuations as illustrated in Fig. 8.6.

The flow of the mass of the longitudinal order parameter fluctuations (cf. Fig. 8.7) is obtained from the self-energy of the σ fields at zero momentum and frequency. The flow of λ can then be computed from the flow of m_σ^2 and α via the relation Eq. (8.29). For m_σ^2 , we have the flow equation

$$\begin{aligned} \partial_\Lambda \frac{m_\sigma^2}{2} = & g_\sigma^2 \int_{k|\Lambda_f} \left[G_f(k) G_f(-k) \right. \\ & \left. - F_f(k) F_f(-k) \right] \\ & + \frac{\lambda}{4} \int_{q|\Lambda_b} [3G_\sigma(q) + G_\pi(q)] \\ & + \frac{(\lambda\alpha)^2}{2} \int_{q|\Lambda_b} [9G_\sigma^2(q) + G_\pi^2(q)] \\ & + 3 \frac{\lambda\alpha}{2} \partial_\Lambda \alpha . \end{aligned} \quad (8.45)$$

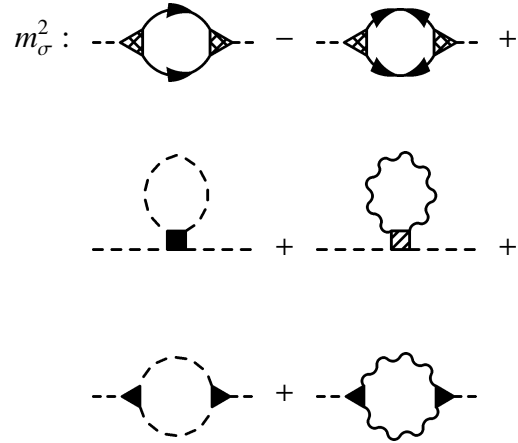


Fig. 8.7. Diagrammatic representation of the contributions to the bosonic mass in the symmetry-broken regime.

The second term in this equation is due to a product of the 3-point vertex γ_{σ^3} and $\partial_\Lambda \alpha$ arising from the cutoff dependence of the expansion point for the effective action. The

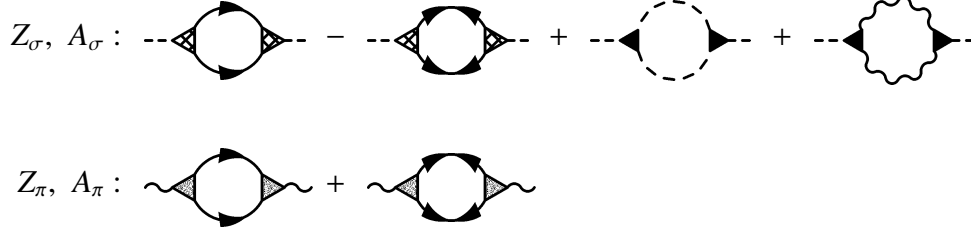


Fig. 8.8. Diagrams renormalizing the bosonic Z - and A -factors for $\Lambda < \Lambda_c$.

flow of Z_σ is obtained from the second frequency derivative of the self-energy of the σ fields, which yields

$$\begin{aligned} \partial_\Lambda Z_\sigma &= g_\sigma^2 \int_{k|\Lambda_f} \partial_{q_0}^2 [G_f(k+q) G_f(-k) - F_f(k+q) F_f(-k)] \Big|_{q=0} \\ &+ \frac{(\lambda\alpha)^2}{2} \int_{k|\Lambda_b} \partial_{q_0}^2 [9G_\sigma(k+q) G_\sigma(k) + G_\pi(k+q) G_\pi(k)] \Big|_{q=0}. \end{aligned} \quad (8.46)$$

The flow of A_σ is given by the same equation with $\partial_{q_0}^2$ replaced by $\partial_{\mathbf{q}}^2$.

In the flow of Z_π there are strong cancellations of different terms originating from bosonic fluctuations. We have shown with a slightly extended truncation in chapter 6 that the effective self-interaction among Goldstone bosons flows to zero such that Z_π remains finite and the Goldstone mode is not renormalized substantially (Pistoletti 2004). We therefore keep only the fermionic fluctuations, that is,

$$\partial_\Lambda Z_\pi = g_\pi^2 \int_{k|\Lambda_f} \partial_{q_0}^2 [G_f(k+q) G_f(-k) + F_f(k+q) F_f(-k)] \Big|_{q=0}. \quad (8.47)$$

For the flow of A_π we obtain the same equation with $\partial_{q_0}^2$ replaced by $\partial_{\mathbf{q}}^2$. The terms contributing to the flow of the Z - and A -factors are illustrated in Fig. 8.8.

In the symmetry broken regime, there are also contributions to the flow of the interaction between fermions and bosons due to vertex corrections with bosonic fluctuations (see Fig. 8.9), yielding

$$\begin{aligned} \partial_\Lambda g_\sigma &= g_\sigma \int_{q|\Lambda_b} \left[F_f^2(k-q) - |G_f(k-q)|^2 \right]_{k=(0, \mathbf{k}_F)} [g_\sigma^2 G_\sigma(q) - g_\pi^2 G_\pi(q)] \\ \partial_\Lambda g_\pi &= g_\pi \int_{q|\Lambda_b} \left[F_f^2(k-q) + |G_f(k-q)|^2 \right]_{k=(0, \mathbf{k}_F)} [g_\sigma^2 G_\sigma(q) - g_\pi^2 G_\pi(q)]. \end{aligned} \quad (8.48)$$

The right hand sides are dominated by the contribution from the π propagator, which tends to reduce g_σ, g_π for decreasing Λ .

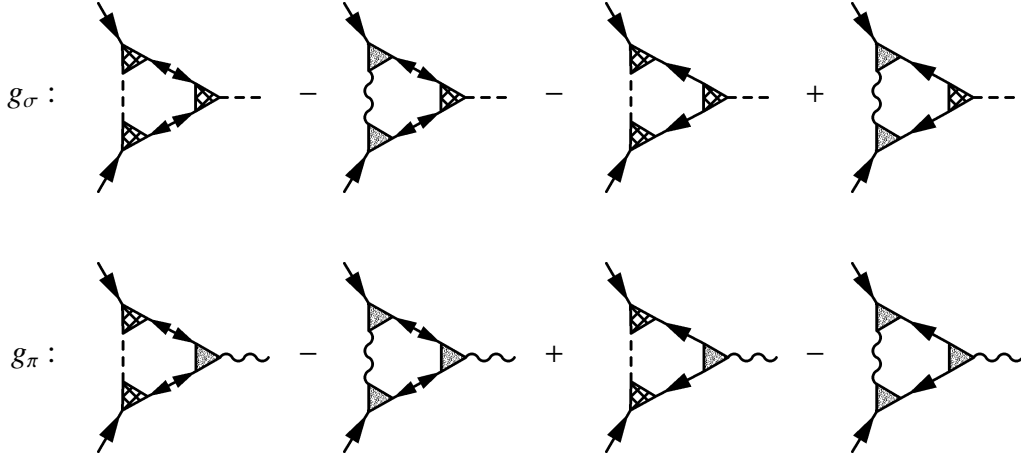


Fig. 8.9. Fermion-boson vertex corrections below Λ_c .

8.4.4 Relation to mean-field theory

Before solving the flow equations derived above, we first analyze what happens when contributions due to bosonic fluctuations are neglected, and relate the reduced set of equations to the usual mean-field theory (Sec. 8.3).

In the absence of bosonic fluctuations, $g = g_\sigma = g_\pi = 1$. Furthermore, the bosonic order parameter α and the fermionic gap Δ are identical: $\alpha = \Delta$. Since the bosonic cutoff is irrelevant here, we can choose $\Lambda_f = \Lambda$. The flow equation for the bosonic mass in the symmetric regime, Eq. (8.38), simplifies to

$$\partial_\Lambda \frac{m_b^2}{2} = \int_{k|\Lambda} G_f(k) G_f(-k), \quad (8.49)$$

where $G_f(k) = G_{f0}(k) = (ik_0 - \xi_{\mathbf{k}})^{-1}$. This equation can be easily integrated, yielding

$$\frac{m_b^2}{2} = \frac{1}{|U|} - \int_{|k_0|>\Lambda} \int_{\mathbf{k}} \frac{1}{k_0^2 + \xi_{\mathbf{k}}^2}. \quad (8.50)$$

m_b vanishes at a critical scale $\Lambda_c > 0$. The flow equation for $\Delta (= \alpha)$ in the symmetry broken regime $\Lambda < \Lambda_c$, Eq. (8.44), is reduced to

$$\partial_\Lambda \Delta = -\frac{2}{m_\sigma^2} \int_{k|\Lambda} F_f(k). \quad (8.51)$$

It is complemented by the flow equation for the mass of the σ field, Eq. (8.45), which becomes

$$\partial_\Lambda \frac{m_\sigma^2}{2} = \int_{k|\Lambda} [|G_f(k)|^2 - F_f^2(k)] + 3\gamma_{\sigma^3} \partial_\Lambda \Delta \quad (8.52)$$

in the absence of bosonic fluctuations, with $\gamma_{\sigma^3} = \lambda\Delta/2 = m_\sigma^2/(2\Delta)$. The propagators G_f and F_f have the usual BCS form, as in Eqs. (8.10) and (8.11).

A numerical solution of the coupled flow equations (8.51) and (8.52) yields a gap Δ which is a bit smaller than the BCS result obtained from the gap equation (8.12). The reason for this discrepancy is the relatively simple quartic ansatz (6.2) for the bosonic potential. The complete bosonic potential is non-polynomial in $|\phi|^2$ even in mean-field theory. Restricted to the zero momentum and frequency component of ϕ it has the form (Popov 1987)

$$U^{\text{MF}}(\phi) = \frac{|\phi|^2}{|U|} - \int_k \ln \frac{k_0^2 + \xi_{\mathbf{k}}^2 + |\phi|^2}{k_0^2 + \xi_{\mathbf{k}}^2} . \quad (8.53)$$

The kernel of the 3-point vertex γ_{σ^3} obtained from an expansion of this mean-field potential around a finite order parameter Δ reads

$$\gamma_{\sigma^3} = -2 \int_k \left[\frac{1}{3} F_f^3(k) - F_f(k) |G_f(k)|^2 \right] \quad (8.54)$$

at zero frequencies and momenta. Inserting this into (8.52), the flow of m_σ^2 can be written as a total derivative

$$\partial_\Lambda \frac{m_\sigma^2}{2} = -\partial_\Lambda \int_{|k_0|>\Lambda} \int_{\mathbf{k}} [|G_f(k)|^2 - F_f^2(k)] , \quad (8.55)$$

where the Λ -derivative on the right hand side acts also on Δ , generating the term proportional to γ_{σ^3} . Integrating this equation with the initial condition $m_\sigma = 0$ at $\Lambda = \Lambda_c$, yields

$$\frac{m_\sigma^2}{2} = K(0) + L(0) - U^{-1} , \quad (8.56)$$

which is the correct mean-field result. With m_σ given by (8.56), the flow equation (8.51) yields the correct mean-field gap. The easiest way to see this, is to write the BCS gap equation in the presence of a cutoff in the form $1 = -U \int_{|k_0|>\Lambda} \int_{\mathbf{k}} \Delta^{-1} F_f(k)$, and take a derivative with respect to Λ .

It is instructive to relate the above flow equations for Δ and m_σ to the flow equations for the BCS mean-field model obtained in a purely fermionic RG (Salmhofer 2004). For a sharp frequency cutoff, those flow equations have the form

$$\partial_\Lambda \Delta = -(V + W) \int_k F_f(k) , \quad (8.57)$$

$$\partial_\Lambda (V + W) = (V + W)^2 \partial_\Lambda \int_{|k_0|>\Lambda} \int_{\mathbf{k}} [|G_f(k)|^2 - F_f^2(k)] , \quad (8.58)$$

where V is a normal two-fermion interaction in the Cooper channel, while W is an anomalous interaction corresponding to annihilation (or creation) of four particles.

With the identification $2/m_\sigma^2 = V + W$ these equations are obviously equivalent to (8.51) and (8.55). The above flow equation for $V + W$ is obtained from a one-loop truncation complemented by additional self-energy insertions drawn from higher order diagrams with tadpoles (Salmhofer 2004, Katanin 2004). These additional terms correspond to the contractions with γ_{σ^3} in the present bosonized RG.

8.5 Results

In subsections 8.5.1 and 8.5.2, analytic properties of our flow equations are discussed. Numerical results for two-dimensional systems are exhibited and interpreted in subsection 8.5.3.

8.5.1 Flow for $\Lambda \lesssim \Lambda_c$

For Λ slightly below Λ_c , the flow equations can be expanded in the order parameter. To leading order, the order parameter α and the gap Δ are identical, $\alpha = \Delta$. The fluctuation term in the flow equation (8.44) for Δ is quadratic in α , and also the flow of g_σ yields only corrections beyond linear order to the relation between α and Δ .

Near Λ_c , the flow equation (8.43) for α can be written as

$$\partial_\Lambda \alpha^2 = -\frac{4}{\lambda} I - \int_{q|\Lambda_b} [3G_\sigma(q) + G_\pi(q)] , \quad (8.59)$$

where $I = \int_{k|\Lambda_f} (k_0^2 + \xi_{\mathbf{k}}^2)^{-1}$, evaluated for $\Lambda = \Lambda_c$. Note that we have replaced the ratio m_σ^2/α^2 by λ in the first term on the right hand side of the flow equation. Integrating the flow equation one obtains

$$\alpha^2 = \left[\frac{4}{\lambda} I + \int_{q|\Lambda_b} [3G_\sigma(q) + G_\pi(q)] \right]_{\Lambda=\Lambda_c} (\Lambda_c - \Lambda) \quad (8.60)$$

for $\Lambda \lesssim \Lambda_c$. The order parameter α and the fermionic gap are thus proportional to $(\Lambda_c - \Lambda)^{1/2}$ for $\Lambda \lesssim \Lambda_c$.

Inserting Eq. (8.60) into the flow equation (8.45) for m_σ^2 and neglecting the last fluctuation term, which is of higher order in α , one obtains

$$\partial_\Lambda m_\sigma^2 = -4I - \lambda \int_{q|\Lambda_b} [3G_\sigma(q) + G_\pi(q)] . \quad (8.61)$$

This shows that the flow of α and m_σ^2 is indeed consistent with the relation $m_\sigma^2 = \lambda \alpha^2$ following from the ansatz for the bosonic potential.

8.5.2 Infrared asymptotics

In the infrared limit ($\Lambda \rightarrow 0$), the key properties of the flow can be extracted from the flow equations analytically as already demonstrated in chapter 6 for the general σ - Π model with $N-1$ Goldstone bosons. The behavior of the bosonic sector depends strongly on the dimensionality of the system. We consider dimensions $d \geq 2$, focusing in particular on the two- and three-dimensional case. The bosonic order parameter and the fermionic gap saturate at finite values in the limit $\Lambda \rightarrow 0$. The fluctuation corrections to $\partial_\Lambda \alpha$ and $\partial_\Lambda \Delta$ involve the singular Goldstone propagator G_π only linearly and are therefore integrable in $d > 1$. The fermion-boson interactions g_σ and g_π also saturate. The finiteness of Z_π and A_π is guaranteed by the correct implementation of symmetries (see chapter 6, Pistolesi 2004). We choose $\Lambda_b = \Lambda$ in the following. The choice of Λ_f (as a function of Λ) will be discussed and specified below.

The flows of m_σ^2 , λ , Z_σ , and A_σ are dominated by terms quadratic in G_π for $\Lambda \rightarrow 0$, see Fig. 8.10. Using $m_\sigma^2 = \lambda \alpha^2$, we obtain the asymptotic flow equation for λ from Eq. (8.45) in the simple form

$$\partial_\Lambda \lambda = \lambda^2 \int_{q|\Lambda} G_\pi^2(q) . \quad (8.62)$$

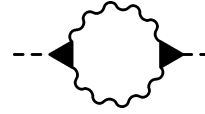


Fig. 8.10. Goldstone fluctuations determining the infrared asymptotics for $\Lambda \rightarrow 0$.

The above integral over G_π^2 is proportional to Λ^{d-4} for small Λ in dimensions $d < 4$, implying that λ scales to zero in $d \leq 3$. In two dimensions one obtains $\int_{q|\Lambda} G_\pi^2(q) = \frac{1}{4\pi^2 A_\pi Z_\pi} \Lambda^{-2}$ for small Λ , such that the rescaled variable $\tilde{\lambda} = \lambda/\Lambda$ obeys the flow equation

$$\frac{d\tilde{\lambda}}{d \log \Lambda} = -\tilde{\lambda} + \frac{\tilde{\lambda}^2}{4\pi^2 A_\pi Z_\pi} , \quad (8.63)$$

which has a stable fixed point at $\tilde{\lambda}^* = 4\pi^2 A_\pi Z_\pi$. Hence, the bosonic self-interaction vanishes as

$$\lambda \rightarrow 4\pi^2 A_\pi Z_\pi \Lambda \quad \text{for } \Lambda \rightarrow 0 \quad (8.64)$$

in two dimensions in agreement with Eq. (6.37). Consequently, also the radial mass m_σ^2 of the Bose fields vanishes linearly in Λ . In three dimensions one has $\int_{q|\Lambda} G_\pi^2(q) \propto \Lambda^{-1}$ for small Λ such that λ and m_σ^2 scale to zero logarithmically for $\Lambda \rightarrow 0$. Since m_σ^2 is the dominant contribution to the denominator of G_σ at small momenta and frequencies, the scaling of m_σ^2 to zero as a function of Λ implies that G_σ (at $\Lambda = 0$) diverges as

$$G_\sigma(sq) \propto s^{-1} \quad \text{for } d = 2 \quad (8.65)$$

$$G_\sigma(sq) \propto \log s \quad \text{for } d = 3 \quad (8.66)$$

in the limit $s \rightarrow 0$ matching Eq. (6.35). Although derived from an approximate truncation of the functional flow equation, this result is *exact* even in two dimensions, where the renormalization of m_σ^2 is very strong. This is due to the fact that the scaling dimension of m_σ^2 is fully determined by the scaling dimension of the Goldstone propagator and the existence of a fixed point for $\tilde{\lambda}$, but does not depend on the position of the fixed point (Pistoletti 2004).

The flow of Z_σ is given by

$$\partial_\Lambda Z_\sigma = \frac{(\lambda\alpha)^2}{2} \int_{q|\Lambda} \partial_{p_0}^2 G_\pi(p+q) G_\pi(q) \Big|_{p=0} \quad (8.67)$$

for small Λ . The integral over the second derivative of $G_\pi G_\pi$ is of order Λ^{d-6} . In two dimensions the coupling λ vanishes linearly in Λ , such that $\partial_\Lambda Z_\sigma \propto \Lambda^{-2}$, implying that Z_σ diverges as Λ^{-1} for $\Lambda \rightarrow 0$. Hence, the term $Z_\sigma q_0^2$ with $|q_0| = \Lambda$ in the denominator of G_σ scales linearly in Λ , as m_σ^2 . In three dimensions $\int_{q|\Lambda} \partial_{p_0}^2 G_\pi(p+q) G_\pi(q) \Big|_{p=0}$ diverges as Λ^{-3} , while λ vanishes only logarithmically. Hence $\partial_\Lambda Z_\sigma \propto (\log \Lambda)^{-2} \Lambda^{-3}$, which is larger than in two dimensions. Integrating over Λ one finds $Z_\sigma \propto (\Lambda \log \Lambda)^{-2}$, which means that $Z_\sigma q_0^2$ vanishes as $(\log \Lambda)^{-2}$ in the infrared limit. This yields a sub-leading logarithmic correction to the mass term m_σ^2 in the denominator of G_σ . An analogous analysis with the same results as just obtained for Z_σ also holds for the momentum renormalization factor A_σ . A strong renormalization of longitudinal correlation functions due to Goldstone fluctuations appears in various physical contexts (Weichman 1988, Zwerger 2004).

Recently, a singular effect of Goldstone fluctuations on the fermionic excitations in a superfluid was found in Gaussian approximation (Lerch 2008). This singularity appears only after analytic continuation to real frequencies, and its fate beyond Gaussian approximation remains to be clarified.

Since m_σ^2 and λ scale to zero in the infrared limit in $d \leq 3$, all purely bosonic contributions to the effective action scale to zero. On the other hand, the fermion-boson coupling remains finite. One is thus running into a strong coupling problem, indicating a failure of our truncation, if fermionic fields are integrated too slowly, compared to the bosons. The problem manifests itself particularly strikingly in the flow equation for the order parameter, Eq. (8.43), in two dimensions. Since $m_\sigma^2 \propto \Lambda_b$ for small Λ_b , the fermionic contribution to $\partial_\Lambda \alpha$ is of order Λ^{-1} if one chooses $\Lambda_f = \Lambda_b = \Lambda$, leading to a spurious divergence of α for $\Lambda \rightarrow 0$.

The problem can be easily avoided by integrating the fermions fast enough, choosing $\Lambda_f \ll \Lambda_b$ in the infrared limit. In our numerical solution of the flow equations in the following section we will choose $\Lambda_b = \Lambda$ and $\Lambda_f = \Lambda^2/\Lambda_c$ for $\Lambda < \Lambda_c$, which matches continuously with the equal choice of cutoffs for $\Lambda > \Lambda_c$. The fermionic contribution to $\partial_\Lambda \alpha$ in Eq. (8.43) is then finite for small Λ , since the factor $\Lambda_f' = 2\Lambda$ in $\int_{k|\Lambda_f}$ compensates the divergence of m_σ^{-2} in front of the integral. Since the fermions

are gapped below Λ_c , one could also integrate them completely (set Λ_f to zero), and then compute the flow driven by Λ_b only.

The freedom to choose fermionic and bosonic cutoffs independently was exploited also in a recent fRG-based computation of the fermion-dimer scattering amplitude in vacuum (Diehl 2007).

8.5.3 Numerical results in two dimensions

In this section, we present a numerical solution of our flow equations from Sec. 8.4.3 in two dimensions. Technically, we employ a fifth-order Runge-Kutta integration routine to solve coupled, ordinary differential equations. At each increment of the Runge-Kutta routine, two-dimensional integrations over the whole Brillouin zone have to be executed. For this purpose, we employ an integrator for singular functions with relative error of less than 1%. In particular, for $\Lambda \approx \Lambda_c$ it is imperative to operate with sufficiently accurate routines as the integrands are large and small deviations result in a significant spread in the final values for $\Lambda \rightarrow 0$. For further details on the numerical procedure, we refer to Appendix A.

We fix our energy units by setting the hopping amplitude $t = 1$. We choose a chemical potential $\mu = -1.44$ corresponding to an average electron density of 1/2 (quarter-filled band). This choice represents the generic case of a convex Fermi surface remote from van Hove singularities. The only varying input parameter is the Hubbard U , which determines the initial value of the bosonic mass via $m_b^2 = |2/U|$. Initially, the flow starts in the symmetric regime with $\Lambda = \Lambda_0 = 100$, where Eqs. (8.38 - 8.41) determine the evolution. The critical scale is determined by the condition $m_b^2(\Lambda_c) = 0$. In the symmetry-broken regime ($\Lambda < \Lambda_c$), Eqs. (8.43 - 8.48) determine the evolution.

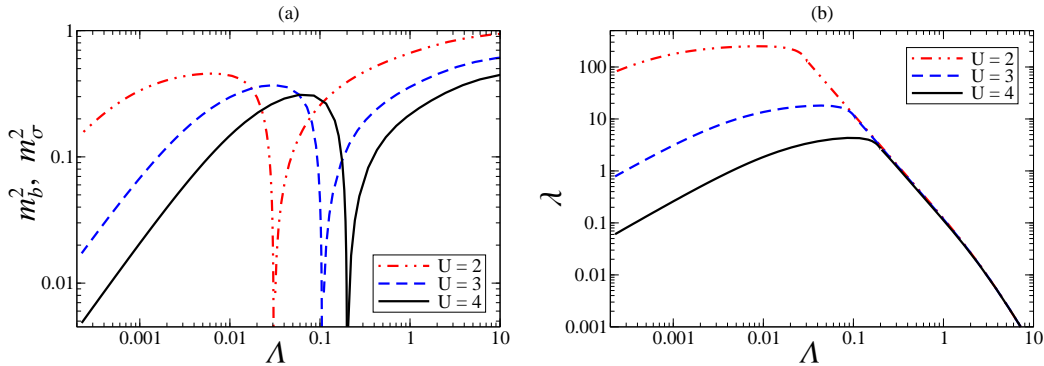


Fig. 8.11. (a): Flows of the bosonic mass, m_b^2 for $\Lambda > \Lambda_c$ and m_σ^2 for $\Lambda < \Lambda_c$. (b): Quartic coupling λ .

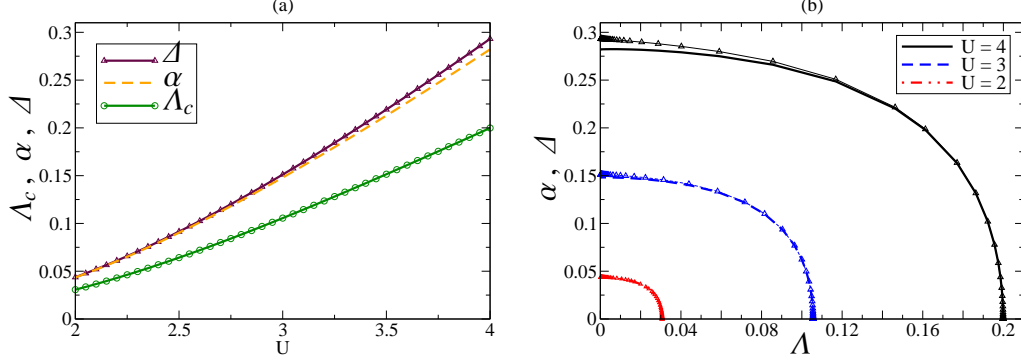


Fig. 8.12. (a): Fermion gap Δ , order parameter α , and the critical scale Λ_c versus Hubbard U . (b): Exemplary flows for Δ (triangles) and α (lines) each corresponding to one point in (a).

In Fig. 8.11 characteristic flows of the bosonic mass and the quartic coupling are shown in double-logarithmic plots for different choices of the Hubbard U . The sharp de- and increase of the bosonic mass marks the region around Λ_c . For small Λ , the flow reaches the infrared asymptotic regime (see Sec. 8.5.2). The scale Λ_{IR} at which this scaling sets in decreases for decreasing U . The numerically obtained scaling $m_c^2, \lambda \propto \Lambda$ is consistent with the analytical result of Sec. 8.5.2.

In Fig. 8.12 (a) we compare the fermion gap with the bosonic order parameter (final values at $\Lambda = 0$) and the critical scale as a function of U . In Fig. 8.12 (b) the flow of Δ and α as a function of Λ is shown for various choices of U . We observe $\Delta, \alpha \propto (\Lambda_c - \Lambda)^{1/2}$ for $\Lambda \lesssim \Lambda_c$ as derived below Eq. (8.60). The ratio Δ/Λ_c , where Δ is the final gap for $\Lambda \rightarrow 0$, is approximately 1.4 for the values of U studied here. As a result of fluctuations, the gap is reduced considerably compared to the mean-field result

$$\frac{\Delta}{\Delta_{\text{BCS}}} \approx 0.25 \quad (8.68)$$

for $2 \leq U \leq 4$. The main reduction here stems from the bosonic self-interactions in the symmetric regime leading to a substantial decrease of Λ_c via the second term of Eq. (8.38). A reduction of the gap compared to the mean-field value is generally present even in the weak coupling limit $U \rightarrow 0$. In fermionic perturbation theory second order corrections reduce the prefactor of the BCS gap formula even for $U \rightarrow 0$ (Martin 1992). The reduction obtained here is slightly stronger than what is expected from a fermionic renormalization group calculation (Gersch 2008).

For $\Lambda < \Lambda_c$, Goldstone fluctuations slightly reduce α via the term involving $G_\pi(q)$ in Eq. (8.43). On the other hand, the term due to the Goldstone mode in Eq. (8.44)

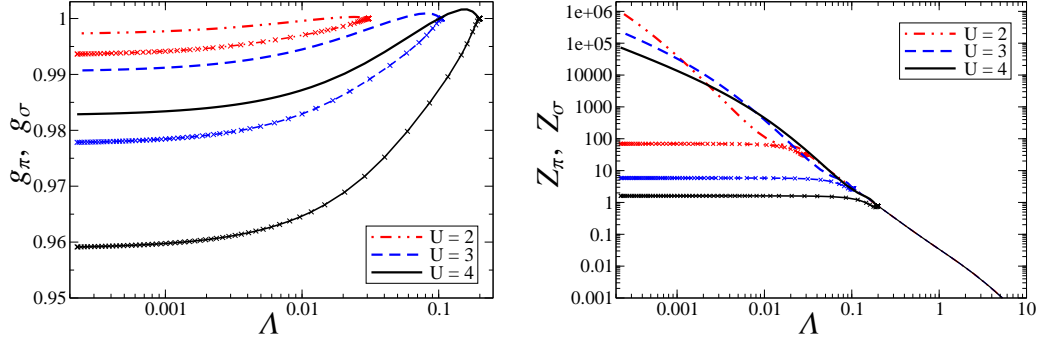


Fig. 8.13. Left: Flows of fermion-boson vertices, g_σ (lines), and g_π (lines with crosses), for $\Lambda < \Lambda_c$. Right: Flows of Z_σ (lines) and Z_π (crosses).

enhances the fermionic gap Δ relative to α , such that Δ is generally slightly larger than α . This difference will become larger upon increasing the interaction strength as one enters the regime of a Bose gas made of tightly bound fermions. Here, however, for relatively weak interactions, the impact of Goldstone fluctuations on both α and Δ is very modest. By contrast, the impact of Goldstone fluctuations is known to be dramatic at finite temperatures (not treated here) in two dimensions, since they drive the order parameter to zero (Goldenfeld 1992).

In the right plot of Fig. 8.13, we show flows of the Z-factors of the σ - and π -field, respectively. In the symmetric regime, the evolution is independent of U . At Λ_c , the ϕ -field splits into the σ - and π -modes with Z_σ diverging in the limit $\Lambda \rightarrow 0$ as $Z_\sigma \propto \Lambda^{-1}$ (cf. Sec. 8.5.2). The Z-factor of the Goldstone field saturates for $\Lambda \ll \Delta$. The flows for the A-factors (not shown) parametrizing the momentum dependence of the σ - and π -propagators exhibit very similar behavior.

Finally, in the left plot of Fig. 8.13 we show flows of the fermion-boson vertices g_σ and g_π for $\Lambda < \Lambda_c$. Their relative changes are only of the order of a few percent (note the scale of the vertical axis) with g_σ being a bit larger than g_π .

8.6 Conclusion

Truncating the exact fRG flow, we have derived approximate flow equations which capture the non-trivial order parameter fluctuations in the superfluid ground state of the attractive Hubbard model, which has been chosen as a prototype model for attractively interacting fermions. The superfluid order parameter is associated with a bosonic field which is introduced via a Hubbard-Stratonovich decoupling of the

fermionic interaction. Below a critical scale Λ_c , the bosonic effective potential assumes a mexican hat shape leading to spontaneous symmetry breaking and a Goldstone mode. The bosonic order parameter is linked to but not equivalent to a fermionic gap. The fermionic gap is significantly smaller than the mean-field gap, mostly due to fluctuations above the scale Λ_c . Transverse order parameter fluctuations (Goldstone mode) below Λ_c lead to a strong renormalization of radial fluctuations. The radial mass and the bosonic self-interaction vanish linearly as a function of the scale in two dimensions, and logarithmically in three dimensions, in agreement with the exact behavior of an interacting Bose gas (Pistolesi 2004). On the other hand, the average order parameter, the fermionic gap, and the interaction between fermions and bosons are affected only very weakly by the Goldstone mode.

Supplementing the flow equations derived above by a shift of the chemical potential, to keep the density fixed, one may also try to deal with larger values of U (see also Outlook 9.3.3). Eagles (1969) and Leggett (1980) have shown that already the BCS mean-field theory captures many features of the condensed Bose gas ground state made from strongly bound fermion pairs in the limit of strong attraction. Beyond mean-field theory, the difference between the fermionic gap and the order parameter α increases at larger U .

It will also be interesting to extend the present analysis to $T > 0$, in particular in view of the possibility of a finite fermionic gap in the absence of long-range order in a Kosterlitz-Thouless phase at low finite temperatures (see also Outlook 9.3.2).

Part III

Summary

Conclusions

The topic of this thesis has been the computation of the effects of order parameter fluctuations in two- and three-dimensional interacting Fermi systems with emphasis on symmetry-broken phases and quantum critical behavior. For this purpose, we have solved flow equations within the functional RG framework for fermionic (single-particle) and bosonic (collective) degrees of freedom at zero and finite temperature.

9.1 Key results

Three important methodological advancements were achieved during this work.

9.1.1 Non-Gaussian fixed points

We demonstrated in chapters 5, 6, and 7 how to compute RG flows of quantum critical fermion systems at zero and finite temperature where the interaction vertex is attracted towards a *non-Gaussian fixed point* with nontrivial critical exponents.

In chapters 5 and 6, we extended the Hertz-Millis theory formulated entirely in terms of a bosonic order parameter field to phases with discrete and continuous symmetry-breaking. Extending the previous work by Millis (1993), we computed the shape of the T_c -line in the vicinity of the QCP for the case where even the zero temperature theory is described by a non-Gaussian fixed point. We fully captured the interplay and relative importance of quantum and thermal fluctuations in the vicinity of the QCP.

In chapter 7, we set up a renormalization group framework for coupled theories of fermions interacting with their own collective order parameter fluctuations at quantum criticality. As a first application, we considered the semi-metal to superfluid QCP of attractive Dirac fermions in two dimensions possibly relevant for cold atoms on the honeycomb lattice and graphene. At the QCP, the fermion-boson coupling becomes relevant and induces anomalous exponents for both the fermion and boson propagator, respectively.

9.1.2 Goldstone modes

Systems whose spectrum contains massless *Goldstone bosons* as a consequence of spontaneously breaking a continuous symmetry were analyzed in chapters 6 and 8.

In chapter 6, we devised a truncation of the effective action for zero temperature phases with continuous symmetry-breaking (σ - Π model) that yields the *exact* momentum behavior of the longitudinal and transversal (Goldstone) mode, respectively. The Goldstone mode strongly renormalizes the longitudinal propagator while all singularities in the Goldstone channel cancel as a consequence of symmetries – both modes therefore exhibit strongly different dependences on momenta. An even simpler truncation also yields the expected critical exponents directly at the critical point where both modes become degenerate. Additionally, the σ - Π model permits investigation of the finite temperature effects in particular correctly reproducing the Mermin-Wagner theorem.

In chapter 8, we thoroughly studied the impact of the Goldstone mode in fermionic superfluids at zero temperature. The Goldstone mode only weakly affects the fermion-boson vertex, the fermionic gap, and the order parameter. In the infrared regime, the fermions decouple from the flow and the collective bosonic sector described by the σ - Π model yields the exact momentum scaling of the transversal and longitudinal mode.

9.1.3 Non-universal and universal quantities

In chapters 7 and 8, the functional RG was implemented as a versatile framework for coupled fermion-boson systems to compute *universal* as well as *non-universal* quantities simultaneously. The emergence of –bosonic and universal– effective theories from microscopic –fermionic and non-universal– models upon lowering the energy scale is a strength of the Fermi-Bose RG approach. In addition to the singular terms also collected in other RG methods, our flow equations also capture finite but possibly large contributions which affect non-universal quantities such as the position of a QCP, or the size of a fermionic gap. Furthermore, the energy scale at which the universal asymptotics sets in can also be computed conveniently within this framework enabling a controlled comparison of the size of the various couplings with their residual low energy phase-space volume.

9.2 Criticism

Despite the methodological advancements of this thesis, some sore spots, subject to valid criticism, remain. Three central shortcomings of this work are as follows.

As outlined in section 2.1, in many microscopic models such as the repulsive Hubbard model the situation of competing ordering tendencies arises. For an accurate

computation of non-universal properties and to obtain certain qualitative phenomena such as the generation of an attractive d-wave coupling from antiferromagnetic spin fluctuations, it is not sufficient to take into account only one ordering channel.

In chapter 8, the attractive Hubbard model was considered in a parameter regime where the Cooper channel is undoubtedly the most dominant channel and it was therefore justified to utilize only one Hubbard-Stratonovich field for superfluid order. In the future, one would want to either (i) decouple the microscopic four-fermion interaction into multiple bosonic channels and a posteriori check how much the results depend on the precise decoupling procedure (Baier 2004), or (ii) perform a combined fermionic plus bosonic RG study, that is, first integrate out the high energy modes with a fermionic RG and subsequently perform the Hubbard-Stratonovich decoupling at a scale Λ_b when only a few dominant bosonic susceptibilities are left over. Then, the results have to be checked on their dependence on the switching scale Λ_b . A similar strategy has been adopted within a fermionic RG plus mean-field theory approach in Reiss (2007).

The number of couplings employed in the truncations of this thesis has been kept to a minimum and often involved merely multiplicative Z-factors for the frequency and momentum dependencies of the various propagators. Although it is impressive how much interesting physics one can extract already on this level, to ascertain the results and improve on quantitative accuracy, it is necessary to parameterize the self-energies and vertices on a frequency and/or momentum grid resulting in a more elaborate numerical effort. In some circumstances, as for example in the superfluid Kosterlitz-Thouless phase (see subsection 9.3.2), this is necessary to obtain even the correct qualitative behavior.

It is under debate how well the functional RG copes with strongly coupled systems (Salmhofer 2007). On the one hand, non-Gaussian fixed points in the infrared regime are captured at least qualitatively. The system is strongly coupled in only a limited region of phase-space and the small phase-space volume when the cutoff goes to zero is helpful in controlling the vertex expansion when truncating the exact effective action. On the other hand, truly strongly coupled systems when the local interaction exceeds the bandwidth are strongly coupled everywhere in phase-space and cannot be treated in manageable truncations yet (Metzner 2005).

9.3 Outlook

There exist numerous interesting directions for future research based on the work presented in this thesis. We here list three of them and describe the strategy for an RG treatment as well as the operational risks associated with each.

9.3.1 QED₃ (extending chapter 7)

We have shown in chapter 7 how to compute RG flows for coupled fermion-boson systems at quantum criticality. An interesting extension concerns Quantum Electrodynamics in 2 + 1 dimensions which has been advocated as a model for the zero temperature behavior in underdoped high T_c superconductors (Franz 2002, Herbut 2002).

Massless QED₃ can be tuned to a QCP by varying the number of fermion flavors to a critical $N_{f,\text{crit}}$. For fewer flavors than $N_{f,\text{crit}}$ the ground state spontaneously breaks the chiral symmetry while for more flavors than $N_{f,\text{crit}}$ the gauge interaction is weakened and the ground state is chirally invariant. The properties of QED₃, in particular the momentum dependence of the fermion and gauge boson propagator (*universal*) at the QCP and $N_{f,\text{crit}}$ (*non-universal*), are presently only poorly known (Kaveh 2005, Strouthos 2008 and references therein). To investigate this in a functional RG setting, one would replace the effective action written in Eq. (7.4) with the fermion-boson action of QED₃. The minimal truncation includes a fermion and (gauge) boson self-energy, possibly in the form of Z-factors. The flow of the renormalized gauge coupling (g) generates four-fermion interactions (λ_f) in the chiral sector necessitating two interaction channels for the truncation. Diverging four-fermion interactions signal the onset of chiral symmetry-breaking and thus permit the determination of $N_{f,\text{crit}}$ (Gies 2006). The set of flow equations is depicted graphically in Fig. 9.1.

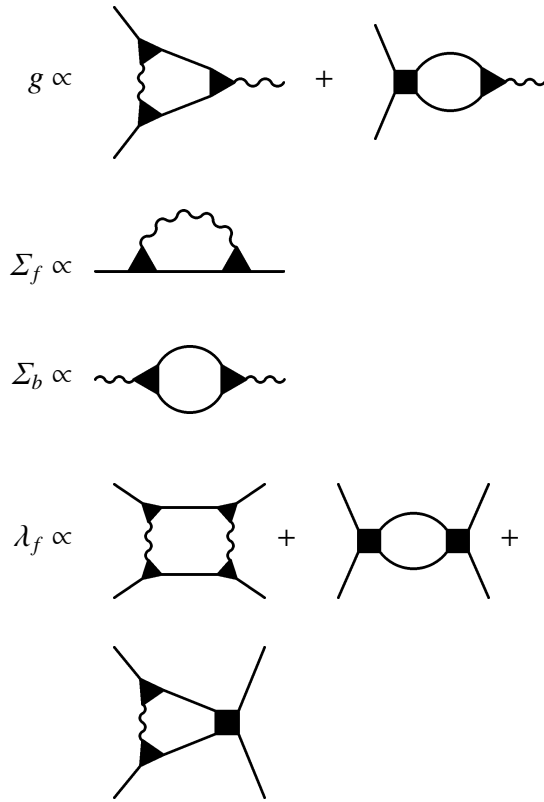


Fig. 9.1. Diagrammatic representation of the set of flow equations for QED₃. Wiggly lines stand for gauge bosons and straight lines for fermions.

Operational risks here involve the fulfillment of gauge symmetry and the dependence on the choice of gauge-fixing, typically Landau gauge. To get warmed up, one may want to start with an effective model for QED₃ without gauge bosons –the Thirring model in 2 + 1 dimension (Hands 1995, Christofi 2007, Gies 2008).

9.3.2 Superfluid Kosterlitz-Thouless phase (ext. chapter 8)

The correct finite temperature extension of the truncation employed in the ground-state study for two-dimensional fermionic superfluids in chapter 8 must yield the qualitative features peculiar to the Kosterlitz-Thouless phase (Kosterlitz 1973, Kosterlitz 1974, Goldenfeld 1992). Although there is *no spontaneous symmetry-breaking*, this phase is characterized by a line of fixed points and a temperature dependent anomalous dimension for the order parameter field. The order parameter correlation function decays algebraically due to the presence of a massless Goldstone mode. At the transition temperature, the superfluid density jumps to a universal value due to a conspiracy of vortex and Goldstone excitations (Nelson 1977). The single-particle spectrum displays a gap around the Fermi level reminiscent of pseudo-gap phenomena in the cuprates which also fall into the Kosterlitz-Thouless universality class (Rohe 2001, Eckl 2002).

To date, no satisfactory study of the Kosterlitz-Thouless phase starting from a microscopic fermionic model and capturing the above features has been performed and would clearly be desirable. First attempts within the functional RG framework for bosonic systems have been put forward in (Gräter 1995, v. Gersdorff 2001). However, in both studies the flow runs back into the symmetric phase, though very slowly, therefore not capturing the vanishing of the β -function of the superfluid density in the Kosterlitz-Thouless phase. Notwithstanding the notorious difficulties of the bosonic sector, capturing the gap in the single-particle spectrum without symmetry-breaking seems in reach. Since the anomalous part of the fermionic self-energy, that normally gaps the spectrum, vanishes, one has to parametrize the frequency- and momentum dependence of the *normal* self-energy of the fermions rather accurately.

The crucial diagram is shown in Fig. 9.2 where the order parameter field renormalizes the fermion self-energy. The gap should be visible in the temperature dependence of the specific heat deviating strongly from the linear temperature behavior expected in a (gapless) Fermi liquid. The scale-dependent specific heat can be computed via temperature derivatives of the thermodynamic potential in Eq. (3.22):

$$C^\Lambda(T) = -T \frac{\partial^2 U^\Lambda(T)}{\partial T^2}. \quad (9.1)$$

Operational challenges lie in the numerical implementation of the normal fermion self-energy on a momentum- and frequency grid.

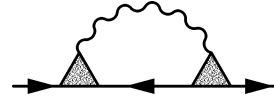


Fig. 9.2. Contribution to the normal fermion self-energy in the superfluid phase. The wiggly line stands for the boson propagator and the straight line for fermions.

9.3.3 BCS-Bose crossover (ext. chapter 8)

Upon increasing the attractive interaction in a superfluid Fermi gas, the nature of the fermion pairs evolves from BCS-type Cooper pairs to tightly bound bosons which undergo Bose-Einstein condensation (Leggett 1980). Nozières and Schmitt-Rink first considered this BCS-Bose crossover for lattice fermions and they extended Leggett's approach to finite temperatures (Nozières 1985).

An interesting extension of chapter 8 concerns the properties of the attractive Hubbard model when increasing the attraction U to larger values (Singer 1996, Keller 1999, Keller 2001, Burovski 2006). The main addition to the RG truncation already included in chapter 8 is a constraint to keep the density fixed during the RG flow. Implementing a flow equation for the density can be achieved by differentiating the flow equation of the thermodynamic potential, Eq. (3.22), with respect to the chemical potential:

$$\partial_\Lambda n^\Lambda = -\frac{\partial}{\partial \mu} \partial_\Lambda U^\Lambda . \quad (9.2)$$

Including the fermionic, bosonic and fluctuation contributions (Ohashi 2002, Diehl 2007) to the density is necessary to self-consistently adjust the chemical potential to keep the density constant during the RG flow. As a first step, one would try to understand and reproduce the Hartree mean-field theory in the zero sound channel within the RG equations analogously to the mean-field BCS model (Salmhofer 2004). Subsequently, a Hartree plus BCS-model with fixed density would have to be, at least qualitatively, reproduced by the RG flow. Finally, the order parameter fluctuations are added in and the effects thereof studied.

Deutsche Zusammenfassung

Die vorliegende Dissertation entwickelt Renormierungsgruppenstrategien zur Berechnung makroskopischer Eigenschaften von wechselwirkenden Fermi-Systemen. Besonders das Verhalten bei niederen Energien ist interessant, da hier wechselwirkungsinduzierte, kollektive Phänomene auftreten. Durch Herleitung und Lösung von Renormierungsgruppengleichungen analysieren wir in dieser Arbeit den Einfluss von Ordnungsparameterfluktuationen auf thermodynamische Observable und Korrelationsfunktionen in Fermi-Systemen mit spontaner Symmetriebrechung und quantenkritischem Verhalten.

Die Dissertation ist in zwei Hauptteile gegliedert. Teil I stellt das theoretische Rüstzeug der Arbeit bereit; in Teil II wird dieses dann auf verschiedene Problemstellungen angewendet.

In Kapitel 2 werden fundamentale Konzepte der Physik korrelierter Fermionen und der Renormierungsgruppe, die zum Verständnis der in Teil II folgenden Anwendungen notwendig sind, vorgestellt. Das Herzstück des ersten Teils stellt Kapitel 3 dar, in dem die einteilchenirreduzible Darstellung der funktionalen Renormierungsgruppe hergeleitet wird.

In Abschnitt 3.1.1 wird erläutert wie man die in Superfelder gebündelten fermionischen und bosonischen Freiheitsgrade in den Formalismus einbringt, so dass man simultan zu den fermionischen auch die kollektiven, bosonischen Fluktuationen ausintegrieren kann; dies wird in den Kapiteln 7 und 8 in die Praxis umgesetzt.

Im Hinblick auf Anwendung in den Kapiteln 5, 6 und 8, erweitern wir in Abschnitt 3.2.2 den Formalismus auf symmetriebrochene Systeme. In Abb. 3.1 zeigen wir die durch einen nichtverschwindenden Erwartungswerts einer bosonischen Feldkomponente im Minimum des effektiven Potentials modifizierte Hierarchie der Vertexfunktionen.

Der zweite Teil der Dissertation ist vier verschiedenen Anwendungen der in Teil I vorgestellten Konzepte und Methoden gewidmet.

In Kapitel 5 verallgemeinern wir die ursprünglich von Hertz und Millis entwickelte Renormierungsgruppentheorie, die Fermionen auf einen Schlag ausintegriert und die daraus resultierende effektive, bosonische Theorie mit Hilfe von Flussgleichungen analysiert, auf Phasen mit diskreter Symmetriebrechung. Im Gegensatz zu Millis können wir durch das Lösen unserer Flussgleichungen bei endlichen Temperaturen auch stark wechselwirkende, nicht-Gaußsche Fluktuationen behandeln, die das Verhalten entlang der im quantenkritischen Punkt mündenden Phasengrenze dominieren.

Im ersten Schritt studieren wir bosonische Propagatoren mit dynamischen Exponenten $z \geq 2$ in zwei und drei Raumdimensionen. Obwohl das Infrarotverhalten bei endlichen Temperaturen durch einen nicht-Gaußschen Fixpunkt beschrieben wird, bestätigen wir das von Millis in Gaußscher Approximation von der symmetrischen Phase kommend abgeleitete Potenzgesetz, das die Phasengrenze als Funktion des Kontrollparameters in der Nähe des quantenkritischen Punktes beschreibt. Dies ist eine Konsequenz des geringen Phasenraumvolumens, das den Effekt der starken Kopplung im Infraroten unterdrückt. Da wir die Phasengrenze durch Ausloten der Position des Fixpunktes bestimmen, sind wir in der Lage, die kritische Region zwischen der von Millis als Phasengrenze angenommenen Ginzburg-Linie und der *wahren* Phasengrenze numerisch auszumessen: Während beide Linien in drei Raumdimensionen kaum voneinander abweichen, öffnet sich in zwei Raumdimensionen eine ausgeprägte Lücke zwischen Ginzburg-Linie und Phasengrenze bei endlichen Temperaturen.

Im zweiten Schritt nehmen wir uns im Abschnitt 5.5.3 das bis dato nicht untersuchte Quanten-Ising-Modell in zwei Raumdimensionen mit dynamischem Exponent $z = 1$ vor. Nun liegt auch die Grundzustandstheorie unterhalb der oberen kritischen Dimension, was die von Millis gemachte Näherung –um den nicht-wechselwirkenden Gaußschen Fixpunkt zu entwickeln– vollständig invalidiert. Wie in Abb. 5.6 illustriert, weicht in diesem Fall die Ginzburg-Linie auch bei Temperatur null von der Phasengrenze ab. Resultate der numerischen Lösung der Flussgleichungen sind in Abb. 5.7 und 5.8 abgebildet. Für die Phasengrenze als Funktion des Kontrollparameters finden wir Wurzelverhalten mit einer logarithmischen Korrektur, siehe Gl. (5.49).

In Kapitel 6 analysieren wir Fälle, wo der quantenkritische Punkt einer Universalitätsklasse zugehörig ist, in der eine kontinuierliche Symmetriegruppe gebrochen wird. Dann treten masselose Goldstone-Moden auf, die das kritische Verhalten radikal beeinflussen –besonders in niedrigen Dimensionen.

Basierend auf dem in Abschnitt 6.2 definierten $\sigma - \Pi$ Modell, das den Goldstone-Anregungen mit einem separaten Propagator Rechnung trägt, führen wir analog zu Kapitel 5 eine Flussgleichungsstudie in der Nähe eines quantenkritischen Punktes durch. Wir fokussieren uns dabei auf Systeme mit quadratischer Frequenzabhängigkeit –also dynamischer Exponent $z = 1$ – in den Propagatoren beider, radialer und transversaler, Anregungen des Systems. Die Flussgleichungen spiegeln das Mermin-Wagner-Theorem richtig wider: Der Ordnungsparameter, und damit die kritische Temperatur,

wird in Raumdimensionen kleiner gleich *zwei* von thermisch angeregten Goldstone-Moden zu null gedrückt.

Als ein unerwartetes Hauptresultat finden wir in Abschnitt 6.4.3, dass die Form der Phasengrenze bei endlicher Temperatur in der Nähe des quantenkritischen Punktes in *drei* Raumdimensionen nicht von der Anzahl der Goldstone-Moden abhängt.

Abseits der Phasengrenze, in der symmetriebrochenen Phase, extrahieren wir in Abschnitt 6.5 das exakte Infrarotverhalten beider Propagatoren und der Wechselwirkungen analytisch aus den Flussgleichungen. Die effektive Selbstwechselwirkung der Goldstone-Moden fließt aus Symmetriegründen zu Null (siehe Gl. (6.34)), und der Goldstone-Propagator behält seine unrenormierte, quadratische Frequenz- und Impulsabhängigkeit bei. Die radiale Mode und deren Wechselwirkungen hingegen werden, wie in Gl. (6.35-6.37) zusammengefasst, stark durch die Goldstone-Moden renormiert.

In Kapitel 7 berechnen wir Renormierungsgruppenflüsse gekoppelter Fermi-Bose Theorien, die sich durch ihr kompliziertes, und ob der beiden masselosen Propagatoren am quantenkritischen Punkt daher mit anderen Methoden bisher nur unzureichend erforschbares, Infrarotverhalten auszeichnen.

Wir analysieren attraktiv wechselwirkende Dirac-Fermionen (siehe Abb. 7.2); hier treibt die Wechselwirkungstärke bereits in Molekularfeldtheorie einen kontinuierlichen Quantenphasenübergang von einem Halbmetall zu einer Superflüssigkeit (siehe Abb. 7.1 und Abschnitt 7.2.1). Physikalisch treten Dirac-Fermionen in Kohlenstoffschichten und in optischen Honigwabengittern in kalten, atomaren Quantengasen auf.

Unsere Trunkierung und Flussgleichungen der Fermion-Boson Wirkung, in Abb. 7.4 diagrammatisch dargestellt, ermöglichen die Berechnung aller quantenkritischen Exponenten in unmittelbarer Nähe des quantenkritischen Punktes. Abb. 7.5 zeigt die Werte der anomalen Dimensionen der Fermionen und Boson direkt am quantenkritischen Punkt für verschiedenen Raumdimensionen. Wie unter Gl. (7.33) erläutert, impliziert eine anomale Dimension des Fermionfeldes den Zusammenbruch des Fermiflüssigkeitsverhalten: Die lineare Frequenzabhängigkeit der Selbstenergie wird zu einem fraktionellen Potenzgesetz, das die hohe Zerfallsrate der niederenergetischen Quasiteilchen in der Nähe des Dirac-Punktes beschreibt.

In Abschnitt 7.4.1 werden numerische Flüsse der in der Trunkierung vorkommenden Parameter präsentiert. Durch kontrolliertes Verknüpfen der mikroskopischen Anfangsbedingungen, die auch der Molekularfeldrechnung von Abschnitt 7.2.1 zugrundeliegen, ist es uns möglich, zusätzlich zu den universellen Exponenten auch die nicht-universelle, renormierte Position des quantenkritischen Punktes entlang der Kontrollparameterachse mit dem Wert der Molekularfeldrechnung zu vergleichen; Gl. (7.39) veranschaulicht, dass Quantenfluktuationen die Ausmaße des Superflüssigkeitsbereichs im Phasendiagramm Abb. 7.1 drastisch reduzieren.

Die Berechnung des Satzes quantenkritischer Exponenten wird durch die Bestimmung der Potenzgesetze für die Korrelationslänge und die Suszeptibilität als Funktion des Kontrollparameters in Abschnitt 7.4.2 abgerundet.

In Kapitel 8 wird ein Gros der in den Kapiteln 5 bis 7 aufgebauten Neuerungen synthetisiert, und wir präsentieren eine umfassende Analyse des attraktiven Hubbard-Modells bei Viertelbandfüllung, als Prototyp eines fermionischen Systems mit suprafluidem Grundzustand. In einem gekoppelten Fermion-Boson Fluss, der sowohl die Selbstwechselwirkungen des Ordnungsparameters, zwei verschiedene Fermion-Boson Kopplungen, als auch die anomalen Komponenten der fermionischen Selbstenergie berücksichtigt, werden simultan zu diversen nicht-universellen Größen, wie der Energielücke des fermionischen Energiespektrums, auch universelle Infraroteigenschaften des kollektiven, bosonischen Sektors bestimmt.

Strukturell zeichnet sich unsere Analyse durch Unterscheidung des Minimums des bosonischen, effektiven Potentials und der fermionischen Energielücke –beide fallen nur in Molekularfeldtheorie zusammen, siehe Abschnitt 8.4.3– und Trennung der radialen und transversalen Moden (siehe Abschnitt 8.4.3), aus. Letzteres ermöglicht in Anlehnung an Abschnitt 6.5 die exakte Behandlung des Infrarotsektors (siehe Abschnitt 8.5.2).

In Abschnitt 8.5.3 werden numerische Lösungen der gekoppelten Renormierungsgruppengleichungen in zwei Raumdimensionen präsentiert. Ein wesentliches Resultat ist der in Abb. 8.12 dargestellte Vergleich zwischen fermionischer Energielücke, Minimum des effektiven Potentials und kritischer Skala. Die Werte für die fermionische Energielücke sind um etwa einen Faktor vier gegenüber der Molekularfeldtheorie reduziert; hauptsächlich verursacht durch Ordnungsparameterfluktuationen, die bei relativ hohen Energieskalen bereits im symmetrischen Teil des Flusses der Formierung suprafluider Ordnung entgegenwirken.

Die linke Graphik in Abb. 8.13 zeigt, dass beide Fermion-Boson Vertizes, obschon diese durch Goldstone-Fluktuationen renormiert werden (siehe Abb. 8.9), quantitativ nur um wenige Prozentpunkte von ihren nicht-renormierten Ausgangswerten abweichen. Dies ist eine Konsequenz des geringen den Goldstone-Moden zur Verfügung stehenden Phasenraumvolumens.

Der unterschiedliche Verlauf der bosonischen Z-Faktoren ist in der rechten Abbildung von Abb. 8.13 sichtbar: Während der Z-Faktor der radialen Mode als Funktion der Skala divergiert, saturiert der Z-Faktor der Goldstone-Mode, so dass diese ihre quadratische Frequenz- und Impulsabhängigkeit behält –wie bereits in Abschnitt 6.5 analytisch demonstriert.

Die Dissertation schliesst mit einer kritischen Diskussion in Kapitel 9, die sowohl methodische Errungenschaften als auch Optimierungspotenziale der Arbeit und interessante zukünftige Forschungsvorhaben umreißt. Im Anhang A wird die zur numerischen Lösung der Flussgleichungen entwickelte numerische Prozedur erklärt.

Part IV

Appendices

A

Numerical procedure

In this Appendix, we present the programs which were assembled and subsequently used to solve the RG flow equations in this thesis. The exact flow equation, Eq. (3.18), projected on a finite number of parameters represents a system of coupled ordinary differential equations. The right-hand-sides of these equations involve numerical integrations. In chapter 5, the right-hand-sides involve one-dimensional integrations and in chapter 8 two-dimensional momentum integrations over the whole Brillouin zone have to be executed.

Hence, a routine for coupled differential equations was combined with a numerical integration routine which provides the values of the right-hand-sides at each increment of the differential equation solver. A data flow picture is exhibited in Fig. A.1.

The routines employed were taken from the GSL-GNU scientific library¹ and then assembled and modified in a C/C++ code. Specifically, we used the Runge-Kutta-Fehlberg (4, 5) stepping function, `gsl_odeiv_step_rkf45`, for the differential equation solver. This routine adaptively adjusts the step-size for given error margins and proved to be computationally efficient as well as accurate even at very low temperatures. We used relative error margins of $1e-4$ to $1e-8$.

For the numerical integrations, we employed the routine `gsl_integration_qags`. This routine performs well for singular integrands as we encounter at the critical scale or toward the end of the flow. It adaptively adjusts the stepsize within each integration interval to satisfy the error margins. We employed relative error margins of $1e-2$ to $1e-4$. Two-dimensional integrations were executed by linearly combining two one-dimensional routines.

¹ <http://www.gnu.org/software/gsl/>

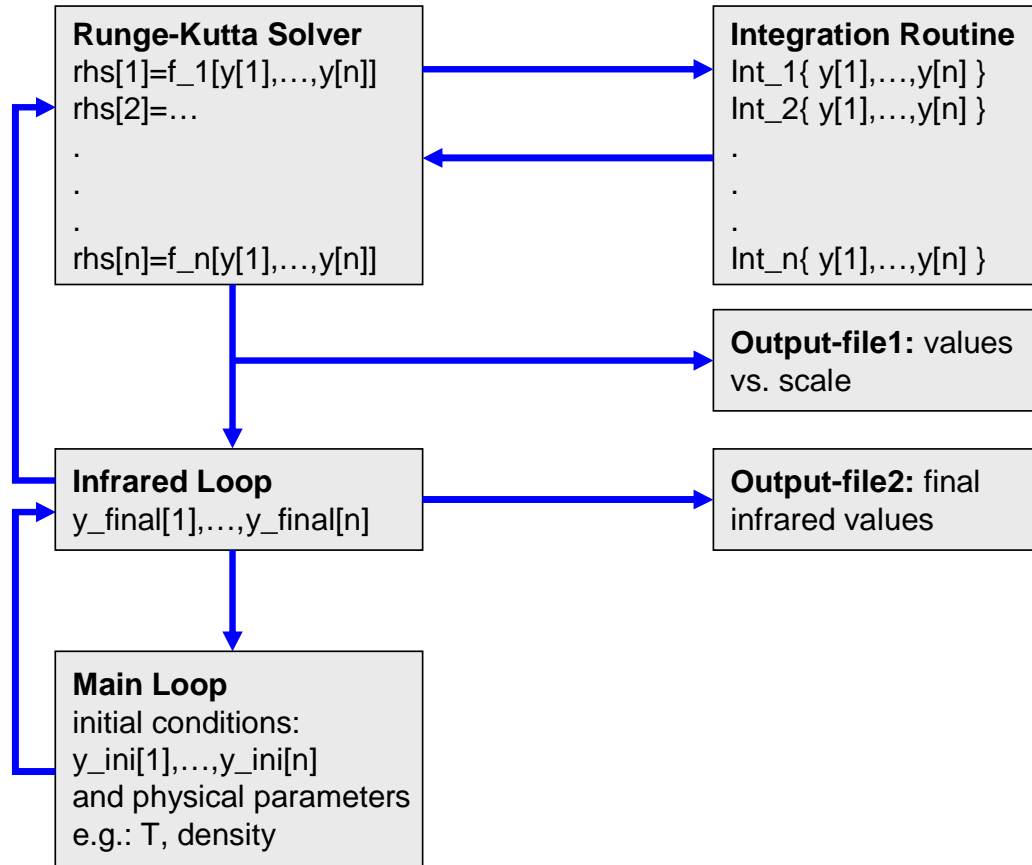


Fig. A.1. Schematic data flow of the program employed to solve the flow equations in this thesis. The maximum number of coupled equations solved simultaneously in chapter 8 was $n \lesssim 15$. Typical computation times for forty consecutive flows as shown in Fig. 8.12 were of the order of several days up to one week on a single modern processor.

B

Academic curriculum vitae

Born on April 24th, 1981 in Frankfurt am Main

EDUCATION

<i>10.2005 - 02.2009</i>	<i>Doctorate - Theoretical Physics (grade: with distinction)</i>
10.2005 - 02.2009	• PhD-Student of W. Metzner, Max-Planck-Institute for Solid State Research, Stuttgart
07.2007 - 09.2007	• Guest researcher with G. Lonzarich, Trinity College, University of Cambridge, UK
10.2005 - 07.2007	• Regular visitor to the Group of C. Wetterich, University of Heidelberg
04.2006 - 08.2006	• Tutor in Statistical Physics and Electrodynamics, University of Stuttgart
<i>10.2001 - 05.2005</i>	<i>Master of Science - Physics (grade: superior)</i>
08.2004 - 05.2005	• M. Sc. in Theoretical Astrophysics with A. Burrows, University of Arizona, Tucson, USA
04.2003 - 07.2004	• Diploma exams, University of Heidelberg
09.2001 - 03.2003	• Prediploma, Technical University Dresden
<i>06.2000</i>	<i>Abitur, Justus-Liebig-School, Darmstadt</i>
06.1997 - 08.1998	• Queen Elizabeth High School, Edmonton, Canada

SCHOLARSHIPS

Max Planck Contract for Doctoral Research
Full scholarship – The University of Arizona
Fulbright Commission Travel Grant
Baden-Württemberg Stipendium

Stuttgart, February 2009

References

- Abanov, A., and Chubukov, A.V., Phys. Rev. Lett. **84**, 5608 (2000).
- Abanov, A., Chubukov, A.V., and Schmalian, J., Adv. in Phys. **52**, 119-218 (2003).
- Abanov, A., and Chubukov, A.V., Phys. Rev. Lett. **93**, 255702 (2004).
- Abrikosov, A.A., Gorkov, L.P., and Dzyaloshinski, I.E., *Methods of Quantum Field Theory in Statistical Physics* (Dover Publications, New York, 2005).
- Altshuler, B.L., Ioffe, L.B., and Millis, A.J., Phys. Rev. B **50**, 14048 (1994); *ibid.* **52**, 5563 (1995).
- Amit, D.J., and Martin-Mayor, V., *Field Theory, the Renormalization Group and Critical Phenomena* (World Scientific, 2005).
- Baeriswyl, D., *et al.*, *The Hubbard Model* (NATO ASI Series, Plenum Press, 1993).
- Baier, T., Bick, E., and Wetterich, C., Phys. Rev. B **70**, 125111 (2004).
- Ballhausen, H., Berges, J., and Wetterich, C., Phys. Lett. B **582**, 144 (2004).
- Bedaque, P.F., Caldas, H., and Rupak, G., Phys. Rev. Lett. **91**, 247002 (2003).
- Belitz, D., Kirkpatrick, T.R., and Vojta, T., Rev. Mod. Phys. **70**, 580 (2005).
- Berges, J., Tetradis, N., and Wetterich, C., Phys. Rep. **363**, 223 (2002).
- Birse, M.C., Krippa, B., McGovern, J.A., Walet, N.R., Phys. Lett. B **605**, 287 (2005).
- Burovski, E., Prokofev, N., Svistunov, B., and Troyer, M., Phys. Rev. Lett. **96**, 160402 (2006); New Journal of Physics **8**, 153 (2006) .

- Castro Neto, A.H., Guinea, F., Peres, N.M.R., Novoselov, K.S., and Geim, A.K., *Rev. Mod. Phys.* **81**, 109 (2009).
- Chin, J.K., Miller, D.E., Liu, Y., Stan, C., Setiawan, W., Sanner, C., Xu, K., and Ketterle, W., *Nature* **446**, 961 (2006).
- Chitov, G.Y., and Millis, A.J., *Phys. Rev. Lett.* **86**, 5337 (2001); *Phys. Rev. B* **64**, 054414 (2001).
- Christofi, S., Hands, S., and Strouthos, C., *Phys. Rev. D* **75**, 101701(R) (2007).
- Chubukov, A.V., and Maslov, D.L., *Phys. Rev. B* **68**, 155113 (2003).
- Chubukov, A.V., Maslov, D.L., Gangadharaiah, S., and Glazman, L.I., *Phys. Rev. B* **71**, 205112 (2005).
- Chubukov, A.V., and Khveshchenko, D.V., *Phys. Rev. Lett.* **97**, 226403 (2006).
- Delamotte, B., Mouhanna, D., and Tissier, M., *Phys. Rev. B* **69**, 134413 (2004).
- Dell'Anna, L., and Metzner, W., *Phys. Rev. B* **73**, 045127 (2006).
- Diehl, S., Gies, H., Pawłowski, J.M., and Wetterich, C., *Phys. Rev. A* **76**, 021602(R) (2007).
- Diehl, S., Krahl, H.C., and Scherer, M., *Phys. Rev. C* **78**, 034001 (2008).
- Diener, R.B., Sensarma, R., and Randeria, M., *Phys. Rev. A* **77**, 023626 (2008).
- Eagles, D.M., *Phys. Rev.* **186**, 456 (1969).
- Eckl, T., Scalapino, D.J., Arrigoni, E., and Hanke, W., *Phys. Rev. B* **66**, 140510(R) (2002).
- Enss, T., PhD Thesis, Max Planck Institute for Solid State Research, arXiv:cond-mat/0504703 (2005).
- Feldman, J., Magnen, J., Rivasseau, V., and Trubowitz, E., *Helv. Phys. Acta* **66**, 497 (1993).
- Franz, M., Tesanovic, Z., and Vafeek, O., *Phys. Rev. B* **66**, 054535 (2002).
- Gersch, R., Honerkamp, C., Rohe, D., and Metzner, W., *Eur. Phys. J. B* **48**, 349 (2005).
- Gersch, R., Reiss, J., and Honerkamp, C., *New J. Phys.* **8**, 320 (2006).

- Gersch, R., Honerkamp, C., and Metzner, W., New J. Phys. **10**, 045003 (2008).
- v. Gersdorff, G., and Wetterich, C., Phys. Rev. B **64**, 054513 (2001).
- Gies, H., and Jaeckel, J., Phys. Rev. Lett. **93**, 110405 (2004).
- Gies, H., and Jaeckel, J., Eur. Phys. J. C **46**, 433 (2006).
- Gies, H., arXiv:hep-ph/0611146 (2006).
- Gies, H., private communication (2008).
- GSL-GNU scientific library, <http://www.gnu.org/software/gsl/>.
- Goldenfeld, N., *Lectures on Phase Transitions and the Renormalization Group* (Perseus Publishing, Oxford, 1992).
- Gräter, M., and Wetterich, C., Phys. Rev. Lett. **75**, 3 (1995).
- Gross, D.J., and Wilczek, F., Phys. Rev. Lett. **30**, 1343 (1973); Phys. Rev. D **8**, 3633 (1973).
- Halboth, C.J., and Metzner, W., Phys. Rev. Lett. **85**, 5162 (2000); Phys. Rev. B **61**, 7364 (2000).
- Hands, S., Kocic, A., and Kogut, J.B., Annals of Physics, **224**, 29 (1993).
- Hands, S., Phys. Rev. D **51**, 5816 (1995).
- Herbut, I.F., Phys. Rev. B **66**, 094504 (2002).
- Herbut, I.F., Phys. Rev. Lett. **97**, 146401 (2006).
- Hertz, J.A., Phys. Rev. B **14**, 1165 (1976).
- Hofstetter, W., *et al.*, Phys. Rev. Lett. **89**, 220407 (2002).
- Honerkamp, C., and Salmhofer, M., Phys. Rev. Lett. **87**, 187004 (2001), Phys. Rev. B **64**, 184516 (2001).
- Jaksch, D., and Zoller, P., Ann. Phys. **315**, 52 (2005).
- Jakubczyk, P., Strack, P., Katanin, A.A., and Metzner, W., Phys. Rev. B **77**, 195120 (2008).

- Katanin, A.A., Phys. Rev. B **70**, 115109 (2004).
- Kaul, R.K, and Sachdev, S., Phys. Rev. B **77**, 155105 (2008).
- Kaveh, K., and Herbut, I.F., Phys. Rev. B **71**, 184519 (2005).
- Keller, M., Metzner, W., and Schollwöck, U., Phys. Rev. B **60**, 3499 (1999); Phys. Rev. Lett. **86**, 4612 (2001).
- Kopper, C., and Magnen, J., Ann. Henri Poincaré **2**, 513 (2001).
- Kosterlitz, J.M., and Thouless, D.J., J. Phys. C **6**, 1181 (1973).
- Kosterlitz, J.M., J. Phys. C **7**, 1046 (1974).
- Krahl, H.C., and Wetterich, C., Phys. Lett. A **367**, 263 (2007).
- Leggett, A.J., in *Modern Trends in the Theory of Condensed Matter*, edited by A. Pekalski and R. Przystawa (Springer, Berlin, 1980).
- Lerch, N., Bartosch, L., and Kopietz, P., Phys. Rev. Lett. **100**, 050403 (2008).
- Litim, D.F., Phys. Rev. D **64**, 105007 (2001).
- Lobo, C., Recati, A., Giorgini, S., and Stringari, S., Phys. Rev. Lett. **97**, 200403 (2006).
- Löhneysen, H. v., Rosch, A., Vojta, M., and Wölfle, P., Rev. Mod. Phys. **79**, 1015 (2007).
- Martín-Rodero A., and Flores, F., Phys. Rev. B **45**, 13008 (1992).
- Metzner, W., Castellani, C., and Di Castro, C., Adv. Phys. **47**, 317-445 (1998).
- Metzner, W., Rohe, D., and Andergassen, S., Phys. Rev. Lett. **91**, 066402 (2003).
- Metzner, W., Prog. Theor. Phys. Suppl. **160**, 58 (2005).
- Micnas, R., Ranninger, J., and Robaszkiewicz, S., Rev. Mod. Phys. **62**, 113 (1990).
- Millis, A.J., Phys. Rev. B **48**, 7183 (1993).
- Nambu, Y., http://nobelprize.org/nobel_prizes/physics/laureates/2008/index.html (2008).

- Negele, J.W., and Orland, H., *Quantum Many-Particle Systems* (Addison-Wesley, Reading, MA, 1987).
- Nelson, D.R., and Kosterlitz, J.M., Phys. Rev. Lett. **39**, 19 (1977).
- Nepomnashchy, Y.A., Phys. Rev. B **46**, 6611 (1992), and references therein.
- Neumayr, A., and Metzner, W., Phys. Rev. B **58**, 15449 (1998).
- Nozières, P., *Theory of Interacting Fermi Systems* (Westview Press, 1964).
- Nozières, P., and Schmitt-Rink, S., Journal of Low Temp. Phys. **59**, 195 (1985).
- Oganesyan, V., Kivelson, S.A., and Fradkin, E., Phys. Rev. B **64**, 195109 (2001).
- Ohashi, Y., and Griffin, A., Phys. Rev. Lett. **89**, 130402 (2002).
- Pawlowski, J.M., Litim, D.F., Nedelko, S., and L. v. Smekal, Phys. Rev. Lett. **93**, 152002 (2004).
- Peskin, M.E., and Schroeder, D.V., *An Introduction to Quantum Field Theory* (Westview Press, 1995).
- Pistolesi, F., Castellani, C., Di Castro, C., and Strinati, G.C., Phys. Rev. B **69**, 024513 (2004); Phys. Rev. Lett. **78**, 1612 (1997).
- Polchinski, J., Nucl. Phys. B **231**, 269 (1984).
- Politzer, H.D., Phys. Rev. Lett. **30**, 1346 (1973).
- Popov, V.N., *Functional integrals and collective excitations* (Cambridge University Press, Cambridge, 1987).
- Quintanilla, J., Haque, M., and Schofield, A.J., Phys. Rev. B **78**, 035131 (2008).
- Randeria, M., in *Bose-Einstein Condensation*, edited by A. Griffin, D. Snoke, and S. Stringari (Cambridge University Press, Cambridge, England, 1995), pp. 355-392.
- Rech, J., Pepin, C., and Chubukov, A.V., Phys. Rev. B **74**, 195126 (2006).
- Reiss, J., Rohe, D., and Metzner, W., Phys. Rev. B **75**, 075110 (2007).
- Rohe, D., and Metzner, W., Phys. Rev. B **63**, 224509 (2001).
- Rosa, L., Vitale, P., and Wetterich, C., Phys. Rev. Lett. **86**, 958 (2001).

- Rosch, A., Phys. Rev. B **64**, 174407 (2001).
- Rüegg, Ch., Normand, B., Matsumoto, M., Furrer, A., McMorro, D.F., Krämer, K.W., Güdel, H.-U., Gvasaliya, S.N., Mutka, H., and Boehm, M., Phys. Rev. Lett. **100**, 205701 (2008).
- Sachdev, S., *Quantum Phase Transitions* (CUP, Cambridge, U.K., 1999).
- Salmhofer, M., *Renormalization An Introduction* (Springer, Berlin Heidelberg, 1999).
- Salmhofer, M., Honerkamp, C., Metzner, W., and Lauscher, O., Prog. Theor. Phys. **112**, 943 (2004).
- Salmhofer, M., Ann. Phys. (Leipzig) **16**, No. 3, 171 (2007).
- Schütz, F., Bartosch, L., and Kopietz, P., Phys. Rev. B **72**, 035107 (2005).
- Schütz, F., and Kopietz, P., J. Phys. A **39**, 8205 (2006).
- Sebastian, S.E., Harrison, N., Batista, C.D., Balicas, L., Jaime, M., Sharma, P.A., Kawashima, N., and Fisher, I.R., Nature **441**, 617 (2006).
- Shankar, R., Rev. Mod. Phys. **66**, 129 (1994).
- Shin, Y., Schunck, C.H., Schirotzek, A., and Ketterle, W., Nature **451**, 689 (2008).
- Singer, J.M., Pedersen, M.H., Schneider, T., Beck, H., and Matuttis, H.G., Phys. Rev. B **54**, 2 (1996).
- Solyom, J., Adv. Phys. **28**, 201 (1979).
- Stewart, G.R., Rev. Mod. Phys. **73**, 797 (2001).
- Strack, P., Gersch, R., and Metzner, W., Phys. Rev. B **78**, 014522 (2008).
- Strouthos, C., and Kogut, J.B., arXiv:0804.0300 (2008).
- Tetradis, N., and Wetterich, C., Nucl. Phys. B **422**, 541 (1994).
- Uchoa, B., and Castro Neto, A.H., Phys. Rev. Lett. **98**, 146801 (2007).
- Voit, J., Rep. Prog. Phys. **57**, 977 (1994).
- Weichman, P.B., Phys. Rev. B **38**, 8739 (1988).

- Weinberg, S., *The Quantum Theory of Fields Vol. I*, (CUP, Cambridge, 2005).
- Wetterich, C., Z. Phys. C **57**, 451 (1991).
- Wetterich, C., Phys. Lett. B **301**, 90 (1993).
- Wetterich, C., Phys. Rev. B **77**, 064504 (2008).
- Wilson, K.G., and Kogut, J., Phys. Rep. C **12**, 75 (1974).
- Wölfle, P., and Rosch, A., J. Low Temp. Phys. **147**, 165 (2007).
- Zanchi, D., and Schulz, H.J., Phys. Rev. B **61**, 13609 (2000).
- Zhao, E., and Paramekanti, A., Phys. Rev. Lett. **97**, 230404 (2006).
- Zwerger, W., Phys. Rev. Lett. **92**, 027203 (2004).